Erlend Gustav Rikardsen Hauge

Scaling in the Si Off-gas Systems

The Effect of Alkali Content

Master's thesis

NTNU
Norwegian University of
Science and Technology

Erlend Gustav Rikardsen Hauge

Scaling in the Si Off-gas Systems

The Effect of Alkali Content

NTNU
Norwegian University of
Science and Technology

Preface

This thesis titled, "Scaling in the Si off-gas systems - The effect of alkali content" was written for the course TMT4900 and was carried out at the Department of Materials Science and Engineering at the Faculty of Natural Sciences at the Norwegian University of Science and Technology(NTNU), during the spring semester of 2022. This thesis is also a continuation of the specialisation project with the same name.

Abstract

The aim for this thesis was to investigate the composition of the scales from the chimney of two silicon furnaces and one ferrosilicon furnace. The investigation of composition is meant to get a better understanding of the underlying mechanism for the formation of the fouling in scales seen for both silicon and ferrosilicon furnaces. When the scales start to accumulate in the chimney it leads to multiple problems and forces industries to have regular shutdowns. With a greater understanding of the underlying mechanism the process can be adjusted to make the process more efficient by avoiding or minimizing the fouling problem. This can then lead to less downtime by reducing regular shutdowns.

Two samples from two silicon furnaces and one sample from a ferrosilicon furnace was split and prepared for investigation. The fouling samples were selected based on interesting attributes like colour or shape for the EPMA analysis, but there was no difference in the resulting images. The only noticeable difference was between the furnaces. The analysis was carried out to characterize the samples and investigate its inherent phase composition. The remaining sample that was not utilized for the EPMA analysis was later crushed down to produce representative homogeneous samples. These samples were then doped with a known amount of alumina for so to be characterised with XRD. The alumina helped with quantitatively determining the amorphous content. The XRD quantified the crystal phases. The representative samples were also used for ICP-MS analysis, the analysis was carried out by ALS Scandinavia at their lab in Luleå. The representative samples were also sent to Elkem Technology lab for quantification of silicon metal by a Fedorov analysis. The representative samples were also tested in a wetting furnace also known as sessile drop furnace(SDF) to determine the softening temperature. The composition of the samples tested in the SDF were also tested in five different prediction models for softening temperature.

Wavelength dispersive x-ray spectroscopy identified five different phases: silica, silicon carbide, silicon metal, ferrosilicon and a slag phase. The silicon carbide, silicon metal and the ferrosilicon are very likely a product of condensation reactions, but silicon carbide could also come from the charge material. The condensation reactions are a direct result of unreacted SiO gas in the chimney. X-ray powder diffraction(XRD) quantified five different phases as well as the amorphous content. The crystal phases were cristobalite, quartz, tridymite, silicon carbide and magnetite. The fouling sample was prior to investigation expected to be amorphous, but the result from every furnace indicated the presence of a large amount of crystalline content. Cristobalite and tridymite was formed by the exposure to temperatures above 820°C, because amorphous silica will crystallize above 820°C. Tridymite does however require potassium to both form and be stable at standard state. The amorphous content varied from 40 to 50% of the fouling.

The composition from ICP-MS was adjusted for oxides and then compared to the composition of Microsilica that was produced during the same time period as the fouling formed. The result differed for all furnaces, but generally the fouling had increased CaO, Al_2O_3 and Fe_2O_3 content. The K_2O, Na_2O and MgO was generally reduced in the fouling sample. The softening temperature was measured consistently above 1600°C and slightly below 1600°C for one sample. This result does not really say anything conclusive about the scales, but there is a chance that the fouling is not formed due to melting phases.

2

Sammendrag

Hensikten med denne masteren har vært å undersøke komposisjonen av avsetningen som finnes i pipen på silisiums og ferrosilisiums verk. Resultatet vil kunne brukes til å oppnå en bedre forståelse av hvilke faktorer som bidrar til oppbygningen av avsetningen. Dermed kan man unngå at avsetningen tar plass ved å gjøre endringer på operasjonen av ovnene. Avsetning i avgass kanaler leder til at industri er tvunget til å ha regelmessige nedstengninger slik at overflatene kan bli rengjort. Dermed kan dette også føre til færre nedstengninger.

To prøver fra pipen til to silisiums verk og en prøve fra pipen på en ferrosilisiums ovn ble undersøkt. Prøvene som ble valgt ut for EPMA analyse ble valgt basert på interessante egenskaper som farge og form, men de resulterende bildene viste ingen forskjell. Den største forskjellen ble sett mellom ovnene. Analysen ble gjort for å karakterisere og undersøke prøvens sammensetning av faser. Prøvemateriale som ikke ble brukt til EPMA ble knust ned til representative homogene prøver. For XRD ble prøvene så dopet med aluminium slik at den amorfe mengden kunne kvantifiseres. XRD kvantifiserte også krystallfasene. De representative prøvene ble også sendt til ALS Scandinavia i Luleå for å karakteriseres med ICP-MS. Prøver ble også sendt til Elkem Technology lab for kvantifikasjon av silisiums metall ved hjelp av en Fedorov analyse. Representative prøver ble også brukt til å karakterisere mykningstemperaturen i en sessile drop furnace(SDF). Komposisjsonen av disse prøvene som ble testet i SDF ble også testet i fem forskjellige model for prediksjon av mykningstemperatur.

Wavelength dispersive x-ray spectroscopy(WDS) ble brukt til å karakterisere fem forskjellige faser: silisium, silisiumkarbid, silisium metall, ferrosilisium og en slagg fase. silisiumkarbid, silisium metal og ferrosilisium er veldig sannsynlig resultatet av kondensasjonsreaksjoner, silisiumkarbid kan også ha kommet fra ovnsmaterialet. Kondensasjonsreaksjon er et direkte resultat av ureagert SiO i pipen på grunn av ustabil drift. X-ray powder diffraction(XRD) kvantifiserte fem forskjellige faser i tilegg til den amorfe mengden. De målte krystallstrukturene var cristobalitt, kvarts, tridymitt, silisiumkarbid og magnetitt. Før undersøkelse av prøver var det forventet at prøven skulle være amorf, men resultatet fra hver ovn tilsier at det er en god del krystallint materiale i pipene. cristobalitt og tridymitt kan dannes når Mirosilica er utsatt for temperaturer over 820°C, fordi dette er når nukleeringen starter for amorf silika. tridymitt krever kalium til stede for å formere siden stoffet både promoterer dannelsen samt stabiliseringen av krystallstrukturen slik at den kan eksistere ved standard tilstand. Amorf mengde varierte fra 40 til 50% for prøvene.

Komposisjonen fra ICP-MS ble justert for oksider og så sammenlignet med Microsilica komposisjonen fra samme tidsperiode som avsetningsprøven var tatt. Resultatet var forskjellig for alle ovnene, men generelt så var det økt CaO, Al_2O_3 og Fe_2O_3 innhold. Mengden K_2O, Na_2O og MgO var generelt redusert for avsetningsprøvene. Mykningstemperaturen ble målt jevnt over 1600°C og i ett tilfelle rett under 1600°C. Resultatet sier ikke mye konklusivt om avsetningen, annet enn at det er en sjanse for at avsetningen ikke er et resultat av smeltefaser.

Contents

List of Figures

List of Tables

9

1 Introduction

Fouling is a process that describes unwanted material depositing on solid surfaces. The deposits lead to a multitude of problems like clogging of transport pipes and reduction on the lifetime of off-gas filters. When the fouling builds up it eventually forces the industries to have regular shutdowns to clean off the deposits from the surface where the fouling occurred. The problem of fouling on heat exchangers has been estimated of being a loss of 0.25% of the total gross domestic production in industrialized countries[11]. The reduced energy recovered from the heat exchangers have also been estimated to lead to an 1-2.5% increase of CO_2 emissions. The increase in CO_2 emissions is estimated based on the energy being supplied by a non-renewable source.

Fouling can be divided into several types: particulate fouling, scaling, corrosion fouling, etc. Scaling forms hard and highly adhered layers which is exactly what is seen in the silicon industry. Scaling is formed through precipitation which is crystallisation of saturated solutions. The underlying mechanism for the fouling of the silicon industry is not understood completely. It could potentially be the product of precipitation, this thesis will try and shed some light on the underlying mechanism for three different furnaces.

Fouling is also a problem that pertains to a lot of industries. When the temperature of the off gas is increasing the fouling has a tendency of also increasing. This does create a problem when systems for energy recovery are implemented. For maximum energy recovery the temperature should be kept high by not diluting the off gas with too much air. The increased temperature will however lead to an increase in the tendency of deposits forming. If other factors that lead to fouling can be reduced, then the off gas temperature can potentially be increased. The relevancy of this problem is at an all-time high, since there is currently a global energy crisis.

There has not been much published regarding the fouling issue for the silicon industry. This thesis aims give a better the understanding of the underlying mechanism through characterizing the fouling samples from three different furnaces. The knowledge gained from this thesis can then potentially be utilized to run the process more optimally by reducing the need to shut down the process. The knowledge could also potentially lead to being able to run the process at higher temperature for increased energy recovery. This thesis will characterise the fouling of two silicon furnaces as well as the fouling of a ferrosilicon furnace. The samples have been investigated by the means of X-ray powder diffraction(XRD), electron probe microanalysis(EPMA), inductively coupled plasma mass spectrometry(ICP-MS), fusion temperature analysis by using a sessile drop furnace(SDF) and a Fedorov analysis. XRD gives information about the crystalline species as well as the amorphous content. EPMA is used for showcasing and characterising phases of the samples. ICP-MS gives the composition of the samples, while SDF is used to find the softening temperature of the fouling. Fedorov finds the amount of silicon metal as well as the iron content of the samples.

2 Theory

This section will give some background theory that is relevant for the project including a literature review of past publications that are relevant for off gas fouling in silicon and ferrosilicon furnaces.

2.1 Silicon

Silicon is the second most abundant element in the earth's crust and the 14th element on the periodic table. Silicon is usually found as an oxide(SiO_2) in nature[12]. A large fraction of SiO_2 exists in huge deposits of quartzite and quartz sand which is relatively pure SiO_2[1]. Quartz is the the raw material source for silicon used in the production of metallurgical grade silicon. Silicon can be utilized in a wide range of applications and modern technology. Because silicon has semiconducting properties it is applicable to both electronics and solar photovoltaics(PV). Electronic grade silicon requires less impurities than one particle per billion, while solar grade silicon only requires less impurities than one particle per million. Metallurgical grade silicon is not nearly pure enough which means it must be further purified to be utilized in electronics or PV's. Further purification can be achieved through the Siemens process. Silicones is another product that can be made by silicon. Silicones are usually utilized as sealants, adhesives, lubricants, etc. In 2021 Norway was the 4th largest producer of silicon/ferrosilicon with 350 thousand metric tons produced silicon/ferrosilicon[13]. This master thesis will focus on the fouling of chimneys in metallurgical grade silicon and ferrosilicon production.
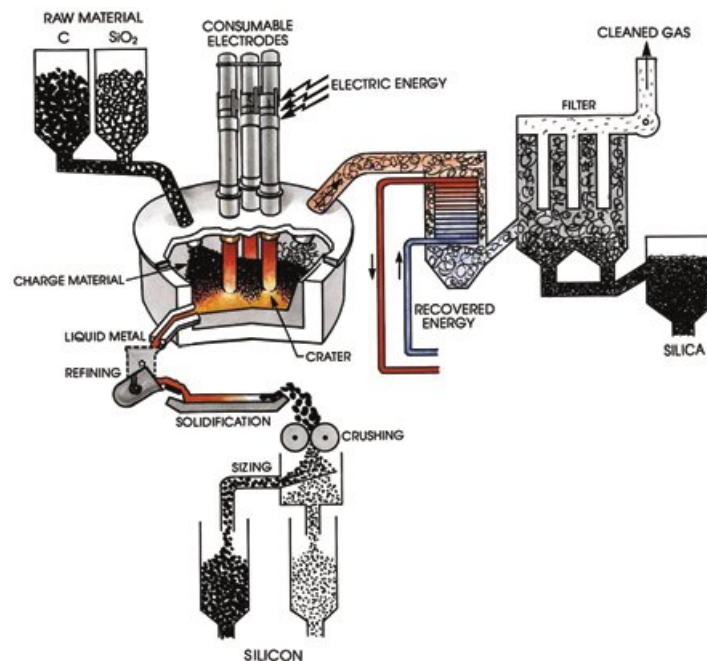
Figure 1: Sketch of a typical silicon production plant illustrating the different parts of the process[1].

2.2 Carbothermic production of silicon

The conventional carbothermic reduction of quartz to silicon has been optimized over several decades and the basic process does not vary a lot across the industry. The main differences are operations like charging, plant design, input material, size and product. The process to produce metallurgical grade silicon is carbothermic reduction of SiO_2(quartz) in an electric submerged arc furnace which produces silicon with a high purity[14]. It is worth noting that quartzite is also used in ferrosilicon metal production, but because of the lower purity of quartzite it is limited to the FeSi production[10]. Carbon is used usually in the form of coal, coke, charcoal and wood chips. The production of ferrosilicon in addition to this adds iron oxide ore, scrap metal or iron pellets as the source of iron. This mix is then heated up through a three-phase alternating current from the submerged electrodes in the charge[10]. This is a very energy-intensive process where roughly 11-13 MWh is used per ton silicon metal that is produced[1]. The simplified ideal reaction for carbothermic reduction of SiO_2 is written as

$$SiO_2(s) + 2C(s) \rightarrow Si(l) + 2CO(g) \tag{1}$$
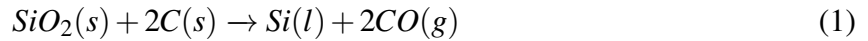
The carbon is a reduction agent agent for the quartz. The temperature required for the carbothermic reduction is above 1811°C[1]. The temperature at the bottom of the electrode is often much higher and varies greatly. The temperature is gradient towards the bottom of the electrode. In this high temperature zone the metal producing reactions take place as well as two reactions forming SiO gas

$$2SiO_2(s) + Si(l) \rightarrow 2SiO(g) \tag{2}$$

$$2SiO_2 + SiC \rightarrow 3SiO(g) + CO(g) \tag{3}$$

$$SiO(g) + SiC(s) \rightarrow 2Si(l) + CO(g) \tag{4}$$
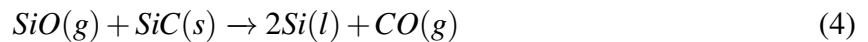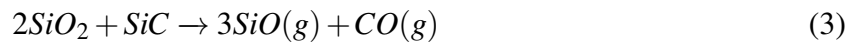
The SiO gas that is produced in the hot temperature zone rises through the charge and can then sequentially react in the lower temperature zone by the following reactions

$$3SiO(g) + CO(g) \rightarrow 2SiO_2(s,l) + SiC(s) \tag{5}$$

$$2SiO(g) \rightarrow Si(s,l) + SiO_2(s) \tag{6}$$

$$SiO(g) + 2C(s) \rightarrow SiC(s) + CO(g) \tag{7}$$
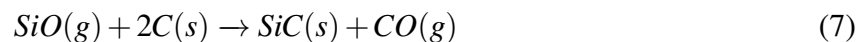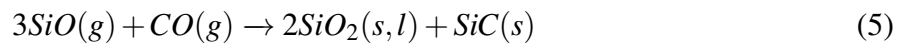
The yield of the process is directly dependent on the amount of SiO gas that reacts by these reactions in the lower temperature zone. The gas that does not react will escape the charge and burn above the charge to form silica fume, given by

$$SiO(g) + \frac{1}{2}O_2 \rightarrow SiO_2 \tag{8}$$

The silica fume is also know as Microsilica and is sold as a biproduct after it has passed through
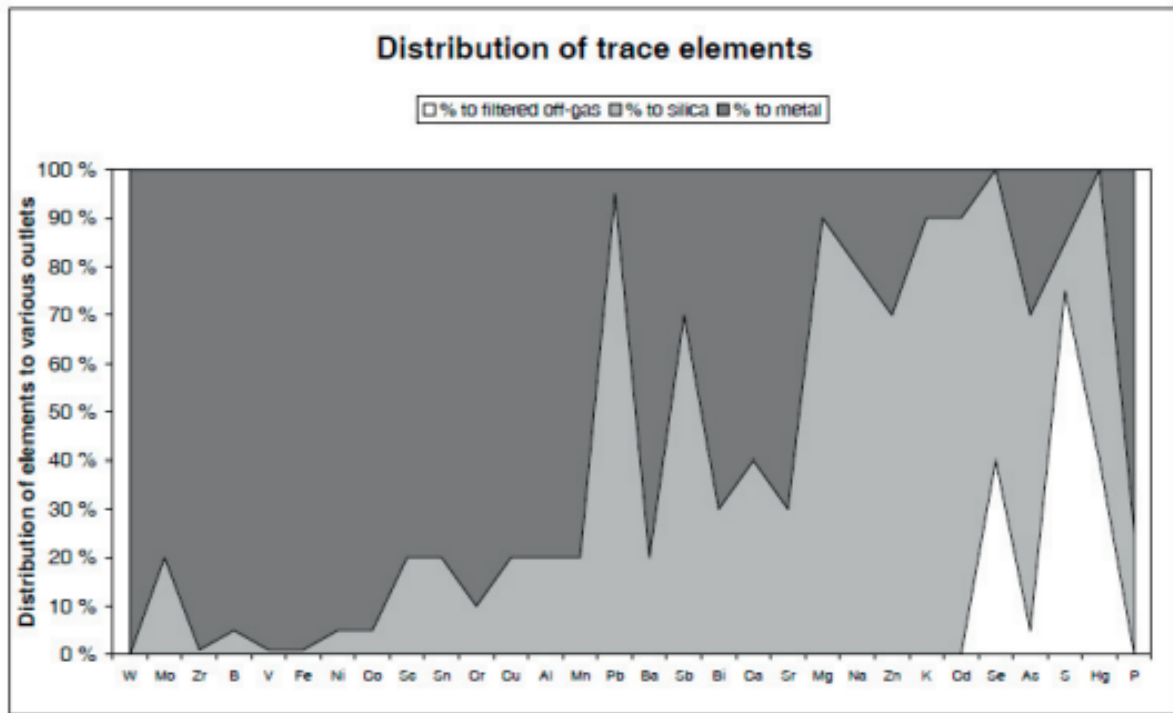
Figure 2: Myrhaugs distribution of elments(Myrhaug 2003[2])

the off gas and is captured in the baghouse filters. Microsilica can be used in various industries but the main use is enhancing the properties of concrete. For every ton silicon metal that is produced roughly 200-400 kg Microsilica is produced[15], depending on the Si-yield of the furnace.

Above the charge the temperature can be as high as 1300°C[16]. While the temperature of the off gas is directly dependent on the amount of excess air that is mixed in. The temperature of the off gas will usually be between 200-700°C[1]. Considering the temperature of the off gas there is a lot of potential thermal energy that can be utilized through energy recovery. The off gas also contains the largest recoverable energy in the process which means that an optimal process utilizes it. In Figure 1 the design of a typical plant is shown including the heat recovery. Running the process with the highest yield possible is a way of reducing the total energy consumption[1]. The backside of the higher yield is a lower amount of silicon in the Microsilica. Which means the relative amount of trace elements will increase in comparison to silicon. The distribution of elements between the off gas, metal and silica have been studied in the past by Myrhaug[2] and the resulting distribution is presented in Figure 2. The size of silica fume is usually smaller than 1 μm and the weight percentage of SiO_2 is usually more than 85%. The particles are also amorphous with a high specific surface area[17].

The quantity of impurities that end up in the Microsilica is very dependent on the quality of the raw material. The composition of raw material including quartz, carbon source and iron source vary greatly dependent on the quality of the material. The carbon sources can vary in the amount of fixed carbon, volatile compounds, moisture and ash. The more non-pure carbons contain ash with oxides the higher the occurrence of oxides like Al_2O_3 and CaO is[1]. All the raw material have some ash in it[14]. Through investigation of six different quartz types in an internal report

4

by Elkem Research in 2004 rereported by Aasly 2008[10] the varying composition can be seen in Table 1.

Table 1: The varying composition of elements from six different quartz types[10]

Unit	Al	Fe	Ca	Mg	Na	K	Ti
%	0.012 - 0.460	0.020 - 0.288	0.001 - 0.010	0.000 - 0.163	0.002 - 0.006	0.001 - 0.063	0.001 - 0.020

There are other properties of the raw material that affect the production as well. For example the mechanical- and thermal strength of the materials mechanical strength is important for maintaining the size of the material. The size of the materials is an important factor since it affects the gas flow within the furnace. When the material is too small the permeability of the charge is reduced, the raw material will be wind sieved where material is lost up the smokestack. Therefor, fines is avoided for the production. Fines can be defined by two different criteria, but the most critical definition is material less than $2mm$ in size[10]. The size of quartz is generally in the range of 10 to $150mm$[1].

The amount of airflow required to lift particles through the off gas is dependent on multiple factors. If the particle is suspended in air the amount of air flow needed is reduced in comparison to if it were laying on top of something. The amount of air is very dependent on density and morphology. Pocovi et al.[3] have studied the minimum required transport velocity to lift minerals and metallic dust in exhaust systems. Among the materials tested was iron fillings with density equal to $7.8g/cm^3$ which very likely gives a better understanding of required airflow for quartz and carbon sources as well. This is probably the case since $\alpha-quartz$ have a density of $2.67g/cm^3$[18] and the carbon sources have an even lower density and both are therefor expected to require less airflow to be lifted. In this report the velocity necessary to avoid permanent suspension in upward airflow was tested, then the resulting constants and exponents have been used to showcase the required velocity in Figure 3. The equation is $V_v = 9.2 \cdot d_p^{0.41}$, where d_p is the mean diameter of the particle. This equation was used to create Figure 3. The equation requires a Reynolds number above 15000 to be applicable which would be a very turbulent flow. The equation is the result of testing the iron fillings with sizes varying between 0.5-1mm. It is difficult to predict how far the model can be extrapolated, but the model gives an idea of how high the flow needs to be at minimum for iron fines. The fines from quartz and carbon sources should require a lower vertical velocity to be suspended.
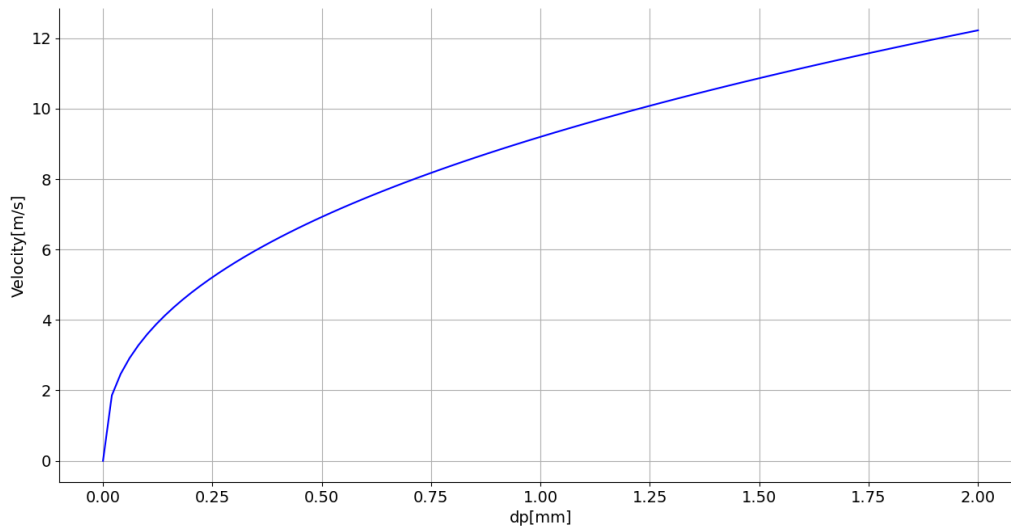
Figure 3: The resulting model for minimum vertical velocity for iron fillings by Pocovi et al.[3]

2.3 Silica phases

Silica can be found as multiple polymorphs including quartz, tridymite, cristobalite, coesite and stishovite. Silica can also be found in an amorphous state like glass or silica fume. Figure 4 shows the phase diagram for silica. Quartz can be divided into two where quartz will directly transform from $\alpha - quartz$ to $\beta - quartz$(573°C), tridymite(870°C) and $\beta - cristobalite$(1050°C) when heated[19]. This is only theoretically since pure quartz will transform directly from quartz to cristobalite at around 1050°C. When cristobalite is cooled down to 270°C it will only have one phase transition directly to $\alpha - Cristobalite$[19]. One important thing to note is that at standard state the only thermodynamically stable phase is $\alpha - quartz$, but a meta stable $\alpha - Cristobalite$ is not abnormal. One thing that is also of key interest for this thesis is that monoclinic tridymite can be found stable in the presence of alkali-metal impurities in standard state[19]. The solid solution of a smaller amount of foreign oxides(alkalis) will distort the silica structure causing the tridymite structure to both form and become stable[20].

It has been proven that crystalline silica polymorphs can be formed through heating of amorphous silica fume with a smaller quantity of impurities of alkali metals like Li, Na, K and Cs. What is worth noting is that Na would favour the formation of cristobalite at 1000°C, while K in a higher amount relative to Na would promote the formation of a mixture of cristobalite and tridymite at a lower temperature of 800°C. The mixture would be shifted towards producing more tridymite and less cristobalite at 1000°C[19].
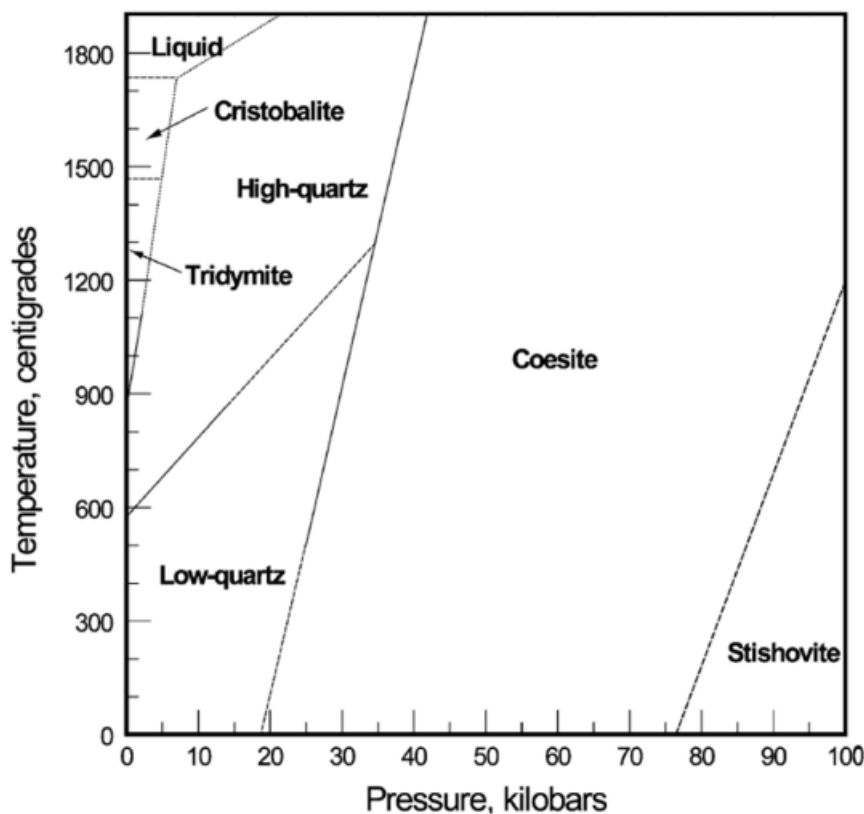
Figure 4: Phase diagram for silica[4].

The formation of polymorphs from amorphous silica is of key interest for this thesis considering amorphous silica is the main solid component in the off gas. In a report by Zhang et al.[5] silica fume from a Chinese ferrosilicon furnace was thermally treated with temperatures ranging from 700-1100C in air. In the analysis of the samples crystalline metastable cristobalite was identified. The report found that the silica would start to nucleate around 800°C. Foreign species like K, Na, Mg and other alkalis were found in the samples both during the nucleation and crystallisation. The key takeaway from the conclusion of the report was that formation of cristobalite was affected by species like Fe, Na, Mg and K. These species would reduce the crystallization temperature while also accelerating the transformation[5].

The samples in Zhang et al.[5] were around 10 grams and heated to the final calcination temperature at a rate of 10°C/min. The final temperature was held for 3 hours, and it ranged from 700-1100°C with a 100°interval between each parallel. Zhang also tested samples with Thermogravimetric Analysis - Differential Scanning Calorimetry (TG - DSC) where three separate stages for mass loss was found up to 1300°C[5]. During the first stage 2.2wt% was removed in the range of 93-200 degree C. This initial loss was concluded to be absorbed water content which then evaporated. The second stage was from 490-1002°C and the weight loss was 3.2%wt. This loss was determined to be linked to the combustion of ash and free carbon because of the exothermic peak. But in the same stage an endothermic peak was observed at 820°C which was determined to be related to the nucleation of the sample. An exothermic peak was observed between 1000-1100°C which is believed to be the crystallization since this is an exothermic process[5].

7

The result from the TG - DSC was in aggreement with the XRD result where the difference of the crystallisation can be seen in Figure 5. There is a clear difference between the three temperatures from 700-900°C. Where at 700°the sample is still amorphous and at 800°the samples is starting to crystallize while the result from 900°C suggest a very crystallized sample. Considering the exothermic peak observed between 1000-1100°C there is still the potential for amorphous material in the sample at 900°C.
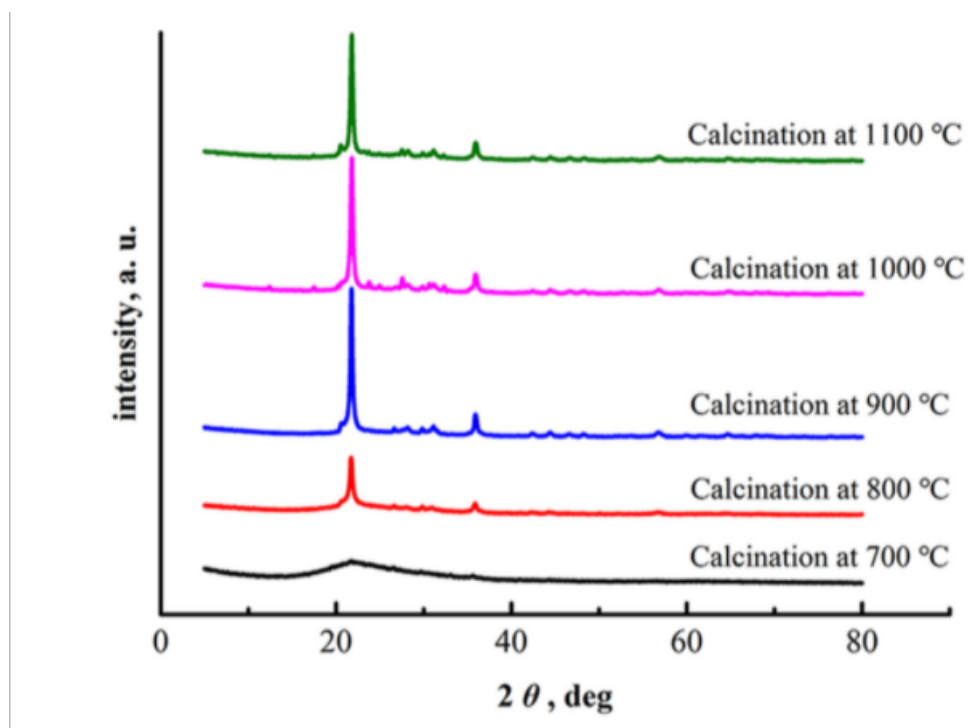
Figure 5: XRD pattern for silica fume for different thermal treatments[5].

The importance of alkali content for the softening temperature can be understood by looking at the phase equilibria and liquidus temperatures of systems like the K-O-Si and Na_2O-K_2O-SiO_2 system. Kracek et al.[21] and Akdogan et al.[6] have studied the K-O-Si system. Both have studied the effect of K_2O on the liquidus of quartz, tridymite and cristobalite. The result of the studies are quite similar which can be seen in Figure 6. What is worth taking note of is the low eutectic point of 742°C with the composition 67wt% SiO_2 and 33wt% K_2O. The main takeaway is the large amount of K_2O required to get a liquidus equal to the temperature directly above the charge(1400°C). The phase transformations here are in accordance to Figure 4.
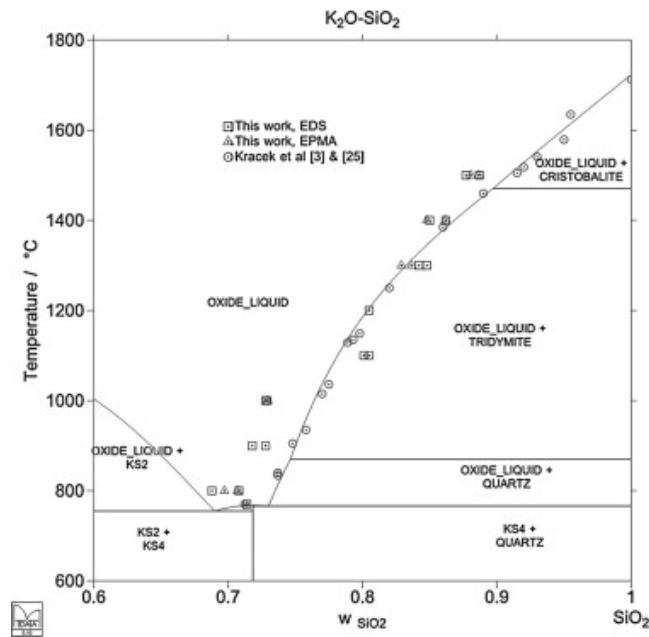
Figure 6: Pseudo-binary phase diagram of K_2O-SiO_2 system in equilibrium with air from Akdogan et al.[6]. The result of measurements is shown for both reports including a calculated solid line.

The Na_2O-K_2O-SiO_2 system was also studied by Kracek et al.[7]. The ternary diagram made from this can be seen in Figure 7. The system is limited to alkali content below 50 mole percent. The system was also simplified by excluding any ternary compounds. Therefor the only compounds seen in the diagram is the binary compounds K_2SiO_3, Na_2SiO_3, $K_2Si_2O_3$, $Na_2Si_2O_5$, $K_2Si_4O_9$ and the crystalline phases of silica. The lowest ternary eutectic temperature of 540°C on this diagram is at the composition of 25.4wt% K_2O, 8wt% Na_2O and 69wt% SiO_2. Another thing to note is that silica is in the form of quartz at this eutectic. This is a composition that would then result in the lowest melting point in a mixture of silica and alkali metals. 540°C is also a lot lower than the expected temperature of the off gas with energy recovery systems considering the waste gas temperature in schei et al.[1] at one plant. This was at Elkem Thamshavn in 1995 and the temperature was 750°C in the boiler to produce steam. The composition of 25.4wt% K_2O, 8wt% Na_2O and 69wt% SiO_2 is however unlikely. But there are other low-melting phases in addition to this and it is hard to predict the melting temperature because of the amount of species that can affect it.

9
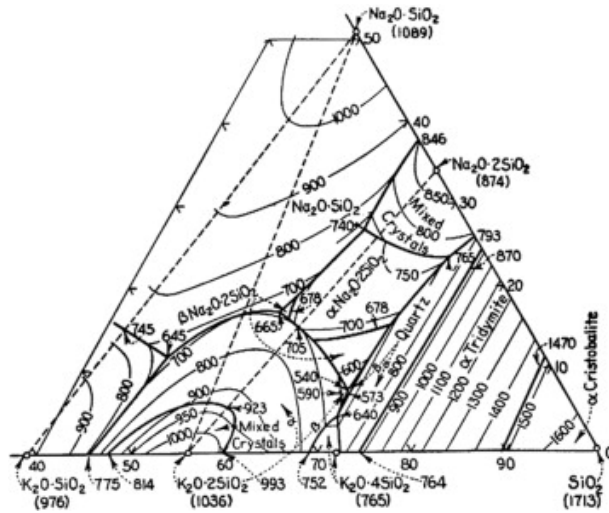
Figure 7: Ternary diagram for the Na_2O-K_2O-SiO_2 system as reported by Kracek[7]

2.3.1 Stoking Crust

The furnace will have three different types of deposits that cause operational problems for the production of silicon and ferrosilicon. These deposits are slag which forms at the bottom and is essentially incompletely converted charge materials, SiC with Si at the bottom of the furnace and crust formation at the top of the charge caused by sintering of charge materials and condensation of SiO by Equation 5 and Equation 6[1]. The problem with these deposits is that they cause obstruction of the process and as result the operation have to be adjusted to accommodate that. The crust formation is the only one that will potentially affect the fouling of the chimney since it pertains to the conditions and mass balance of the off gas.

There are also three different types of crust that form in the furnace depending on the position and composition of the crust namely crater, stoking and side crust. The crater crust is formed in the proximity of the crater and the stoking crust is high in the furnace and is the material that is stoked towards the crater. Silicon carbide is the main component of the crater crust, but because of the high temperature in the proximity of the crater it is also possible for formation of silicon droplets. Even with the high temperature the crust has the possibility of containing traces of condensates[22]. The side crust is as the name suggest formed in the inactive zone of the furnace off to the side close to the crater. The side crust is mainly silicon carbide mixed with oxides forming a green oxide slag. The side crust can also contain condensates, but in a minor amount mainly caused by the small amount of SiO gas travelling through the mass.

The final crust is then located at the top of the charge and is called the stoking crust. This is also the material that is stoked as the name would suggest. Over time this charge will eventually contain cavities. Because the crust is where most of the condensate is found it is very important for the mass balance of the off gas[22]. This layer is also rich in unreacted charge and SiC. Two types of condensates can usually be found in this area white and brown condensate. The composition of brown condensate is a mixture of Si and SiO_2 since it is a direct result of Equation 6. Inside the brown condensates there can be found small silicon spheres which affects the colour of the

10

condensate. This will typically look like Figure 8 which shows brown condensate from a pilot scale experiment by SINTEF in 2011 and later analysed by Jørund Vangskåsen[8]. In a laboratory scale experiment by Ksiazek et al.[23] brown condensate powder was observed accumulating both above the crucible as well as in the off gas tube or ventilation. This is in contrary to how it is expected to be in commercial scale were the SiO is expected to react with oxygen above the charge to form Microsilica. White condensate is also often found in the stoking crust and consists of SiO_2, SiC and Si. The white condensate can appear as porous, foamy layers of whiskers on a surface[24].

The charge is stoked to promote the flow of charge towards the crater. Since condensation and crust formation occurs stoking is necessary to maintain optimal operation conditions. Stoking will cause the gas composition, crater temperature, condensation and chemical reactions in the process to be altered. The process of stoking is more complicated than doing the stoking on a timed schedule since the charge can be overstoked as well as understoked. When the charge is overstoked the permeability is reduced because of the compaction of the charge. The result is that gas will be flowing through channels instead of being spread evenly throughout the charge resulting in a loss of SiO and energy. When the furnace is understoked the permeability will also be lower causing material to not have access to the inner zone of the furnace to be reduced. The direct result of this is a lowered silicon production caused by the SiO gas passing through channels instead of spreading throughout the charge. This will also lead to more SiO gas escaping the charge[22]. Understoking also carries the risk of large cavities forming which can collapse resulting in the release of gas from both the process and volatiles in the carbon material due to sudden heating. This release will both have a higher temperature as well as SiO and CO which both are exothermic reactions potentially releasing large amounts of energy making the potential temperature in the off gas higher in shorter bursts.

(a) 40X (b) 200X
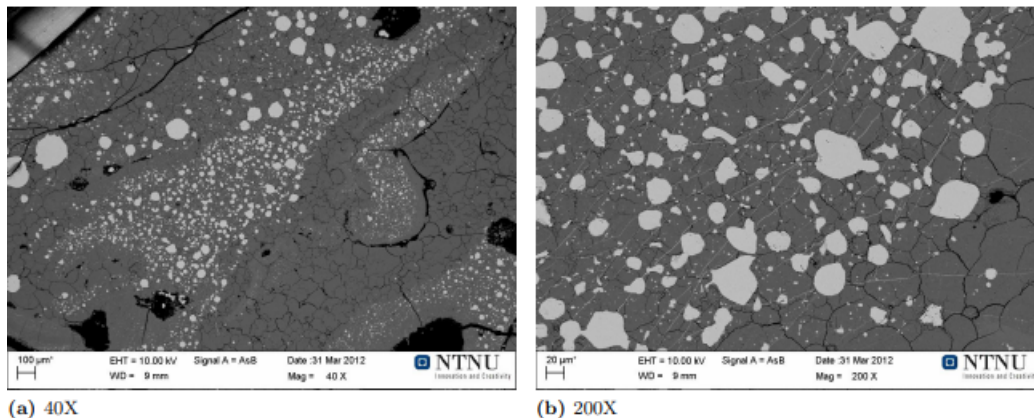
Figure 8: Pale brown condensate from pilot scale sample[8].

2.4 Fouling

Fouling is a problem in a lot of industries where the fouling will eventually clog up the transport pipes as well as reduce the lifetime of off gas filters. The usual solution to the occurrence of clogging is to have regular shutdowns and cleaning of the affected surfaces. Heat recovery systems also have the problem of fouling[25]. The issue of fouling on heat exchangers have been tried mitigated by several methods including changing the design, implementing mechanical removers, coatings or changing the operating conditions[26]. Which measures will be the most effective depends largely on the properties of the fouling.

How the fouling layers build up over time is a very complex and dynamic process, because there are several mechanisms for depositions at play simultaneously. The main parameters influencing the sticking of particles as described by Kleinhans et al.[27] are; particle properties, particle shape and surface roughness, impact angle, particle kinetic energy and its deformation on impaction, substrate properties, substrate roughness and geometry. The substrate is referring to the surface the particle sticks to. The main properties that affect particle and substrate are melt fraction, viscosity and surface tension. What is worth noting is that for silicate-rich ashes the main properties is viscosity and surface tension, but for ash from herbaceous biomass and wood it is mainly the melt fraction[27].

Another effect that is not quite understood in terms of fouling is thermophoresis. This is a force on particles that pushes particles in the opposite direction of the temperature gradient and is very relevant for the silicon industry because the off gas will have a very non-uniform temperature field. This force is very relevant for small particles[27]. Since the temperature of the walls of the off gas is lower than the off gas it will lead to more particles colliding with the walls. When ash particles impact on a cold surface it will solidify and rebound[27]. The initial layer will then form through heterogeneous condensation or migration of small particles to the surface[27]. High amounts of woodchips and biocarbon could then potentially lead to an increased fouling tendency because of an increase in the quantity of particles with a higher melt fraction. The melt fraction of ash particles refers to the total mass of liquid phases or components within the ash particle compared to the mass of the particle. The sticking probability of a particle is dependent on the critical melt fraction and since the off gas of silicon industry is a multi-component system the particles can melt over a wider temperature range. Multiple models for the critical melt fraction have been reported by Kleinhans et al.[27] ranging from 10-15% where particles are assumed to have a likeliness to adhere. The melt fraction can be determined through simultaneous thermal analysis(STA), where the mass change and temperature of the sample and a reference is recorded simultaneous during constant heating[27]. To model the deposition of high temperature ash from fuel combustion it is common to use models based on particle viscosity. The models assume that particles above a critical temperature can deposit. The critical viscosity is calculated based on composition and temperature[28]. Once the particle is above the critical temperature it can be described as a Newtonian fluid. The critical viscosity is the temperature where the viscosity critically changes and this is believed to be at the point where the solid phase start to crystallize from the melt[29].

Agglomeration in bed fluidized bed reactors may take place through two separate mechanisms. Coating induced agglomeration is when ash deposits on a particle, then there is a reaction to form

a liquid phase which binds the particles together. The other mechanism involved ash melting prior to deposition and work as a form of glue between the particles. This mechanism is also known as melt induced agglomeration[30]. Kleinhans et al.[27] have described several more mechanisms for the deposition of ash particles on walls. The mechanisms like the previously mentioned are reaction of a particle, adherence to a sticky surface and condensation on a particle. The differing mechanisms are capture in a porous layer, reducing conditions leading to burning of char particles and sintering of particles. The sintering of ash particles have been observed to happen between 900-1200°C by Gupta et al.[31]. What is important to keep in mind is that the chemical composition will dictate the sintering and melting behaviour heavily. Where Raask et al.[32] found that the sintering temperature was reduced for iron-rich slags.

2.4.1 Fouling in Silicon industry

The problem of fouling is not a recent problem this has been a problem for decades. A study was conducted back in 1993 by Sintef[33] where the composition of the fouling of a ferrosilicon plant was concluded to be both silica fume and fines from the raw material. The fines from raw material were not limited to the off gas, fines of carbon particles would end up affecting the quality of Microsilica. The fouling was also determined to sinter and create melt phases. The problem of sintering of silica fume was very apparent at temperatures above 1000°C. Fines from iron sources would make the resulting deposit very hard. An increase in the velocity of the off gas was found to increase the amount of fines in the off gas. One key thing to note was that it was determined that the problem of fouling could be attributed to the control of the maximum temperatures of the off gas and not the mean process temperature. The resulting conclusion to reduce the problem involved reducing fines in raw material, reduce gas velocity, good process control, off gas design and cooling of the off gas walls. What is worth noting is that this report is quite old and the general process of silicon and ferrosilicon furnaces has been optimised many times since.

2.4.2 Fusion temperature

The fusion temperatures can be found through a test used to study the melting behaviour of ash. The test is done under controlled conditions while observing the change of the ash. The fusion temperatures are divided into four different temperatures, the initial deformation temperature(IDT), the softening temperature(ST), hemispherical temperature(HT) and finally the flow temperature(FT)[34]. There are several standards for the preparation of samples and the characteristic temperatures. When ash fusibility is tested for samples from biomass the characteristic temperatures are different, because the samples appear to be shrinking IDT is replaced with shrinkage starting temperature(SST) and the next step is deformation temperature(DT) while the rest remain the same[27]. The applicability of the test has been questioned, because the heterogeneity of the ash strongly affects the melting temperatures. For example, if the sample contains quartz grains it can lead to a strong compound structure which results in high ash fusion temperatures[27]. The ash particles could be molten, but the quartz particles would lead to no structure change. The test can be done in either reducing or oxidising atmosphere, but reducing atmosphere is reported to reduce the softening temperature of approximately 50 degrees[27].

The coal industry has found a correlation between increased fouling tendencies with lower ash fusion temperature. This has led to aiming to keep the temperature 38°C below AFT for the off gas when exiting the coal burning furnaces[29]. The problem with this approach is that the AFT's vary greatly on the composition of the ash. When coals with higher volatile matter are used it has a tendency of reducing the AFT which leads to increased fouling. Organic compounds and some minerals combine to form these volatile compounds that produces gases when heated[29]. Higher combustibility is also an effect of increased volatile matter in coals.

The softening temperature has a correlation with the type of deposit and how easily removable it is from heat transfer surfaces. Particles that are below softening temperature when hitting a heat adsorbing surface will not form bonded structures. This results in a type of fouling which can easily be removed from the surface. The problem arises when the ash particles are above the softening temperature and been plastic or liquid the resulting deposit will then have a tighter bond and is also harder to remove[29]. How large the difference in IDT and FT is will affect the fouling since a small difference is indicative of a tenacious slag that is difficult to remove, but a large temperature difference indicates a less adhesive deposit[29].

The ash fusion temperatures are affected by some species. For instance, acidic species like SiO_2, Al_2O_3 and TiO_2 will generally produce high melting point ashes. Basic oxides like Fe_2O_3, CaO, MgO, Na_2O and K_2O will in turn lower the melting point[29].

2.4.3 Predicting Ash Fusion temperature

The issues of fouling for coal plants have led to the creation of multiple models to predict the ash fusion temperatures. Some of the models are solely based on the composition, these models can potentially aid in the prediction of ash fusion temperatures in the silicon industry. The composition of anything that travels through the off gas is expected to differ greatly in terms of composition to the coal plants, because coal plants usually have a much higher amount of volatile matter and less silica. Hopefully the models can be extrapolated to a composition much higher in silica and a lot fewer oxides.

Yu et al[35] have made two models that predict the softening temperature for wood-based and herbaceous(no-wood stem) based fuel. The model utilizes a linear correlation coefficient for the prediction. The wood-based biomass model has a correlation coefficient of 0.908 and square deviation of 82.7°C. The herbaceous biomass model has a correlation coefficient of 0.860 and a mean square deviation of 82.7°C. The models were tested and fitted for silica content below 43%[35]. Holubcik et al.[36] have used multiple linear regression to find the correlation between biomass and softening temperature. This model had a correlation coefficient that was 0.937 and a standard deviation of melting temperatures below 60°C. This model has been tested on a higher silica content(64%) making it likely to be more applicable. Suzhen et al.[37] made a regression model with a average deviation of 5.77% and a maximum deviation of 20.58%. This model was then compared to a back-propagation neural network model which is a very complex model. The need for such complex models are because the relation between AFT and composition is complex[37]. The last model that will be tested in this thesis is made by Yin et al.[38] which is apparently the most used regression formula for predicting softening temperature in China. This model was designed to be utilized for silica content above 60% making it potentially the best

suited for this thesis. The model had a fractional error maximum and average of 0.37834 and 0.07180 respectively[38].

3 Experimental

The goal of this thesis is to investigate the composition, structure and softening temperature of the fouling in industrial silicon and ferrosilicon chimneys. Some of the experimental work for Furnace 1 was reported in the specialisation project with the same name. This includes sample preparation, electron probe micro analyzer(EPMA) and inductively coupled plasma mass spectrometry(ICP-MS). X-ray powder diffraction(XRD) and softening temperature analysis has been redone with the same samples, but with a different experimental procedure. The experimental work conducted throughout the thesis will be presented in this chapter. The experimental work will be described in detail from preparation of raw material through the various steps required to prepare the samples for the experiments. The equipment and settings for the equipment used throughout sample preparation will be described and presented. The different analysis methods conducted and its respective settings during the experiments will be presented. An overview of the process from raw material to the different analysis methods is shown in Figure 9.
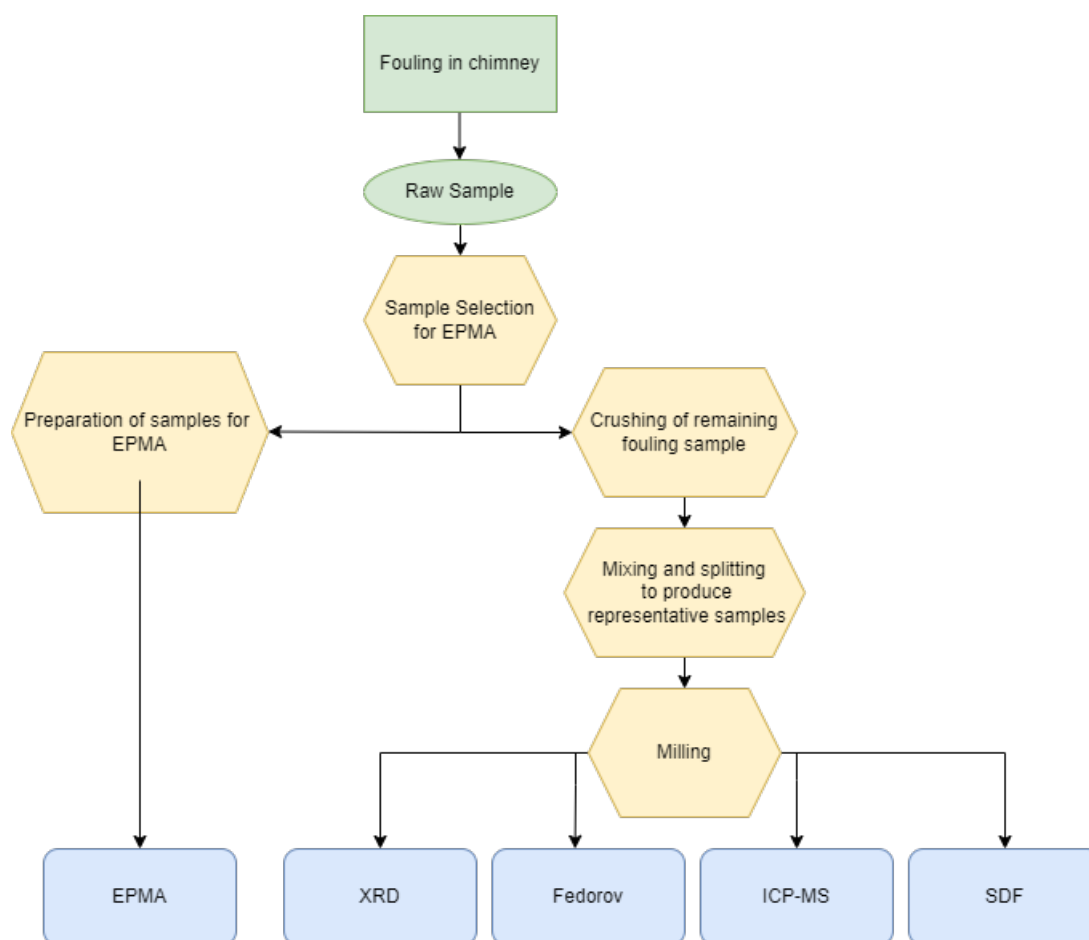
Figure 9: Flowchart representing the preparation of the samples for the different analysis methods. The blue squares are the different analysis methods, while the yellow hexagons are the sample preparation methods.

3.1 Raw Material

The material used in this thesis were sampled from three different furnaces, where two produces metallurgical silicon and the third produces ferrosilicon courtesy of Elkem. The samples were collected a bit further up from the semi-open hood covering the furnace body. One of the furnaces also had samples further up in the chimney. The samples varied a lot in appearance and hardness between the respective furnaces. The furnaces will be referred to as Furnace 1, Furnace 2 and Furnace 3, where Furnace 3 is the ferrosilicon furnace. Furnace 1 and 2 both have a system for energy recovery while Furnace 3 does not. Figure 10 shows the material from Furnace 1 prior to any sample preparation. The fouling samples are very non-heterogeneous. The material varies from being very porous and falls apart when touched, while other parts are hard enough that it required a hammer to disassemble.
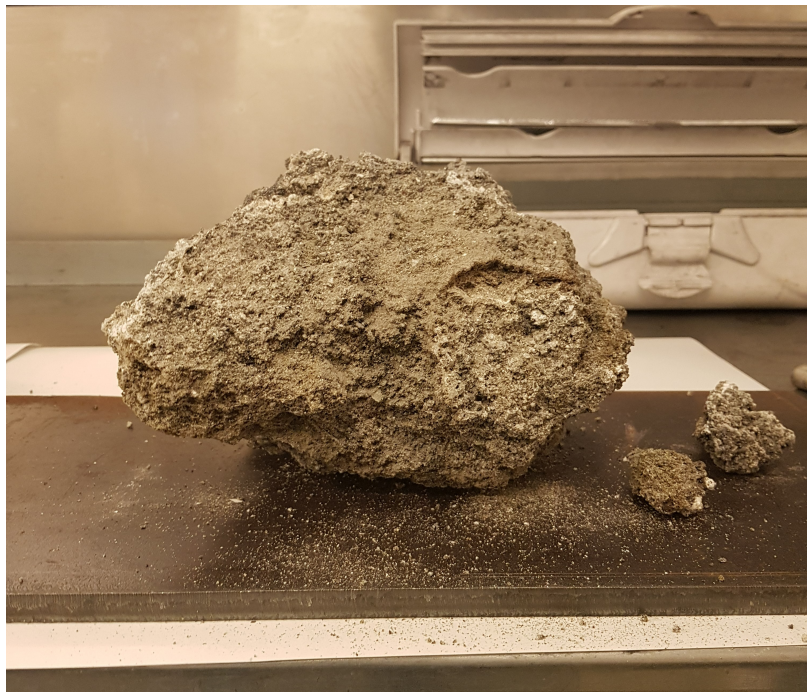
Figure 10: Raw sample from Furnace 1 prior to sample preparation

The material from Furnace 2 was excavated from five different locations where two where close to the furnace and the three other higher up. The samples were also from two different pipes where there had been a difference in temperature. One of the pipes had increased in temperature in the days prior to sampling in comparison to normal temperature. This pipe will be referred to as the high temperature pipe. The samples taken from this pipe can be seen in Figure 11. While the other pipe sampled from had been below normal temperature prior to sampling. These samples can be seen in Figure 12. The samples from Furnace 3 can be seen in Figure 13. This sample was by far the most compact and hard of the samples. The sample is also very different in terms of colour.

Figure 11: Raw sample from Furnace 2 all three samples are from the hot pipe where only the top right sample is closest to the furnace.

Figure 12: Raw sample from Furnace 2 both samples are from the colder pipe where the right sample is closest to the furnace.

Figure 13: Raw sample from Furnace 3 prior to preparation.

3.2 Sample preparation

Sampling from the various raw material is quite important considering the large amount of material each sample consists of. Especially considering how small each sample for SEM analysis needs to be. The samples for SEM analysis was selected based upon visual differences. As can be seen in the sample from Furnace 1 there is a difference in colour which is highlighted in Figure 14. These two phases were sampled from Furnace 1. For Furnace 2 the selection was somewhat the same where the difference in colour was selected in the samples excluding the ones that show a very flat surface indicating this is where the samples were attached to the wall. On these samples it was selected one sample from the flat surface to potentially show the composition that forms the fouling and another sample from the other side to the flat surface. The material from Furnace 3 was largely just black but with one phase that was lighter as well as some areas where it seemed like it had melted together. These differences were sampled for further inspection with EPMA.

The samples for inspection with EPMA was collected by the means of hammer and chisel for the most part, but some samples from Furnace 2 was so soft and brittle that it was possible to collect with a lot less force.
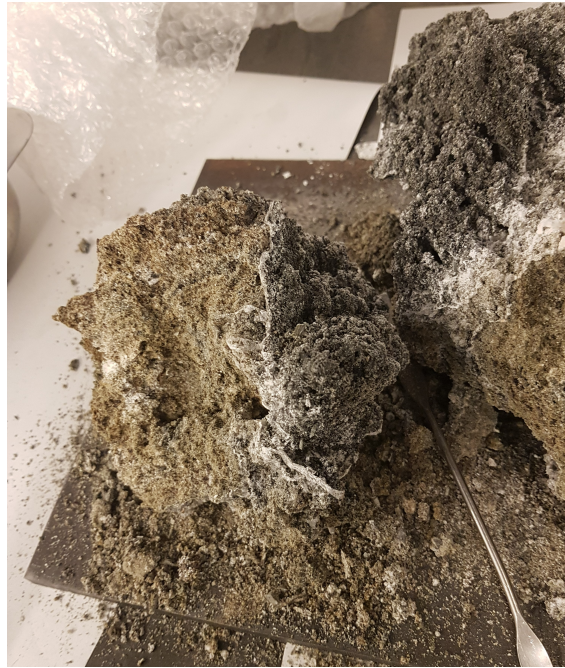
Figure 14: Raw sample during inspection showcasing two separate phases with difference in hardness.

The other analysis methods require samples that were crushed down to a size that makes them more homogeneous and representative off the whole mass. This was done through crushing, mixing, splitting and further milling of the samples. The sample was first split into samples that were large enough to produce enough sample material for all the analysis. The amount for each sample was kept somewhat the same where from Furnace 1 it was produced 9 samples. The same size was used for the latter Furnaces. The initial crushing was done in a pan as shown in Figure 15 to a size that would pass through a riffle splitter. The riffle splitter is a very simple device that essentially splits the material in half through channels going into two separate collecting bins. The splitter lowers the amount of bias for the selection of samples while also reducing the sample size. The splitting was done in such a way that the amount was kept above 75 grams to ensure there would be enough material for all the analysis. The material was transferred to the splitter as evenly as possible to reduce the bias of some channels receiving more matter than others. The resulting collection bins were then selected randomly through flipping a coin while the other bin was discarded.

When the material was split it was transferred to a steel mortar to be crushed further down while also being mixed. When the sample was of a reasonable size it was crushed down into a finer size fraction with a Retsch RS 200 disc milll for 30 seconds. The disk material was made of tungsten carbide. The final milling was to ensure a homogeneous sample as well as help mixing the sample. XRD analysis also required milling of the samples.

Figure 15: One of the samples after initial crushing.

The samples for SEM were cast in epoxy for SEM analysis and EPMA and then polished with the following procedure.

1. MD-Piano 220, with ethanol as lubricant, 250-300rpm, time was dependant on reaching the sample through the epoxy and having uniform lines in the sample

2. MD-Piano 800, with ethanol as lubricant, 250-300rpm, time was dependant on removing old lines and forming new uniform lines

3. MD-Piano 1200, with ethanol as lubricant, 250-300rpm, time same as previous step

4. MD-Piano 2000, with ethanol as lubricant, 250-300rpm, time same as previous step

5. MD-DAC, 3µm suspension, with DP yellow suspension, 250-300rpm, time was dependant on smoothness inspection.

6. MD-NAC, 1µm suspension, with DP yellow suspension, 250-300rpm, time was dependant on smoothness inspection.

The sample was later carbon coated because the sample was not leading electricity leading to bad conditions for good SEM pictures.

3.3   Characterisation

3.3.1   Electron Probe Microanalysis(EPMA)

The prepared samples cast in epoxy was then analysed by electron probe microanalysis(EPMA). This analysis was carried out by Senior Engineer Morten Peder Raanes(NTNU) using a JXA-8500F Field Emission Electron Probe Microanalyzer at NTNU, Trondheim. The different phases in the samples was showcased by utilizing a backscatter detector. Wavelength Dispersive X-ray spectrometer(WDS) was mainly used for the elemental analysis of the samples, but because of the degree of inhomogeneous phases in the samples from Furnace 3 some of these were also characterised through Energy Dispersive X-ray spectroscopy(EDS) over a larger area. A 15 kv acceleration voltage with 14nA beam current was used in the analysis. All the elemental analysis was carried out at a magnification of 150x. X-ray mapping was also utilized on samples where the phases appeared to be some degree of inhomogeneous.

3.3.2   X-ray Powder Diffraction(XRD)

The samples were also characterised by X-ray powder diffraction. Initially the results were expected to be amorphous which is also why the powder was spiked with alumina to quantify the amount of amorphous material. The samples were measured using a Davinci1 diffractometer with CuK_α radiation. The sample was scanned between 10-80°with a variable divergence slit(V6). The parallels had a acquisition time of two hours and a step size of 0.013°.

The presence of amorphous material makes the quantification of phases more complicated due to the lack of crystallinity and long range order. A method to quantify the amount of amorphous phase is using the internal standard method. This method is described in detail in Madsen et al.[39]. This method of analysis relies on the fact that all crystalline phases have been included in the analysis. The method requires an exact amount of crystalline material to be added, also called a spike. This spike allows for the calculation of the other crystal phases as well as the amount of amorphous material. This method is the most common way for quantitative phase analysis while using the Rietveld method according to Madsen et al.[39]. The spike must have a similar mass absorption coefficient as the sample to minimize micro absorption.

The crystalline standard(spike) used was corundum, Al_2O_3 $\alpha - phase$ with a purity of 99,9%. Both the samples and the spike was dried overnight in a furnace at 200°C. Then the samples were sealed to prevent any humidity in the samples before weighing. Roughly 1.8-2.0 grams of sample was mixed with 0.5-0.6 grams of spike(Al_2O_3). The weights were recorded with an accuracy of 4 digits for later calculations. All nine samples from Furnace 1 was quantified, in total fourteen samples from Furnace 2 was quantified while four representative samples was quantified from Furnace 3. The two powders were mixed in a mortar while using a pestle to make the powder as homogeneous as possible. The mixed powder was then placed in a capton holder to be quantified with XRD.

The initial identification of crystalline phases were done in EVA[40] and the parameters from each phase was fetched from International Centre for Diffraction Data(ICDD) PDF-4+ database. The quantification of the crystalline phases was done through TOPAS V5 software[9]. The exact

amount of spike was used in the program, then the program used this to calculate the exact amount of each phase after the peaks have been fitted. To make sure the refinement was run with the exact same parameters for all the samples a standard file with selected settings was utilized. Unit cell parameters and sample displacement was refined for each sample to make the calculated curve best as possible.

3.3.3 Inductive Coupled Plasma Mass Spectrometry (ICP-MS)

To quantify the chemical composition of the samples Inductive Coupled Plasma Mass Spectrometry was performed on nine samples from Furnace 1, five samples from Furnace 2 and three from Furnace 3. The analysis was performed by ALS scandinavia where the concentration of 70 different elements was measured with high precision even at low concentration. ICP-MS allows for the quantification of most elements, but it does not allow for the quantification of carbon which is unfortunate since it is of interest for this thesis.

3.3.4 Sessile Drop Furnace(SDF)

A wetting furnace or Sessile Drop Furnace(SDF) was used to find the softening point of five samples and Microsilica as a reference. The SDF was first ran to find the melting point of iron in reducing atmosphere(CO). This is a test designed to check the thermocouple and if the eventual softening temperatures have to be adjusted. This is done by comparing the observed melting temperature of iron to the theoretical melting temperature($\Delta T = T_{theoretical} - T_{observed}$). This is then used to adjust the softening temperature of the samples by $T_{ST} = T_{observed} + \Delta T$. The softening temperature was measured three times for each sample. Six samples were conducted experiments on. Two samples from both Furnace 1 and Furnace 3 were tested, but only one sample from Furnace 2 this was because Furnace 2 had a much higher purity and was therefor expected to have a higher softening temperature.

The experiments for softening temperature were performed in accordance to international standard ISO 540:2008(E). The powder was initially tested for its size by using a sieve with size $75\mu m$. The particle size was ensured to be below this. Any particles too large would be crushed in a mortar then sieved again. Dextrin was mixed into a 100g/L solution by mixing 5 grams into 50 ml of destilled water. This solution was then used to mix into the powder making a paste. The amount of solution used was kept at a minimum, because the paste would become very sticky if too much solution was used. The paste was then put into a cylinder with 5 mm diameter. The ideal size of the cylinder is a cylinder with height equal to the diameter according to ISO 540:2008(E). When the paste had been applied to the cylinder it was pressed together from both ends. The amount of paste needed for making a cylinder with height equal to diameter was found through trial and error. This pressed powder cylinder was then placed on a aluminium substrate. The substrate was placed in the chamber of the furnace which is designed to allow for rapid heating and cooling. The sample is observed by a digital camera taking a high resolution image every second. The determination of the softening point was done in accordance to the ISO 540:2008(E) standard.

The chamber was first evacuated for all air before being filled with CO gas. The experiments were performed in a reducing atmosphere with 0.1 L/min CO gas flushing the chamber. The furnace was heated to 900°C over 3 minutes. The furnace was held at 900°C for 5 minutes to
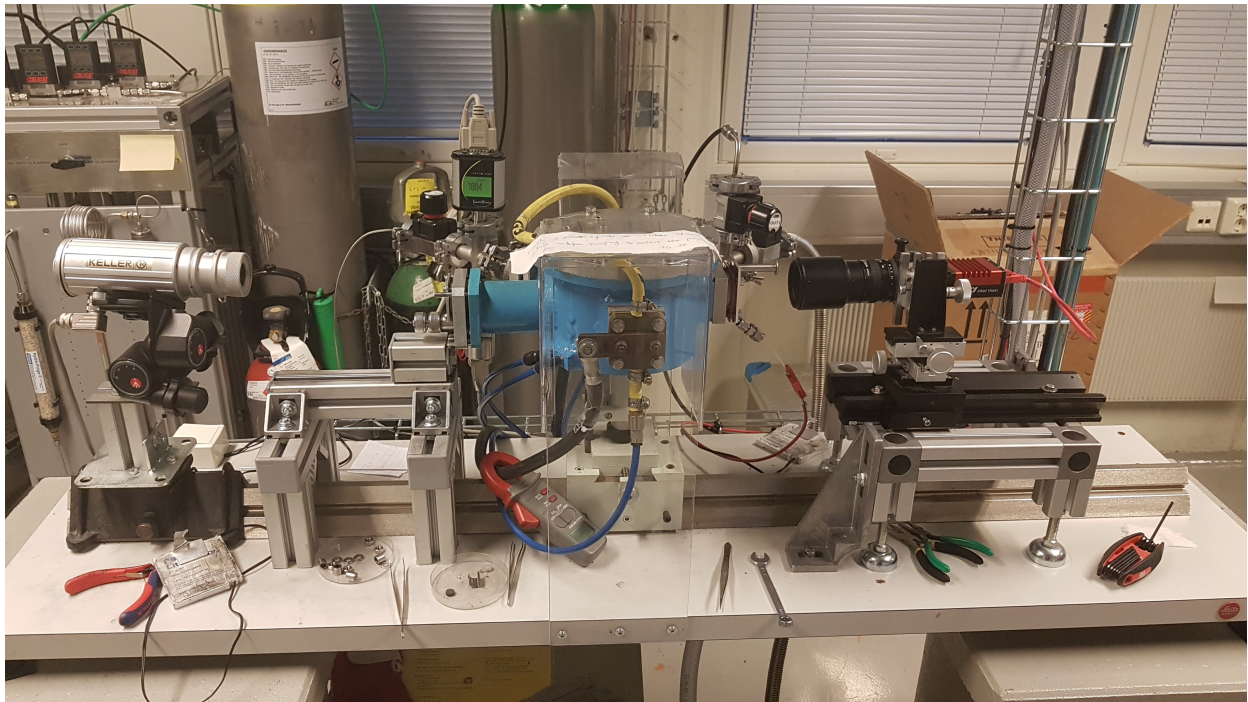
Figure 16: The sessile drop furnace, pyrometer to the left of the blue chamber, camera to the right of the chamber and thermocouple connected through the right side of the chamber.

remove organic matter and the dextrin used to create the shape of the cylinder. The furnace was then further heated at a rate of 50°C/min to 1400°C. Then the rate was adjusted down to a rate of 10°C/min up until 1800°C. The experimental setup is shown in Figure 16. The image shows both the blue chamber as well as the thermocouple which is connected at the bottom right side of the chamber. The image also shows the camera on the right side and the pyrometer on the left. The pyrometer is used as a reference to ensure correct result from the thermocouple. The sample and substrate is inserted from the left side of the blue chamber.

3.3.5 Fedorov analysis

A Fedorov analysis was performed by Elkem Technology Lab on four different samples. The fedorov analysis quantifies the amount of metallic silicon in the samples, but the method cannot remove Fe2+ so any will affect the amount of silicon metal measured. The amount of Fe in the sample is also quantified in the analysis. The samples weighed a minimum of 20 grams each.

4 Results

This section will present the results from the experiments throughout the thesis as well as some of the result done in the specialisation project with the same name. Some of the results from the specialisation project are used for the purpose of comparing the three furnaces. The results that were reused or repurposed is the EPMA and ICP-MS result from Furnace 1.

4.1 XRD

4.1.1 Furnace 1

The resulting XRD plots from Furnace 1 show reoccurring peaks for all the nine samples that were screened in the specialisation project. Through characterization with Diffrac Eva 5.0[40] four phases of SiO_2 were identified, cristobalite, quartz, tridymite and silicon carbide. From Figure 17 the different peaks can be seen for sample 5 most of the peaks are labelled. The remaining XRD plots have been put in Appendix A. The sharp peaks from furnace 1 indicates very crystalline samples. This is in contrary to the expectation of amorphous silica being the main component of the fouling. The relative amount of amorphous material has been quantified which will be compared with the other furnaces later. The main peaks are labelled to the different phases, but some of the remaining small peaks were not. This is because of the overlapping location for expected peaks of the different phases making it hard to distinguish them.
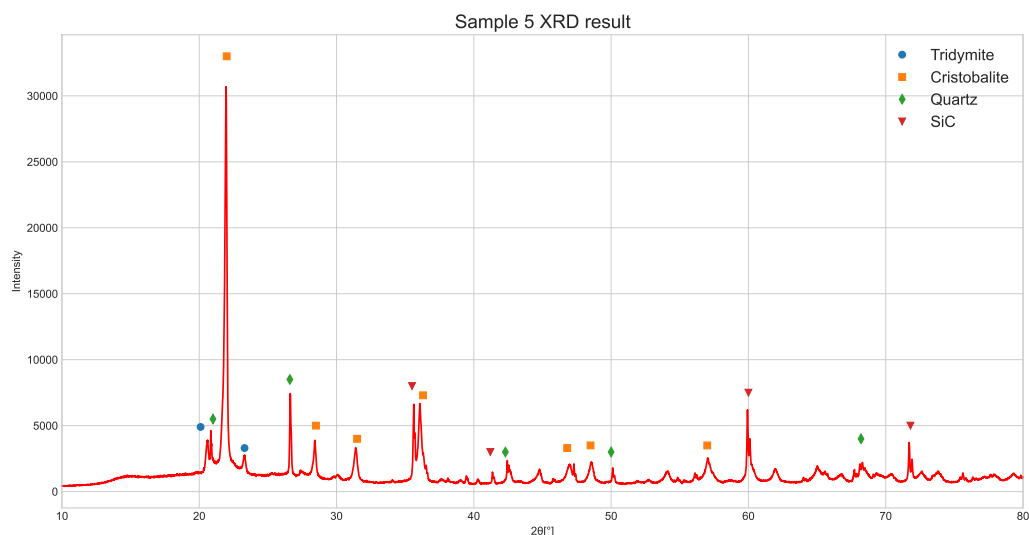
Figure 17: XRD for sample 5 from Furnace 1 with marked peaks.

4.1.2 Furnace 2

Fourteen samples in total from Furnace 2 was quantified and fitted. Three crystalline phases were identified and quantified namely cristobalite, quartz and silicon carbide. The XRD plots from all the samples are more or less the same which is why one have been presented in Figure 18 while the remaining plots can be found in Appendix A. This means the crystalline phases does not vary a lot based on where it is sampled. The peaks are sharp for Furnace 2 as well. Which again indicates a very crystalline sample. The main thing to notice here is the lack of tridymite in comparison to Furnace 1 and the sharp peaks. The main peaks of Figure 18 have been labelled with the according phase, but the smaller peaks remaining all belong to cristobalite and is therefore not labelled.
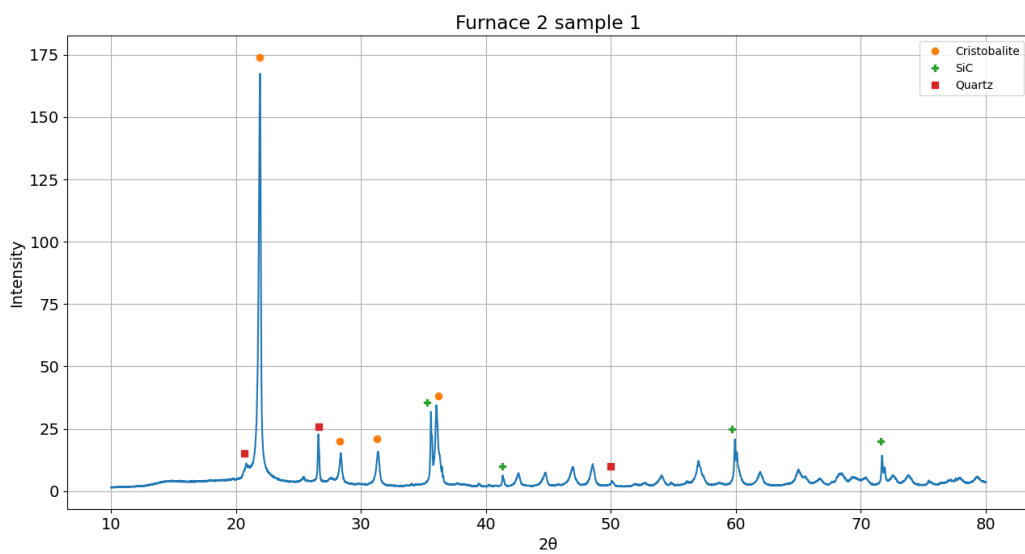
Figure 18: XRD for sample 1 from Furnace 2 with marked peaks.

4.1.3 Furnace 3

The difference between Furnace 3 and the previous furnaces is quite apparent from looking at Figure 19. The sample is showing clear signs of more amorphous phase with the elevated baseline as well as a lot more peaks scattered all over. The phases identified were like those of Furnace 1 but with the addition of Magnetite. Keep in mind this is the only ferrosilicon furnace sampled from. The remaining XRD plots can be found in Appendix A. The quantification of phases from furnace 3 proved to be quite difficult in comparison to Furnace 1 and 2, but the sharp peaks indicating the presence of crystalline phases for this furnace as well.
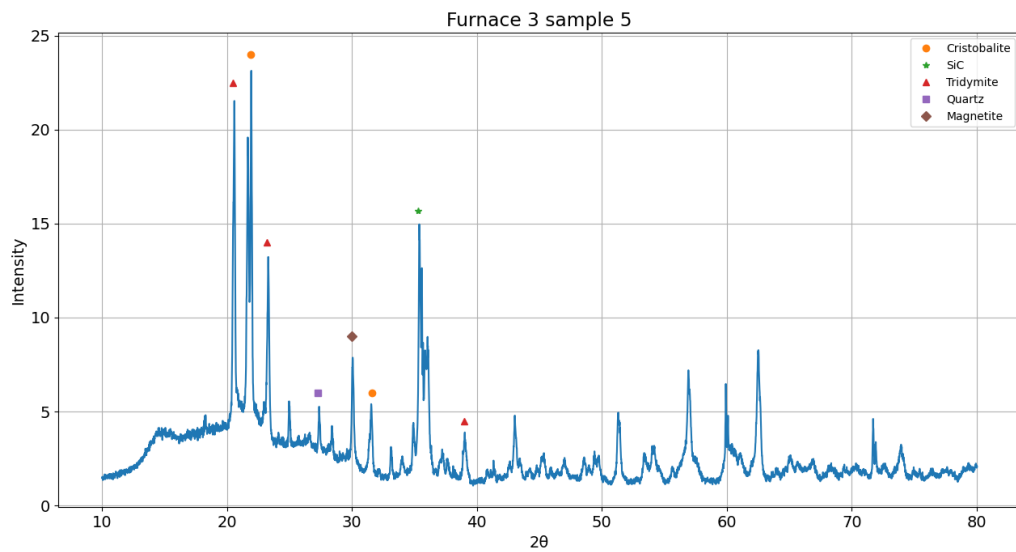
Figure 19: XRD for sample 5 from Furnace 2 with marked peaks.

4.1.4 Comparing crystalline phases

A comparison between the furnaces and the difference in crystalline phases for the Furnaces is shown in Figure 20, here the difference between sample position have been included for Furnace 2. This is the average composition of nine samples from Furnace 1, ten samples from Furnace 2 high, four samples from Furnace 2 low and six samples from Furnace 3. Here high refers to the samples taken way above the hood and the low sample from close to the hood. The error bars are overlapping in some areas but the bars have been broadened to make it easier to read. The main differences can easily be seen as cristobalite, tridymite and silicon carbide quantity from the figure. The furnaces had an amorphous amount ranging between 38% and 50%. The SiC amount spanned from 3.7% to 31%. The amount of quartz is quite low in amount(2.6-5.3%). The amount of quantified Magnetite is very low(0.55%) for Furnace 3.
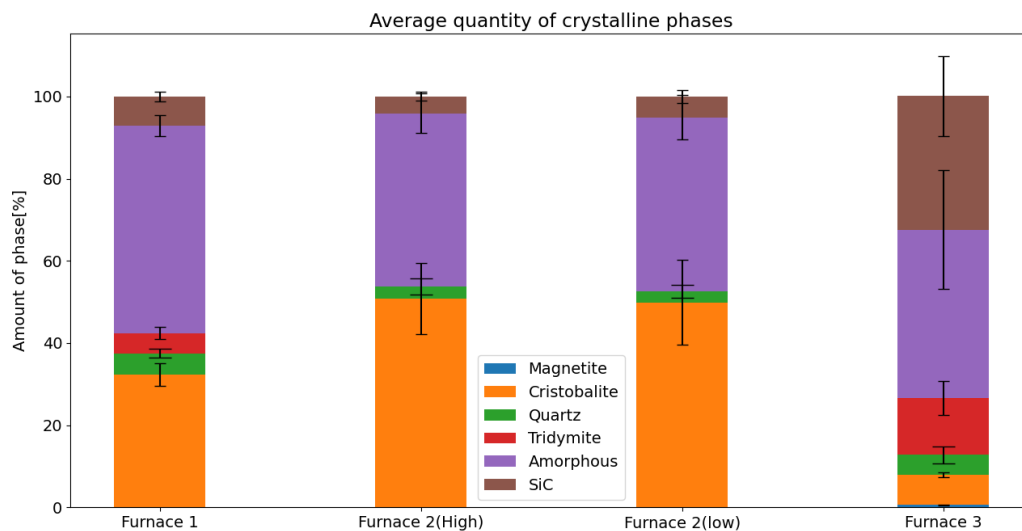
Figure 20: Comparison of average amorphous amount and the average crystalline phases between the furnaces.

4.2 EPMA

Starting off the selection of which samples were done had no bearing in the phases of the different furnaces. This has led to all the data from the different furnaces being represented without being distinguished by where the sample it was collected. This section will focus on combining the backscatter images with the results from WDS/EDS analysis to get a better understanding on how the fouling in the silicon industry is build-up. This section will also compare the differences between the compositions of the different furnaces. The difference between the composition will also be compared to the Microsilica composition taken from the same time period as the fouling. Some of the X-ray mapping showcasing the build-up of composition for the different furnaces will be presented. The result from Furnace 1 was done in the specialization project.

4.2.1 BSE images and WDS analysis Furnace 1

The result from Furnace 1 where the samples from a brown and a darker phase was taken, but no difference can be seen structurally or compositionally. The samples were quantified by the means of WDS where one was performed excluding oxygen and another including the oxides for each sample. In total four samples were quantified where five different phases were identified: silica, silicon carbide, a slag phase, silicon metal and ferrosilicon. The black part of the samples which is unlabelled is the epoxy.

The first BSE image from Furnace 1 can be seen in Figure 21. The white areas is a ferrosilicon phase while the lighter white is silicon metal phase with a 96/wt% purity on average. The silicon carbide, silicon metal and ferrosilicon have been analysed without the inclusion of oxygen. Areas with the silica phase has a very high purity of 99.5-100.3wt% and the slag phase has a very consistent composition. This image is a very representative example of how the composition is in the areas with metal phase. The average phases with standard deviations is shown in Table 2 and Table 3.

Table 2: The average silica and slag phase composition quantified by WDS plus the standard deviation for Furnace 1 in wt%.

Phase	SiO2	K2O	NaO2	MgO	CaO	FeO	Al2O3
Slag	77.7± 4.8	5.16± 0.88	0.623± 0.094	1.02± 0.625	4.94± 2.13	4.26± 1.54	5.63± 1.82
SiO2	100.2± 0.35	0.0618± 0.0229	0.0278± 0.0333	0.00356± 0.00386	0.0534± 0.0197	0.0961± 0.0478	0.128± 0.094

Table 3: The average Si, FeSi and SiC phase composition quantified by WDS plus the standard deviation for Furnace 1 in wt%.

Phase	Si	C	Fe
Si	95.06±1.25	2.151±0.888	0.2195±0.1930
FeSi	53.25±0.68	1.015±0.034	46.89±0.14
SiC	68.21±2.28	30.60±2.19	0.206±0.237
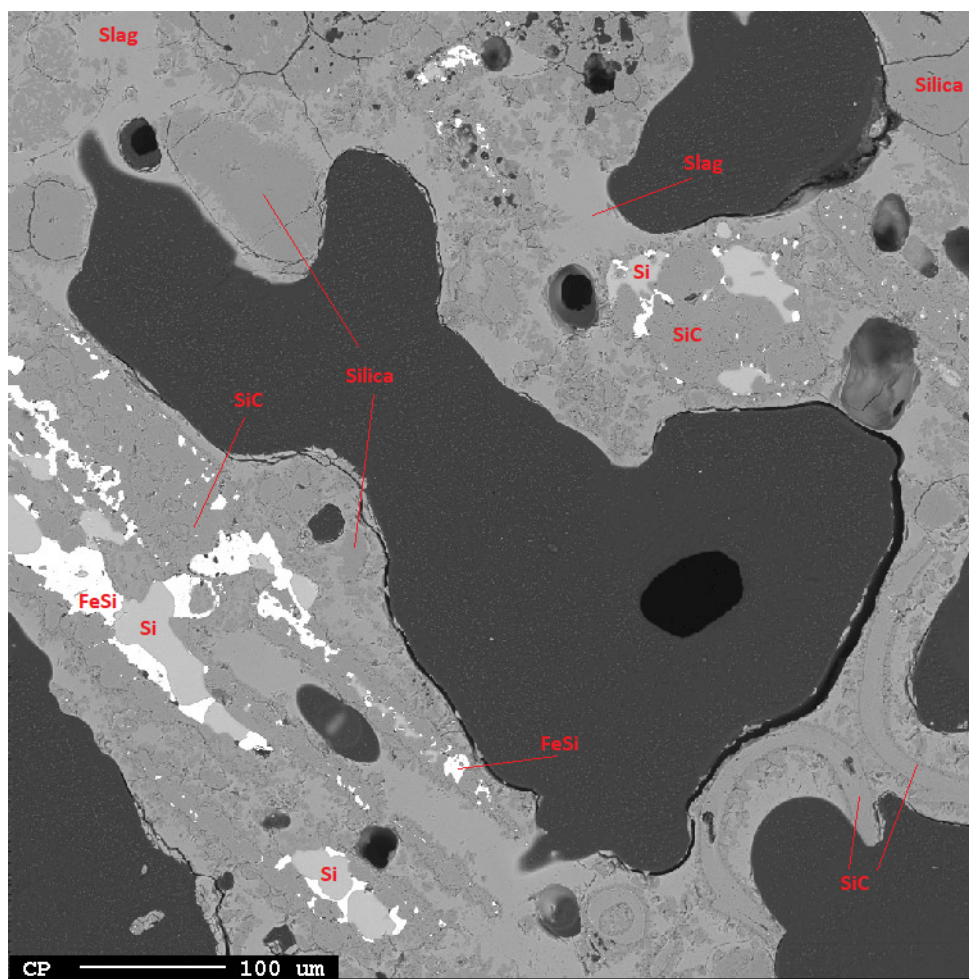
Figure 21: BSE-image of epoxy sample 1 with areas labelled.

In Figure 22 a selection of structures can be seen where the majority is silica phase then a slag phase in between the silica phase. As well as some metal phases and in the top right image at the bottom right typical brown condensate structure can be seen. The amount of metal phases in the samples are seemingly low. The top left image also shows a structure that is very typical for silicon carbide which was quantified to be silicon carbide.
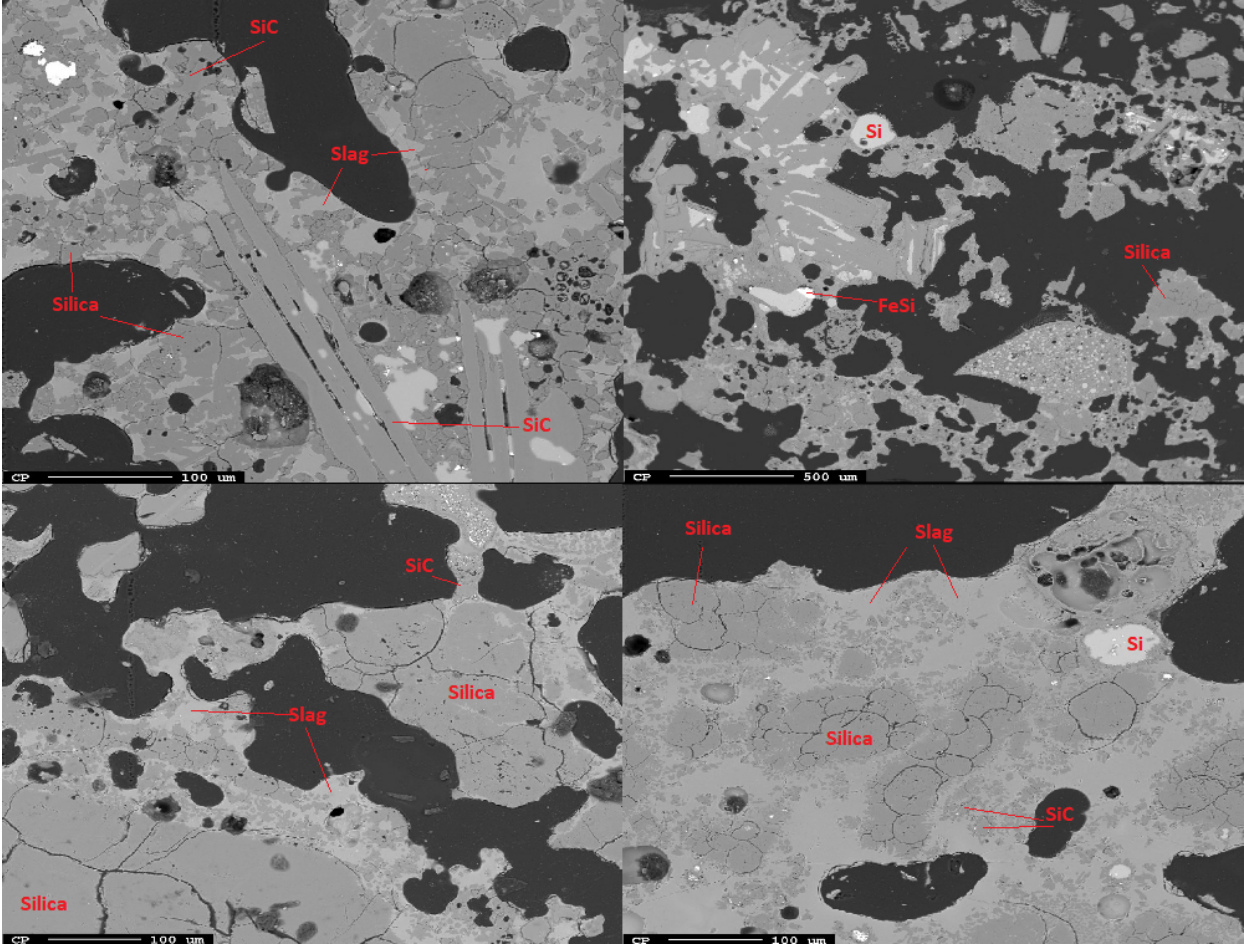
Figure 22: A selection of four BSE images from Furnace 1 to showcase typical structure of phases.

4.2.2 X-ray mapping Furnace 1

The samples cast in epoxy from Furnace 1 was also X-ray mapped. From Figure 23 it can be seen how the phases are not homogeneous, but they have a varying degree of trace elements throughout every phase. What can be seen is the slag phases encapsulates the silica phases in every instance of this figure. This slag phase is the same as were the content of Al, Ca, K, Mg and Fe lights up. There is also one instance of silicon metal on this scan. The area has a lot of cracks where the carbon content can be seen to be very high, but this is likely just epoxy.
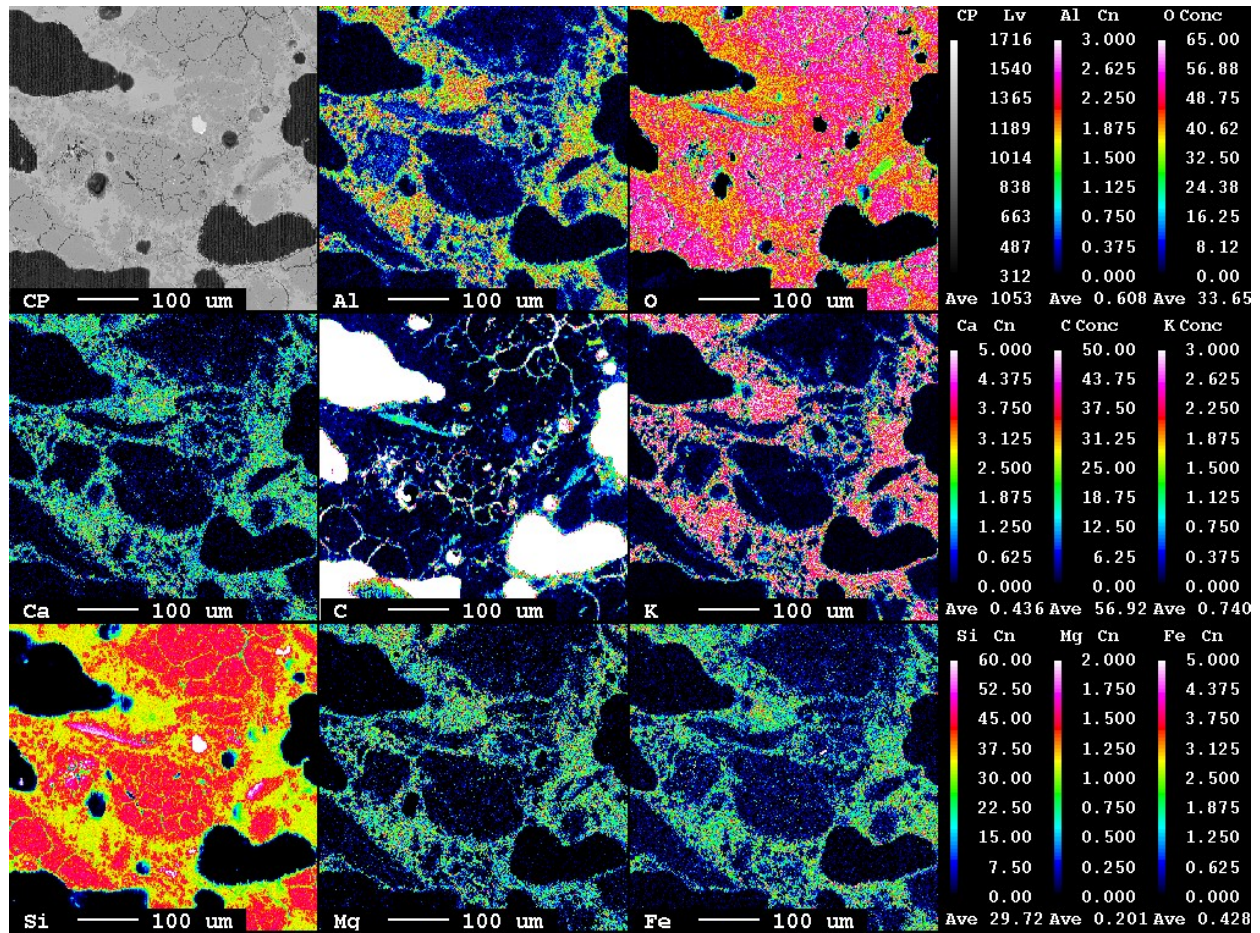
Figure 23: X-ray mapping of SEM sample from Furnace 1 the colour gradients on the right side are in wt%.

The tendency of the x-ray mappings of Furnace 1 are the same which can be seen in Figure 24. Where there is a slag phase encapsulating the silica phase. The amount of trace elements in the slag phase is varying across all the mappings. The silica phase is however relatively pure with a small amount deviating from silica and oxygen. Here the cracks are as well just filled with epoxy creating circular shapes.
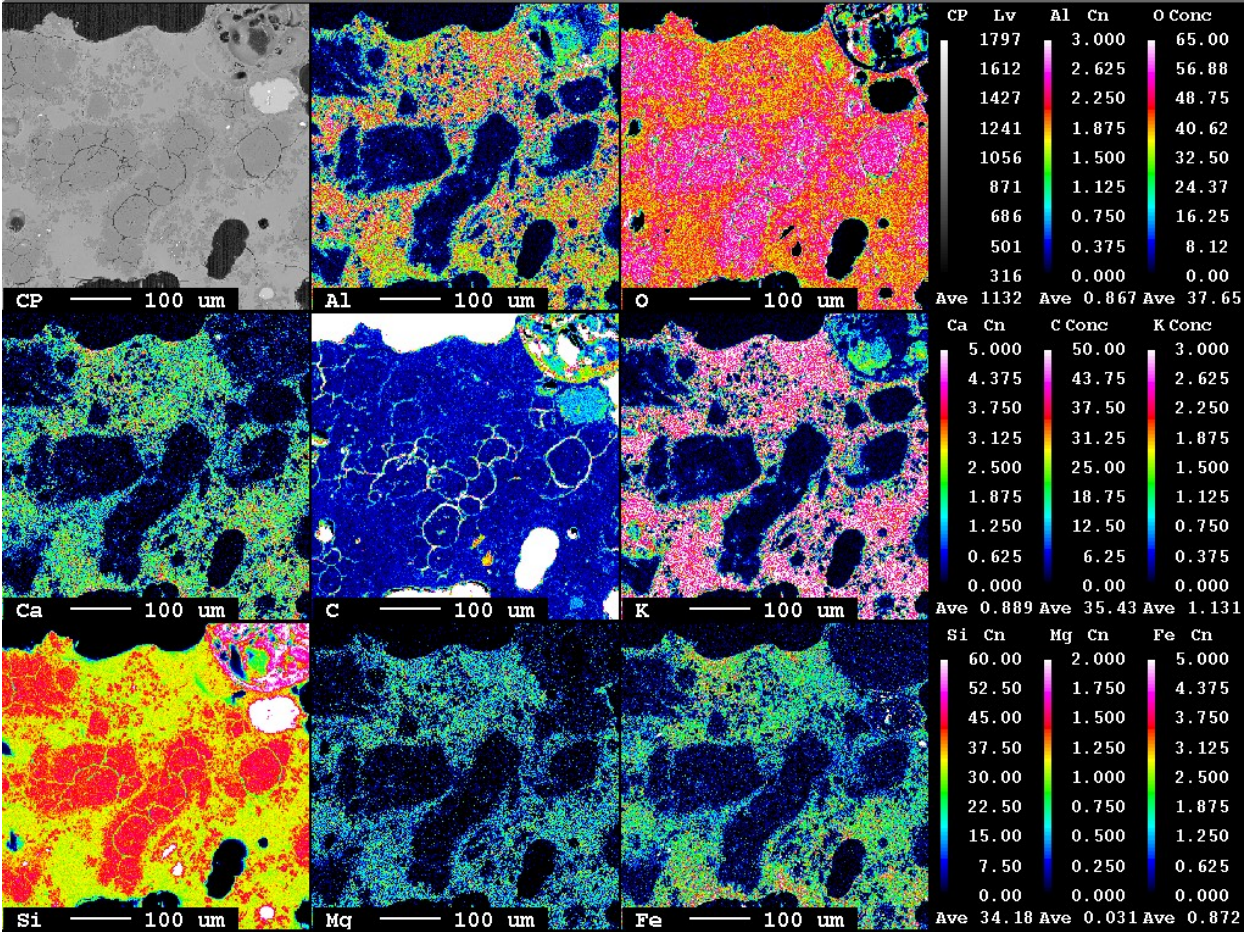
Figure 24: X-ray mapping of SEM sample from Furnace 1 the colour gradients on the right side are in wt%.

4.2.3 BSE images and WDS analysis Furnace 2

The samples from Furnace 2 were collected from differing positions where there was a variation in temperature and elevation. The BSE images from Furnace 2 gives a different impression on how it was build-up. The thing that is very apparent is the lack of slag phase. There were not a lot of instances of a slag phase over 10 samples. The slag phase is a lot smaller in size in comparison to Furnace 1. The samples were quantified by means of WDS where one was performed excluding oxygen and another including the oxides for each sample.

From Figure 25 the atypical structure can be seen for the Furnace 2 samples. Here the red 1 is marking the silica phase, silicon metal and silicon carbide. This was a common occurrence throughout the samples where silicon carbide would be encapsulating the silicon metal phase. The majority of the samples is the silica phase. What is also worth noting is the porosity that the samples of Furnace 2 seemed to be. There can be seen a very small amount of a slag phase in this figure, but it is too small to quantify accurately. The average composition of the phases can be seen in Table 4 and Table 5. What is missing here in the tables in comparison to Furnace 1 is the ferrosilicon in quantity, but that is mainly because the FeSi metal was too small to quantify accurately.

Table 4: The average silica and slag phase composition quantified by WDS plus standard deviation for Furnace 2 in wt%.

Phase	SiO2	K2O	NaO2	MgO	CaO	FeO	Al2O3
Slag	64.5± 1.03	3.15± 2.07	1.83± 0.652	2.39± 1.27	10.2± 7.51	11.7± 11.1	1.06± 1.30
SiO2	98.4± 1.07	0.043± 0.047	0.078± 0.075	0.070± 0.079	0.210± 0.190	0.0494± 0.0513	0.0226± 0.0178

Table 5: The average Si, FeSi and SiC phase composition quantified by WDS plus the standard deviation for Furnace 2 in wt%.

Phase	Si	C	Fe
Si	98.4±1.2	2.30±1.03	0.031±0.027
SiC	70.0±0.6	28.7±2.9	0.0168±0.0189
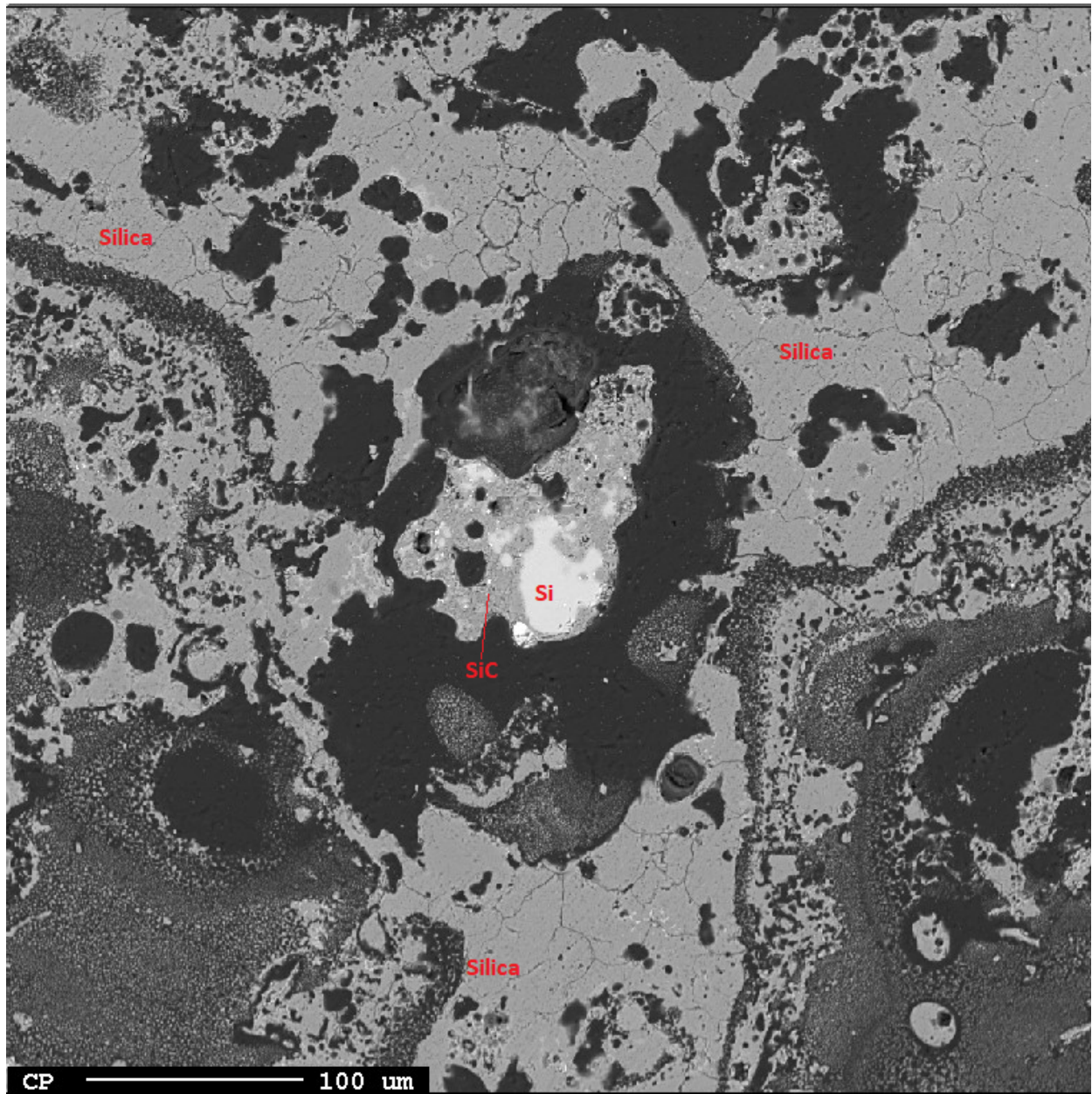
Figure 25: BSE-image of epoxy sample 4 from Furnace 2 with areas labelled.

The four images portrayed in Figure 26 is two images but the left one is with 200x zoom while the right is the same area with 40x zoom. What is clear from the image is the fact that the main phase of the samples is the silica phase. The image also showcases the very common theme of the samples in terms of porousness. The top right image also shows some silicon carbide structures. The bottom image has an some more metal phases and one instance where it forms a circular shape.
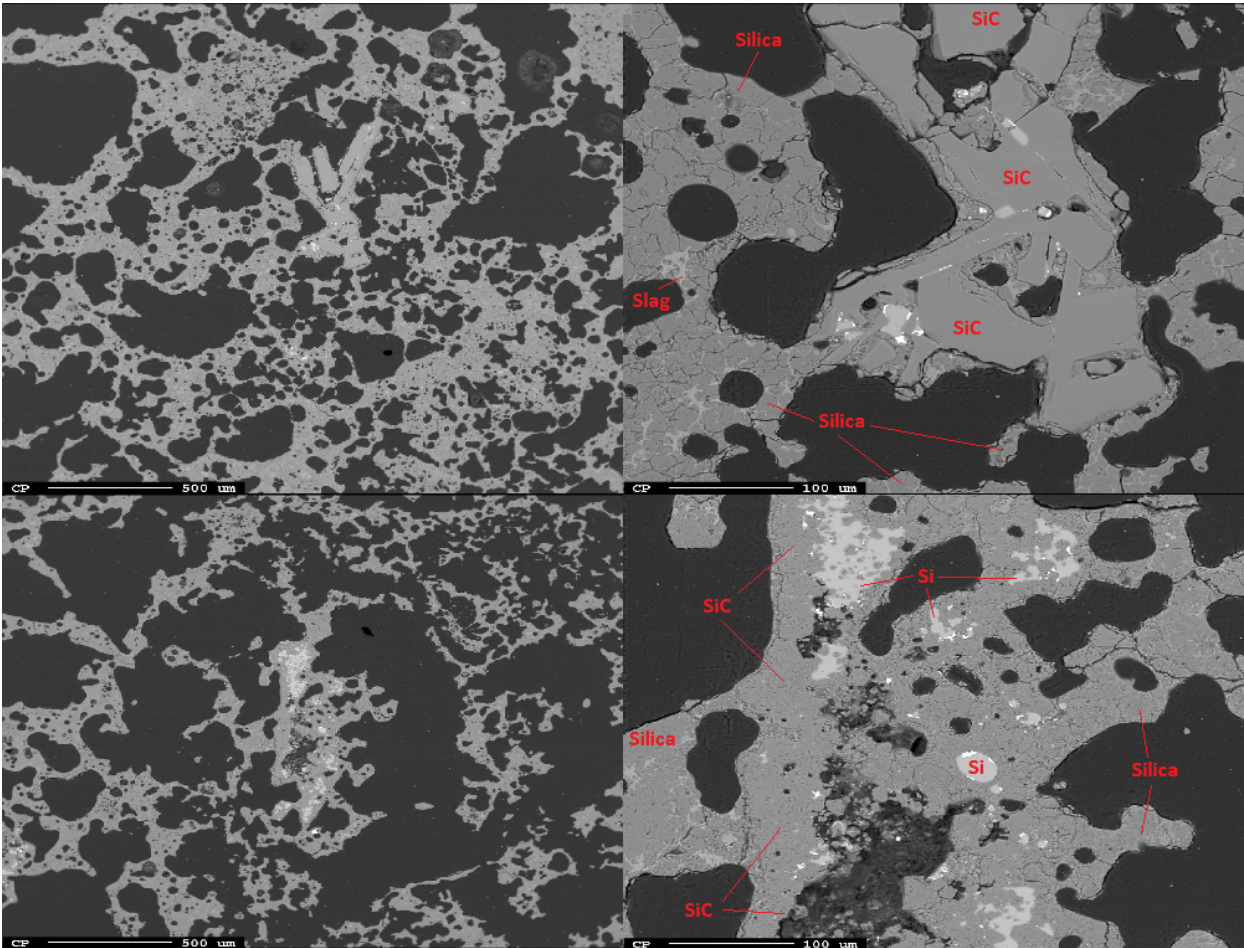
Figure 26: BSE-images from Furnace 2 where the top right pictures are zoomed in to showcase the metal phases of the left pictures.

4.2.4 X-ray mapping Furnace 2

The first image chosen to showcase for the X-ray mapping of Furnace 2 shows a very interesting structure where it seems like it has layered towards the top left corner. This can be seen in Figure 27. The amount of places that light up for the elements Al, Ca, K, Mg and Fe is quite low. The light is quite spread out and there does not seem to be any specific phase with higher content. What can be said is that Ca seems to be present throughout most of the sample with a smaller band forming in the bottom right. There seems to be bands forming of carbon in the middle. Carbon seems to be present throughout the whole sample. With a very high concentration by the red band which would be around 75%.

Figure 27: X-ray mapping of a part of a sample from Furnace 2 the colour gradients on the right side are in wt%.

The image chosen for here is the same as the bottom right picture of Figure 26. This can be seen in Figure 28. The lack of interesting structures was one of the reoccurring problems with the samples from Furnace 2. Therefore it has been x-ray mapped as well. What is quite interesting here is the location of the silicon carbide in comparison to the metallic silicon which can be seen in the bottom left. The fact that this is silicon carbide can be confirmed by viewing the oxygen concentration in the same area. Just like for the last mapping there is not a lot of other elements except some Ca, K and Al. These elements seem to be roughly distributed in the same areas, but the concentration is higher for Ca. The elements are spread out in the silica phase. The concentration increase does not involve a new slag like phase for the most part. A slag like phase is seen in the areas where Ca is white, but the areas are usually too small for accurate quantification.
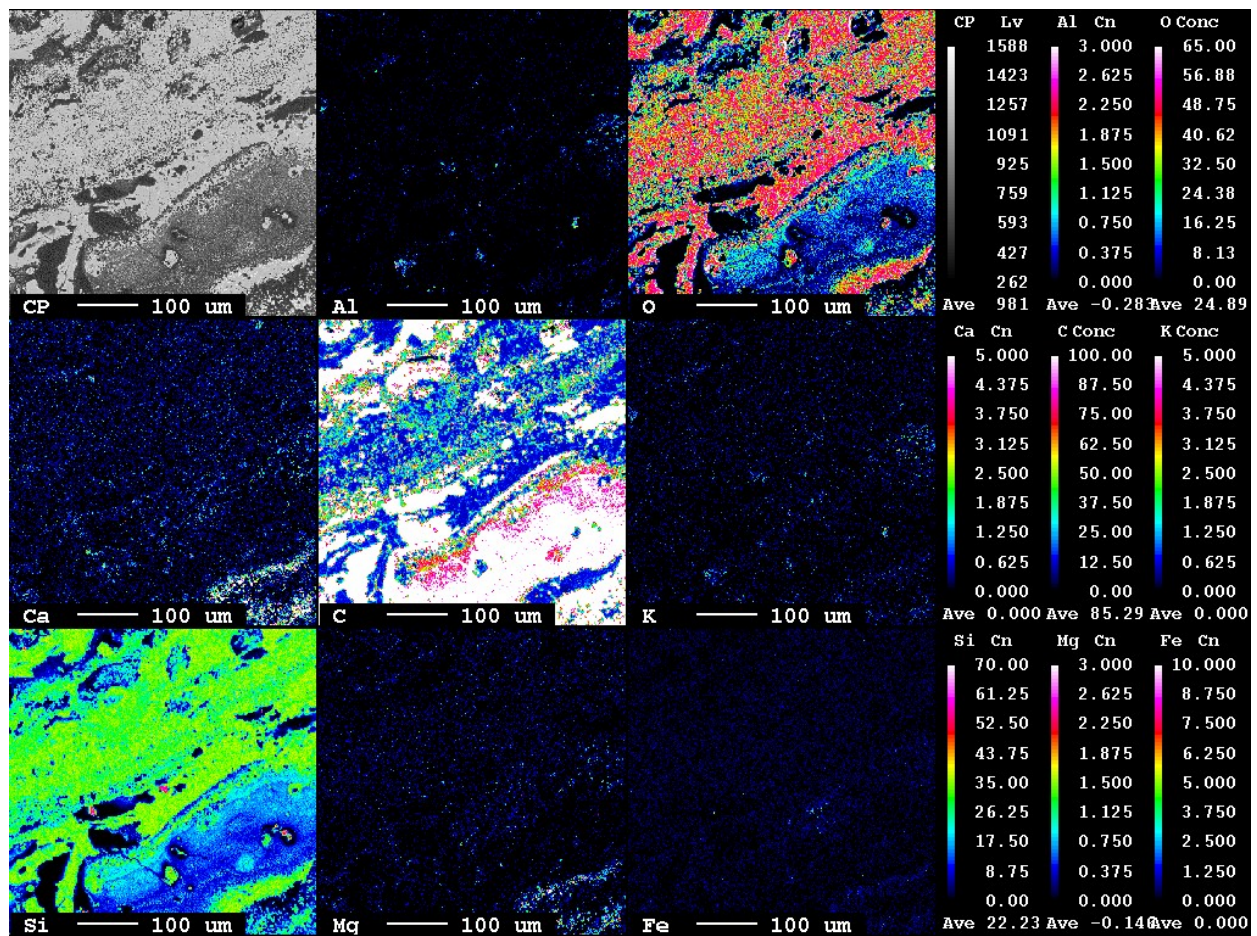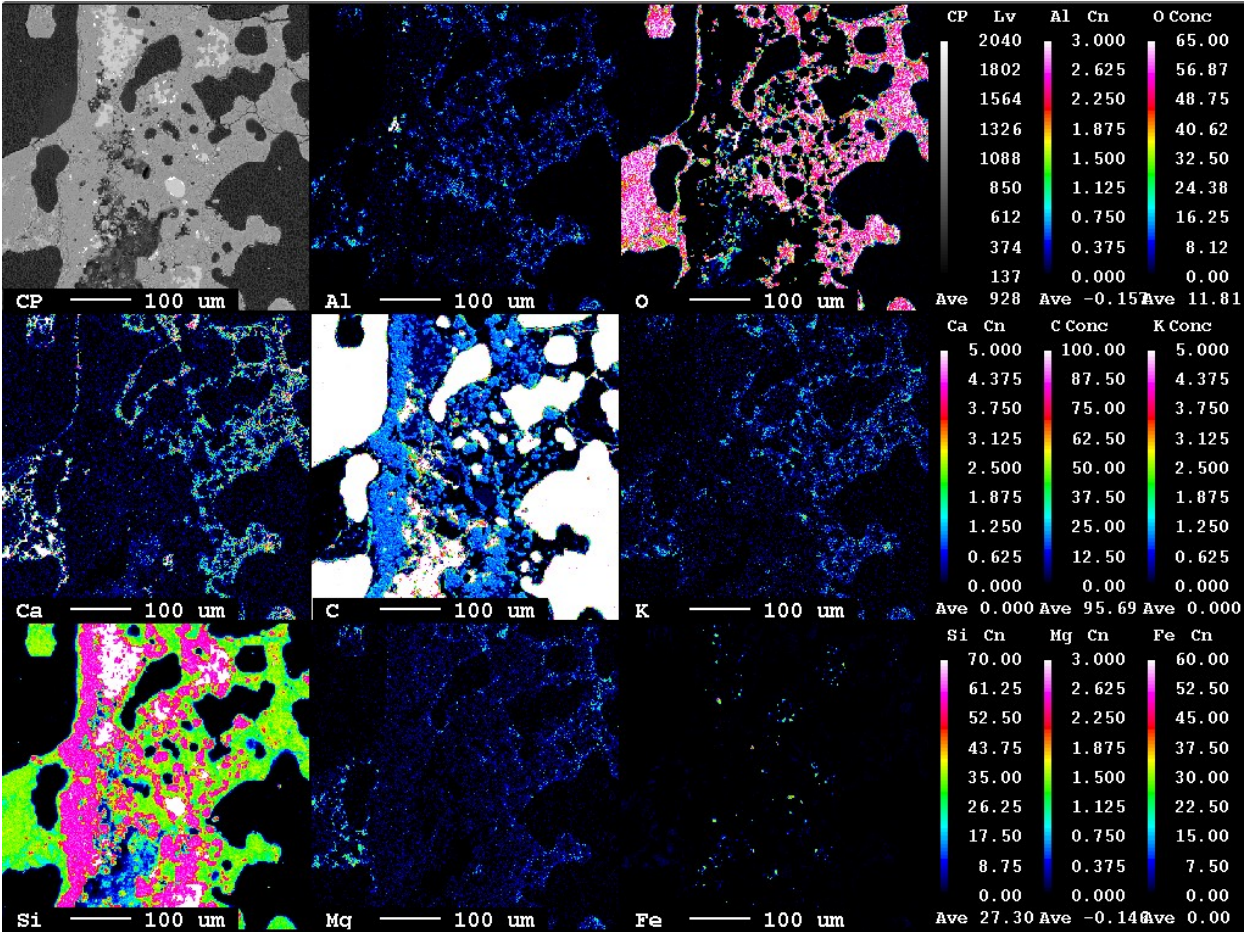

Figure 28: X-ray mapping of a part of sample from Furnace 2 the colour gradients on the right side are in wt%.

4.2.5 BSE images, EDS and WDS analysis Furnace 3

The samples from Furnace 3 showed the same trends throughout all the samples. The samples have a slag phase which is not very consistent in composition or colour. This can be seen in both Figure 29 and Figure 30. The grey slag phase is filled with a smaller lighter grey phase. The composition of the whole slag phase was quantified by means of both EDS over a larger area and WDS. Because of the variance of the slag, it has been done plenty of WDS analysis to get an average. The average of the slag phase, silica phase and FeSi metal can be seen in Table 6 and Table 7. The darker grey phase is the silica phase. A large portion of the metallic phases is ferrosilicon.

Table 6: The average silica and slag phase composition quantified by WDS and EDS plus standard deviation for Furnace 3 in wt%.

Phase	SiO2	K2O	NaO2	MgO	CaO	FeO	Al2O3
Slag	40.1± 11.8	1.30± 0.43	0.255± 0.106	1.35± 0.50	0.742± 0.254	53.0± 11.3	0.659± 0.538
SiO2	96.7± 2.8	0.117± 0.102	0.0479± 0.0285	0.0126± 0.0149	0.0433± 0.0576	0.636± 0.157	0.00277± 0.0201

Table 7: The average Si, FeSi and SiC phase composition quantified by WDS and EDS plus standard deviation for Furnace 3 in wt%.

Phase	Si	C	Fe
FeSi	23.2±9.7	0.842±0.281	74.2±16.1
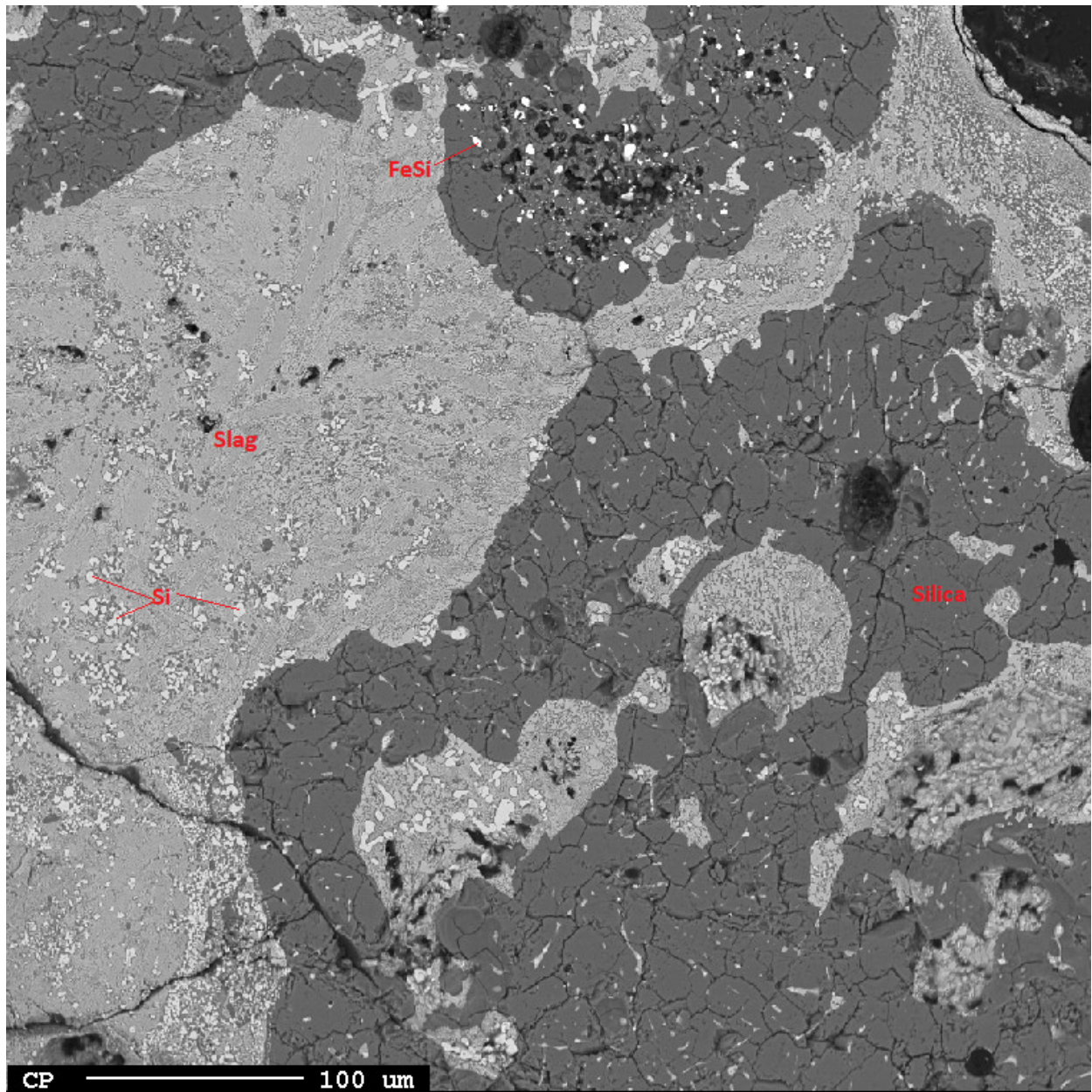
Figure 29: BSE-image from Furnace 3 where the slag phase is grey and silica phase darker grey. With some scattered small metal phases.
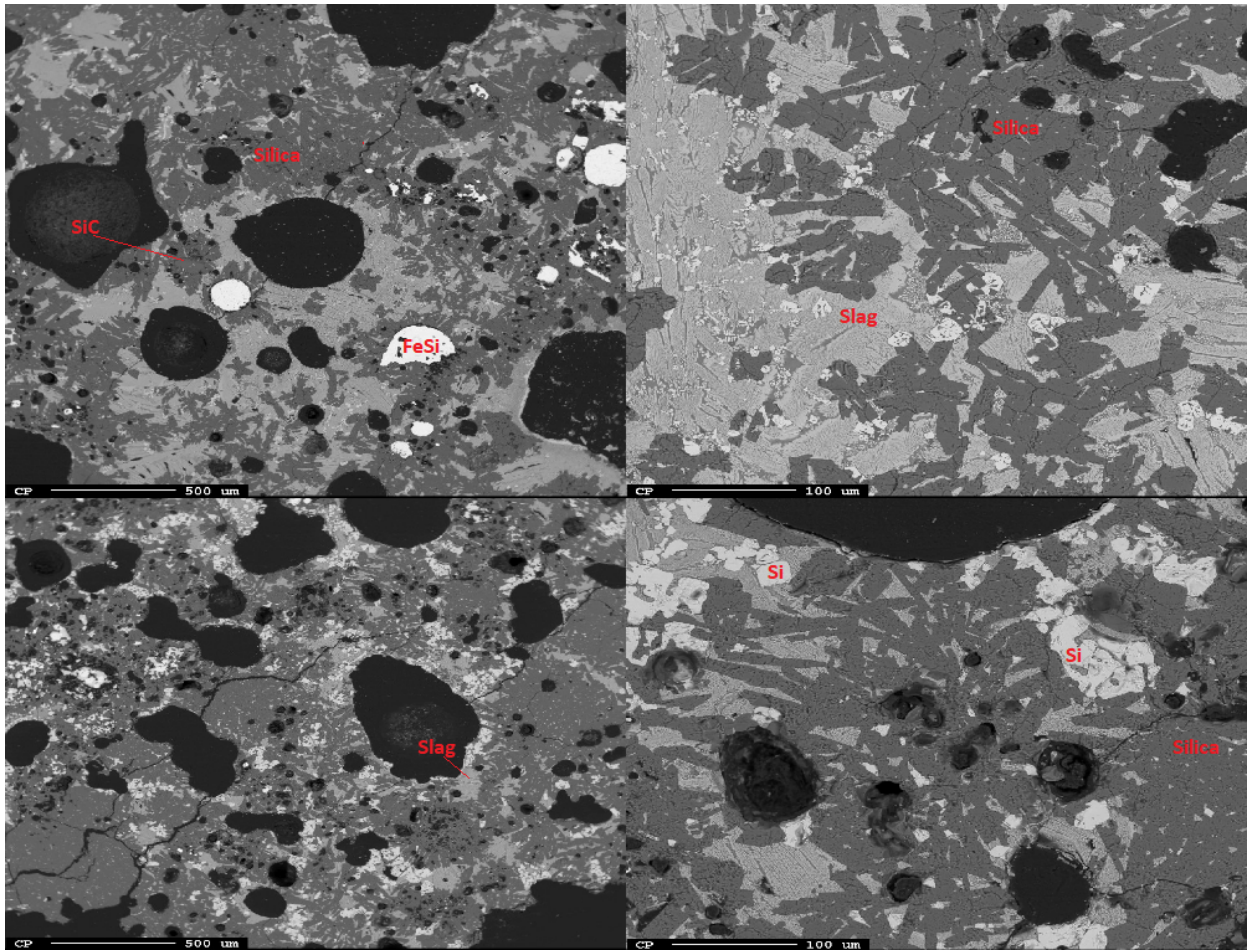
Figure 30: BSE-image from Furnace 3, 40x zoomed pictures on the left while a smaller 200x picture of the same area on the right.

4.2.6 X-ray mapping Furnace 3

What can be seen from Figure 31 and Figure 32 is that there really is a lot of elements other than silicon and iron in the sample. There really is not any structure with an explainable mechanism to it other than it looking like it consists of whatever sticks.
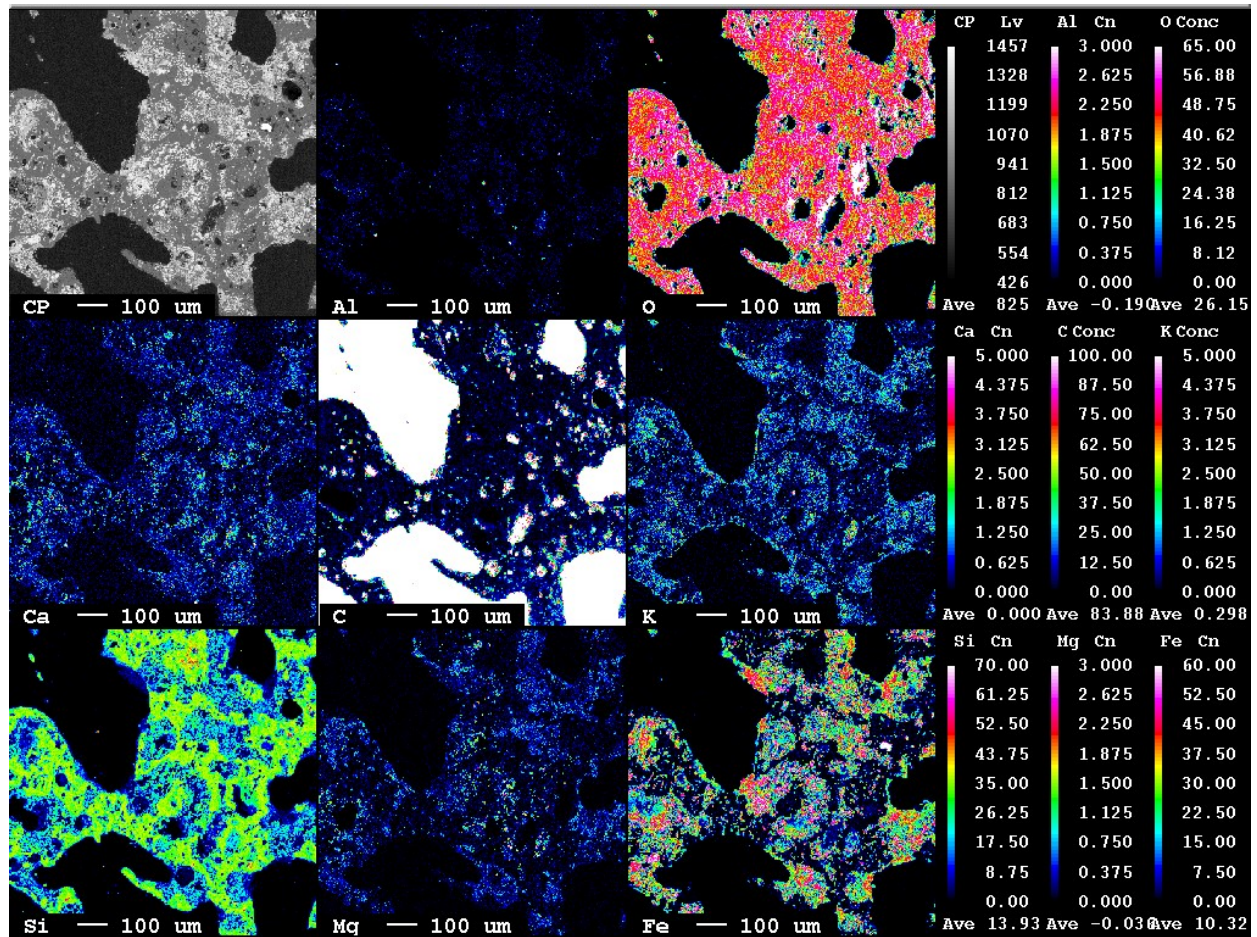
Figure 31: X-ray mapping of SEM sample from Furnace 3 the colour gradients on the right side are in wt%.
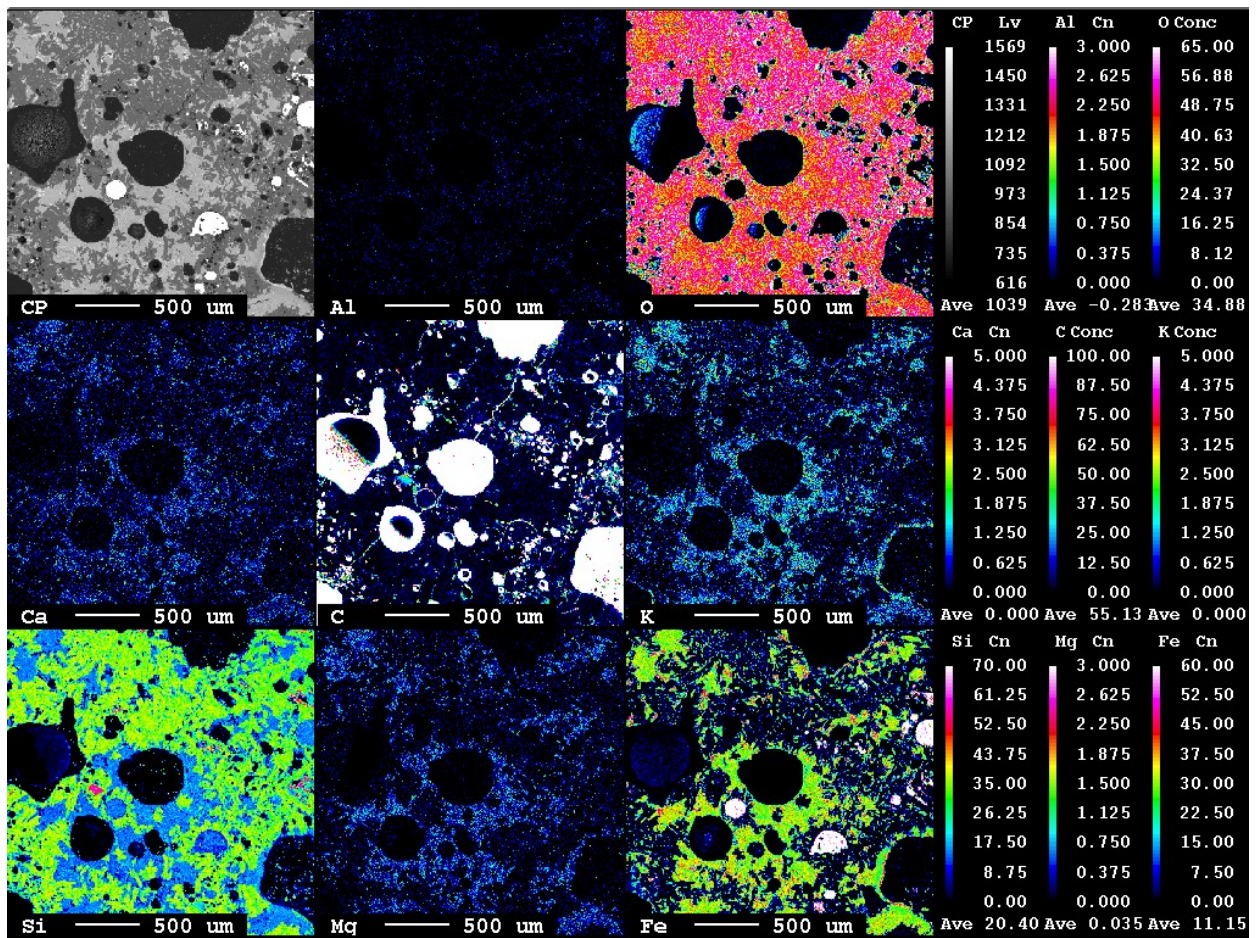
Figure 32: X-ray mapping of SEM sample from Furnace 3 the colour gradients on the right side are in wt%. .

4.3 Comparison EPMA

The two main phases; slag and silica are compared in this section to show the difference between the furnaces. The slag phase is compared in Figure 33. What is worth noting here is that due to a low amount of slag phase in Furnace 2 there is a very high uncertainty on the measurements because of lack of measurements. This is also because the areas for slag phases were considerably smaller in comparison to the other 2 furnaces. Here iron is exceeding the top of the figure. The Fe_2O_3 content of Furnace 3 is 53.0wt% with a standard deviation of 11.3wt%. This has been made to exceed the figure to make the other species readable. The other elements in Furnace 3 are quite low in comparison to the other furnaces. The amount of calcium and iron stand out for Furnace 2, but it has a large uncertainty. Furnace 1 seems to have a roughly equal amount of K, Ca, Al and Fe.
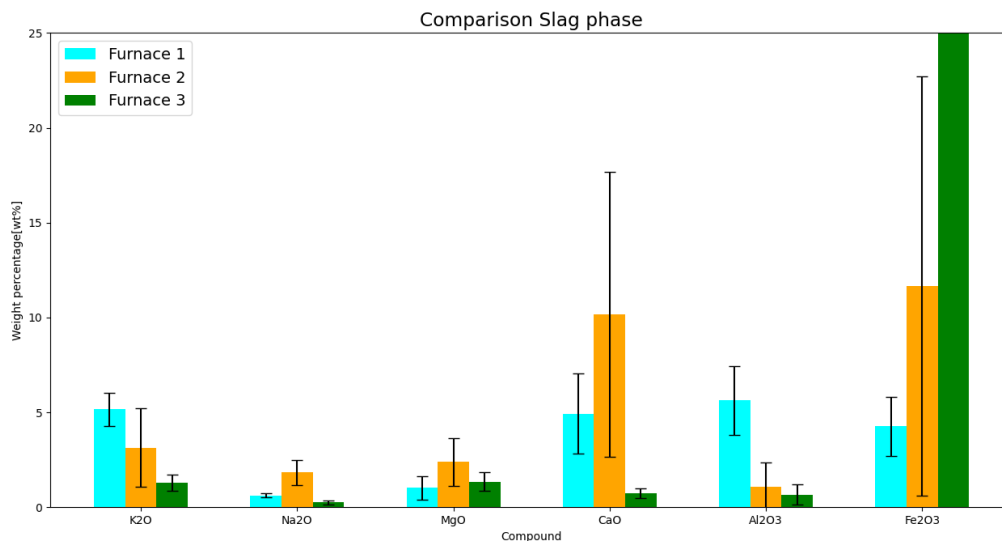

Figure 33: Comparison of the average slag phase composition for the three furnaces.

The composition of the slag phase has also been compared to the Microsilica composition from the same time period, this can be seen in Figure 34. Here as well the composition of FeO is made to exceed the figure for the same reason as the previous figure. The slag phase clearly has a higher amount of every element for every furnace. Furnace 2 has a high amount of Ca and Fe in comparison to Microsilica. Both the alkalis and earth alkalis does not exceed a difference of 5wt% for all the Furnaces, the only exception is CaO for Furnace 2. The amount of aluminium is also quite high for Furnace 1 when compared to the other furnaces. The trend seems to be that this type of phase has quite a bit of iron, but it is worth to keep in mind that Furnace 2 has a large uncertainty and Furnace 3 is a ferrosilicon furnace.

Figure 34: Comparison of the slag phase composition with the average Microsilica composition over the same time period as the fouling formed for all three furnaces.

The silica phase was also compared between the three furnaces in Figure 35. The silica phase is very pure in terms of other elements than SiO_2. This can be seen in that the largest bar is below 0.7wt%. The uncertainties are also quite large for every bar making it possible that the quantity is close to or equal to 0 for many of the species. The interesting thing about this phase is when it is compared to the Microsilica composition in Figure 36. Here it can be seen that the silica phase has a higher purity in comparison to Microsilica. The only exception is for iron where there is slightly more for both Furnace 1 and 2 but the error bars are larger than the bars themselves.

There is no remarkable difference in the composition of the silicon carbide or the silicon metal of the different furnaces. The ferrosilicon is however very different when compared between Furnace 1 and Furnace 3. Furnace 1 has a ferrosilicon with 53.3wt% silicon and 46.9wt% iron, while Furnace 3 has a ferrosilicon with 23.2wt% silicon and 74.2wt% iron. This has not been standardised to 100wt% because the remaining wt% is of carbon which could be a result from carbon coating the samples.

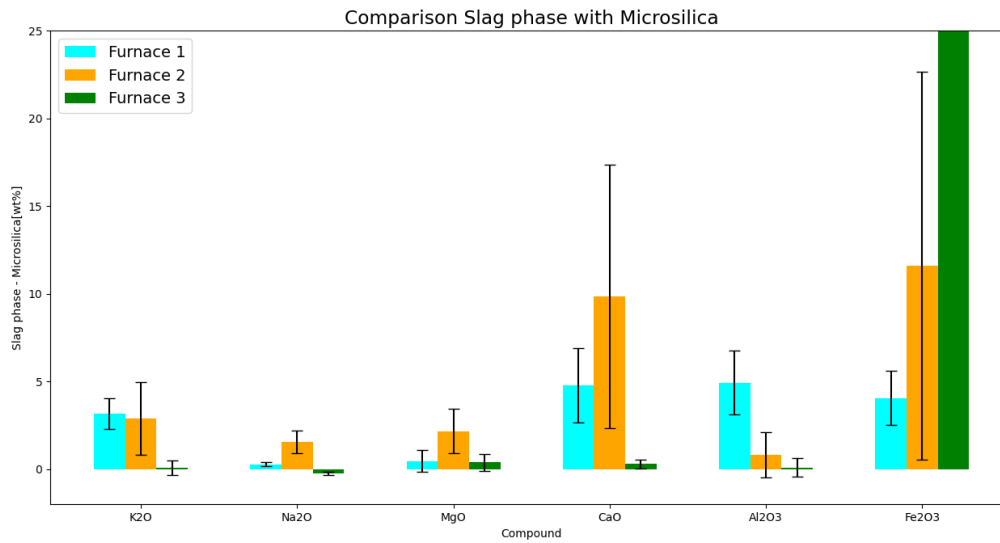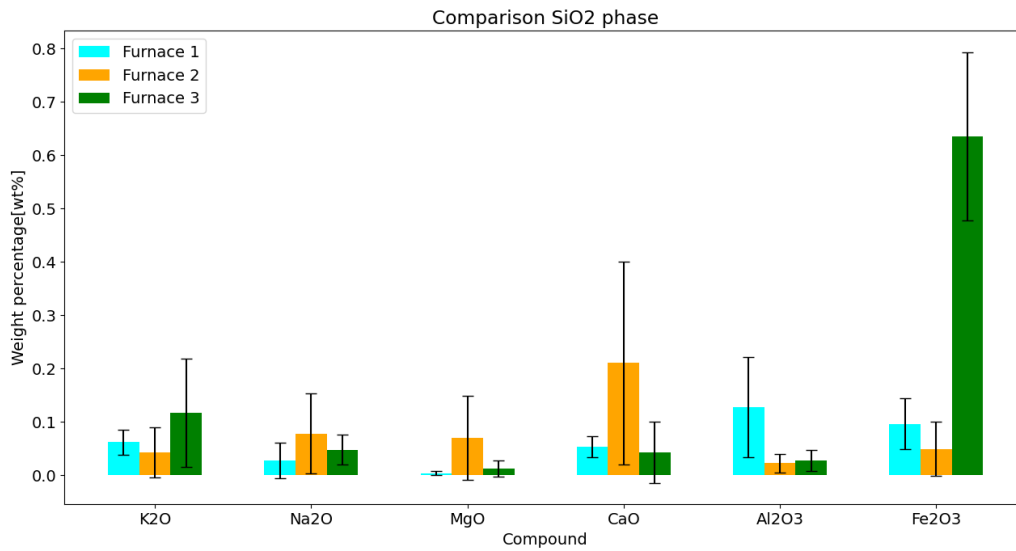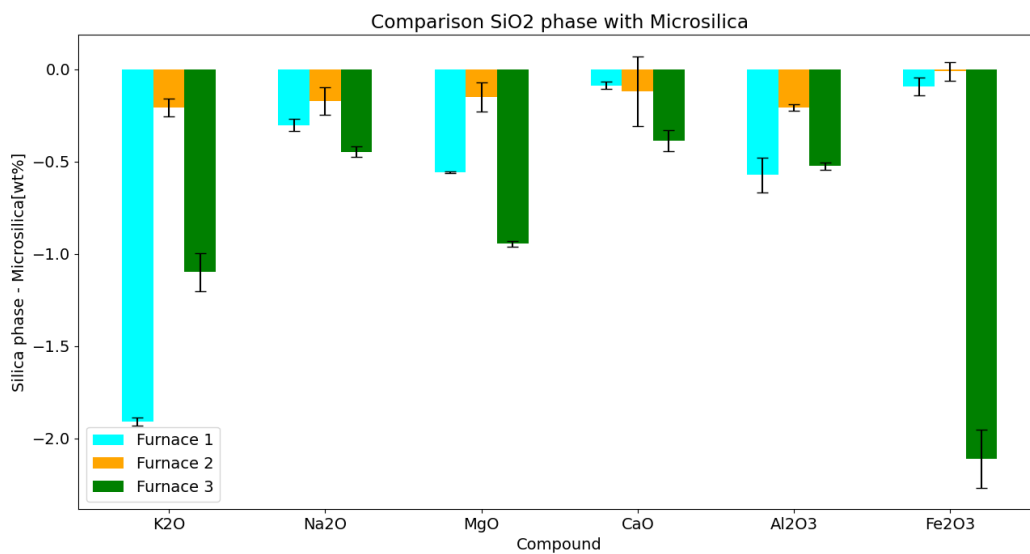Figure 35: Comparison of the silica phase composition for the three furnaces.

Figure 36: Comparison of the silica phase composition with the average Microsilica composition over the same time period as the fouling formed for the three furnaces.

4.4 ICP-MS

The raw results from the ICP-MS analysis done by ALS Scandinavia can be seen in Appendix B. This raw data has been adjusted to oxides to have the weight percentage. The resulting weight percentage average for each furnace can be seen plotted in Figure 37. In total nine samples were tested from Furnace 1, five samples from Furnace 2 and three samples from Furnace 3. What is worth noting is that the amount of iron from Furnace 3 has been made to exceed the figure because it is so large it would obscure all the lower species. The amount of iron in the fouling from Furnace 3 is on average 33.0 with a standard deviation of 0.9. What is apparent from the figure is that Furnace 1 has a higher composition of all compounds excluding Fe and Mg. The amount of alkalis is quite low for both Furnace 2 and 3. The amount of Ca, Al and Fe stand out when Furnace 1 and 2 are compared. Both furnaces are making silicon. While Furnace 3 produces ferrosilicon.
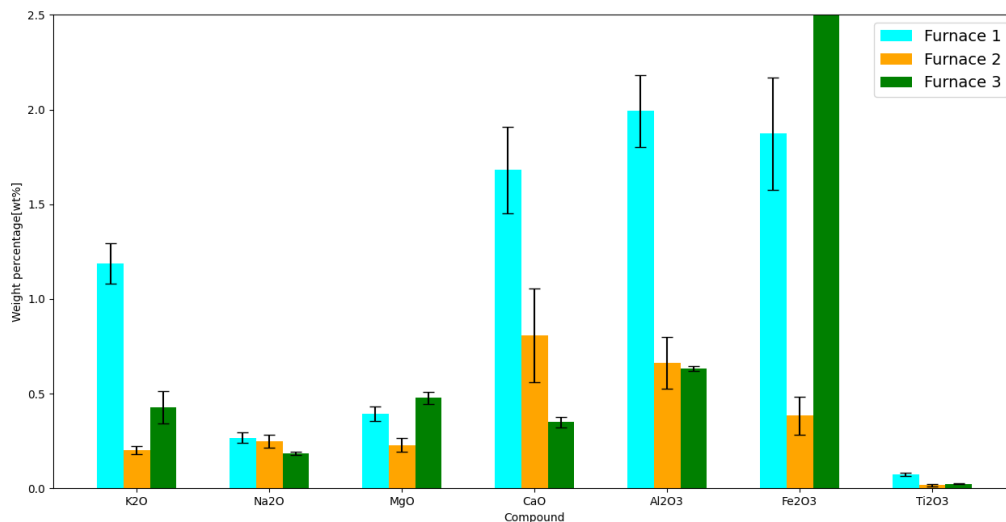
Figure 37: Average composition of oxides with error bars in the fouling samples from all three furnaces.

The composition of Microsilica taken from the same time period is compared to the average fouling composition in Figure 38. Here Si and Fe are exceeding the graph for Furnace 3 because the difference it too large. What is interesting from the graph is that the K, Na and Mg content of the fouling is lower than the Microsilica. While the Ca, Al and Fe is larger for all the furnaces expect Furnace 3 when it comes to Ca. The composition of Furnace 2 does not seem to vary greater than circa 0.5wt% from Microsilica. While Furnace 3 only varies less than 0.75wt% if iron and silicon is excluded. The difference between Furnace 1 and Microsilica is clearly larger in both directions in comparison.
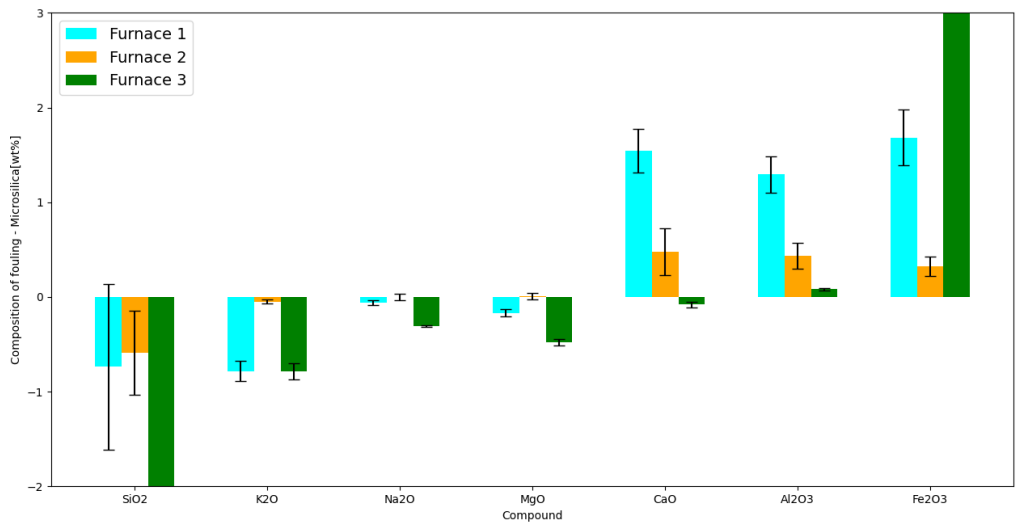
Figure 38: The Microsilica composition compared to the average composition of oxides from the fouling samples.

4.5 SDF

Three parallels were ran to test the softening temperature(ST) on five different fouling samples with differing composition and Microsilica as reference. Furnace 1 has the lowest softening temperature with 1585°C, Furnace 2 had 1653°C and Furnace 3 had 1638°C. Microsilica had a softening temperature of 1711°C. The composition of the samples tested as well as the average softening temperature can be seen in Table 8. The softening temperature was plotted against composition but no trend was found. All the samples were heated beyond their softening temperature which then led to the samples expanding and contracting indicating ongoing reactions. The change in the samples can be seen in Figure 39. The prediction models have also been tested by calculating the predicted softening temperatures for the composition tested with the sessile drop furnace. The result can be seen in Table 9. The difference between the models is quite striking and some of the models seem to predict a very high temperature(5000°C).
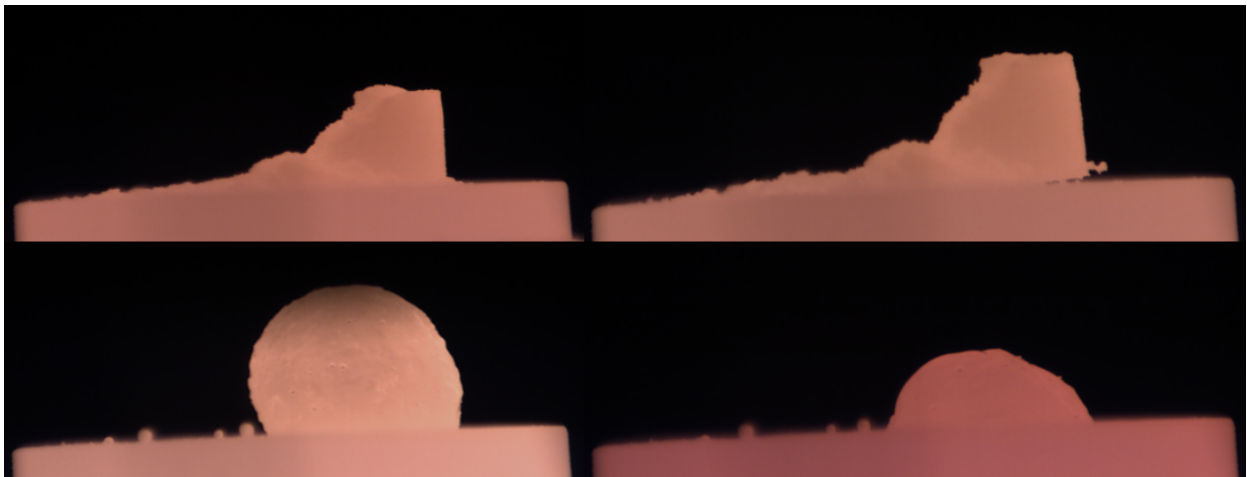
Figure 39: Sample 7 heated up to 1800°C then cooled, showcasing the deformation in steps.

Table 8: The composition and softening temperature(ST) with standard deviation of five samples and Microsilica.

Furnace	F1.1	F1.2	F2.1	F3.1	F3.2	MS
Si	93.2	90.5	96.6	63.7	64.7	97.9
K_2O	1.11	1.402	0.225	0.368	0.489	0.25
Na_2O	0.224	0.314	0.278	0.180	0.191	0.25
MgO	0.344	0.456	0.277	0.455	0.501	0.22
CaO	1.38	2.07	1.15	0.329	0.370	0.33
Al_2O_3	1.84	2.40	0.853	0.622	0.643	0.23
Fe_2O_3	1.63	2.42	0.491	33.6	32.4	0.06
ST	1585± 4	1592± 7	1654± 5	1646± 3	1638± 3	1711± 12

Table 9: Calculated Softening temperature based on composition of the samples tested with SDF with five different prediction models.

Area	Yu et al.[35] herbaceous (°C)	Yu et al.[35] Wood-based (°C)	Holubcik et al.[36] (°C)	Suzhen et al.[37] (°C)	Yin et al.[38] (SiO2 over 60%) (°C)
F1.1	1424	1101	1014	1637	1465
F1.2	1013	1103	1023	1603	1436
F2.1	5141	1100	991	1687	1492
F3.1	1226	1099	989	1418	967
F3.2	1218	1100	986	1425	983
MS	109386	1099	991	1710	1509

4.6   Fedorov Analysis

The result from the Fedorov analysis can be seen in Table 10. Here the Free Si is given with a less than sign. This has to do with the fact that Fe^{2+} cannot be differentiated from metallic silicon. Which means any Fe^{2+} will increase the measured metallic silicon. This means that the given free Si is the maximum amount of silicon metal in the sample. The amount of iron in the sample from Furnace 3 is quite high in comparison to the others. While simultaneously having a much higher silicon metal of $< 5.8\%$. The sample from Furnace 2 clearly has a lot less metallic silicon, but Furnace 1 has $< 1.9\%$ itself which is also quite low.

Table 10: Table with the Fedorov analysis result.

Furnace	Free Si[%]	Fe[%]
Furnace 1	1.9	1.1
Furnace 2 (low)	0.3	0.33
Furnace 2 (High)	0.3	0.37
Furnace 3	5.8	23.4

5 Discussion

The main goal of this thesis is to characterize the fouling from both silicon and ferrosilicon furnaces. This is done to get a better understanding of the underlying mechanism. The softening temperature will be measured for the fouling from the different furnaces. The resulting softening temperature will then be used to compare to softening temperatures models for fly ash used in the coal industry. The result obtained from XRD, EPMA, ICP, SDF and Fedorov will also be discussed.

5.1 Distribution of crystalline phases and amorphous content

The result from the XRD analysis have shown that there are both similarities and differences between the furnaces. The differences in quantity of the phases are shown again in Figure 40. All the furnaces show a high degree of crystallinity, but a good amount of amorphous content as well. Furnace 1 had the highest amount of amorphous content, but the results of Furnace 3 have a large uncertainty because of a worse refinement. The worse refinement is easily explained by looking at the resulting graph in Figure 19.
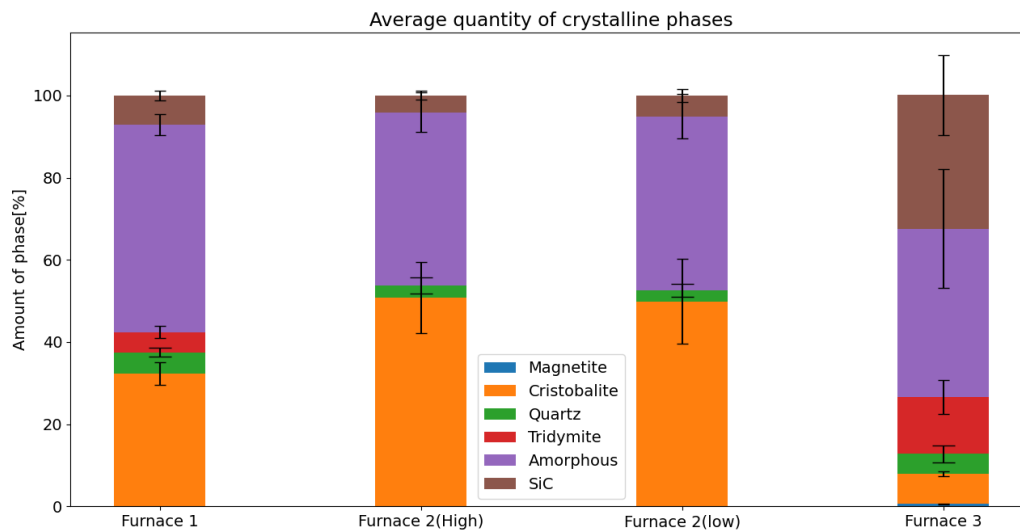
Figure 40: Comparison of amorphous amount and the crystalline phases between the furnaces.

The difference in amorphous content could be the result of a difference in temperature, stability of the furnace process, impurities affecting the crystallisation or the rate of fouling formation. Furnace 1 and Furnace 2 does have a system for energy recovery. This should mean that the average temperature of the off gas of these two furnaces is higher than Furnace 3. Furnace 3 is therefor most likely of having the most amorphous content. The surprising result of Furnace 1 having the highest amount of amorphous content might indicate that the formation of crystalline

phases happen at a higher temperature than the average off gas temperature. This would mean that the stability of the furnace process is more important. But if the fouling has a higher rate of formation for one of the furnaces it is however possible that it prevents crystallisation through isolation of the material. The presence of impurities like Fe, Na, Mg and K should affect the crystallisation since they are known to lower temperature required as well as speed up the process of crystallization. Based on the ICP-MS result this would suggest this would most heavily affect Furnace 3, then Furnace 1 and least affect Furnace 2. The amount of amorphous content for each furnace does give an indication of this not being a very dominating factor. Best guess is that spikes of temperature and rate of formation has a bigger impact.

Cristobalite can also be found in the fouling of all the furnaces. The cristobalite is likely just the result of silica being exposed to temperatures above 820°C causing it to crystallize. Tridymite can also be formed through thermally treating silica fume, but it does require the presence of K to crystallize. The K is expected to distort the lattice and make it possible for it to both form and stabilize at standard state. Tridymite is however not found for Furnace 2 which makes sense since the K content(0.2%) is low for the fouling sample. This does indicate that silica fume is a large part of the deposited fouling from Furnace 1 and 2. Since silica fume is expected to form all the cristobalite and tridymite, but also be the source of most of the amorphous content. Furnace 3 does in total have less tridymite, cristobalite and amorphous content, which indicates the fouling being made up of less silica fume. This is also confirmed by ICP-MS where a major part of it is Fe_2O_3. The small amount of quantified magnetite is therefor also surprising when the amount of Fe_2O_3 is considered. This likely means that the iron oxide is in amorphous form. Furnace 3 does have the most amount of tridymite which is surprising when considering that it also had a lot less K in the ICP-MS result than Furnace 1. This could also just indicate that the refinement was bad for Furnace 3.

The fact that quartz content is found in every furnace does suggest that fines of quartz material has made it to the off gas for all the furnaces. There are many causes that could lead quartz fines in the off gas. For example if the velocity of the air pumped into the furnace is too high, high amounts of fines or a collapsing cavity releasing gas that lifts raw material on top of the charge. Furnace 2 does have the lowest amount of quartz, but there is no way of determining which reason is the dominating factor in the low quartz content in the fouling sample. It also must be considered that the amount of quartz in the sample is relative. If the sample is diluted more than the other furnaces by for example, silica fume, then that would affect the relative amount of quartz. Since some of the samples from Furnace 2 where the most porous and soft it might be the case that they were more diluted by silica fume than the other furnaces.

Another crystalline phase the furnaces had in common was silicon carbide. There are three different potential mechanisms for the silicon carbide in the fouling of the off gas. It could have formed through the condensation reaction

$$3SiO(g) + CO(g) \rightarrow 2SiO_2 + SiC$$
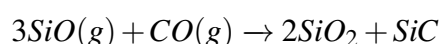
or through the reaction of SiO with carbon

$$SiO(g) + 2C(s) = SiC(s) + CO(g)$$
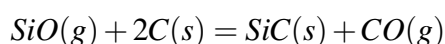
The final option is that silicon carbide formed in the charge material have been transported up to the off gas. This could potentially happen in the event of a large avalanche in the furnace caused

by the build-up of a cavity. The two reactions would be indicators of SiO gas in the off gas. Based on thermodynamics the formation of silica fume is heavily favoured the lower the temperature. Unreacted SiO also indicates an oxygen supply that is too low to convert it all to silica. The reaction between CO and oxygen also becomes more favourable the lower the temperature. The formation of silicon carbide due to condensation reactions would then indicate scenarios where there is an elevated temperature and a lack of oxygen supply. This could be caused by understoking causing the build-up of a cavity which eventually leads to an avalanche releasing large amounts of process gases. This could also lead to a lot of fines and soot moving through the off gas which then leads to carbon and potentially carbide in the off gas. However the structure of silicon carbide does not seen to have a structure that suggest a reaction between carbon particles and SiO. The remaining carbon particle for such a reaction would burn off and the resulting silicon carbide is likely of having a core shell like structure. This is however not seen in the samples for any of the furnaces. The structure of the silicon carbide has in some of the EPMA results had a very flat and needle like structure. This could potentially be the result of a condensation reaction causing it to gradually form the needle by adhering to the crystal structure slowly.

5.2   Composition of the slag phase

The main thing to keep in mind when looking at the result from the ICP-MS figures is that the raw data has been adjusted for oxides assuming that every component is in the most common oxide form. This assumption is wrong, but the extent that this is wrong is hard to judge for other elements than the Si and Fe measured by the Fedorov analysis. Judging by this the amount of SiO_2 and Fe_2O_3 is overestimated and will result in all the other elements being underestimated in Figure 37.

The average composition of fouling from Furnace 1 has a lower purity than the rest of the furnaces in terms of trace elements excluding iron. The reasoning behind this can easily be spotted when the EPMA result is considered. Furnace 1 has a lot more slag phase and a higher content of all the trace elements excluding iron. Furnace 3 does however have a lot more iron in the slag phase. The increase of iron is likely caused by iron fines from the raw material ending up in the chimney. This is the only reasonable reason for the elevated iron content that forms the slag phase and increases the average iron composition to roughly 53wt% of the sample. When considering the size distribution of the Iron source A is 77.2% fines and iron source B is 79.5% fines, then those are very likely the cause for the increased iron content. This means that the fouling of Furnace 3 is likely very different fundamentally than Furnace 1 and Furnace 2 since they both are silicon furnaces without iron fines. The slag phase of Furnace 3 also appears to be very non heterogeneous. If the air inlet has a high enough speed to lift iron fines, it will lift any other fines that are as large as the iron fines. This likely is part of the reason why the phase is so heterogeneous. The slag phase being iron fines is confirmed when the composition of the iron fines in Table 11 are considered. The slag phase is therefore mainly just a combination of silica and iron fines. Iron can be reduced at a lower temperature which could then lead to being reduced in the off gas causing it to form a liquid phase with increased deposition probability. This would however require CO for the reduction. High air intake to lift iron fines would lead to less CO. Increased CO and temperature is possible through the collapse of cavities.

Table 11: Table of composition for the two iron sources used for Furnace 3.

	SiO2	Si	K2O	NaO2	MgO	CaO	Fe2O3	Al2O3
Iron Source A	1.99	0.93	0.026	0.45	0.128	0.67	70.7	0.25
Iron Source B	0.91	0.42	0.02	0.201	0.092	0.1	71.6	0.07

The abundance of the slag phase from Furnace 1 does indicate that it has had an underlying effect on the formation of the fouling. When the composition of both the silica phase and the slag phase is considered, the increase of the average composition is the result of the slag phase. The high fusion temperatures from the tests does however indicate a that a lower melting phase is less likely. The phase is not just silica fume this can be confirmed by looking at the comparison of slag phase with the Microsilica. The phase could however be the result of melt fractions leading to a deposit that is liquid which can then bind silica fume. There really is no other logical reasoning for the phase considering the high amount there is of it. This phase is also likely the phase where tridymite is formed. When compared to Furnace 2 there is a lot less slag phase. The lack of a slag phase is also very likely the reason why there was no tridymite in the average sample since there is nowhere with elevated K levels to form and stabilize it. The slag phase of Furnace 2 does however have more of the oxides Na_2O, MgO, CaO and Fe_2O_3, but with a considerable larger uncertainty. Considering the average composition of the fouling from Furnace 2 it is no surprise that there is a lot less slag phase than Furnace 1. The lack of a slag phase does indicate that the underlying mechanism is far more likely to not be dependent on a phase with a lower melting point. This could then in turn mean that the fouling is not dependent on the composition of the particles and the fouling will form regardless. Then a mechanism could be silica fume deposits then it is heat treated and crystallised. Then there really is nothing that can be done expect keeping control of the temperature and perhaps changing the design to prevent fouling. The slag phase could come from ash found in the raw material. Considering the amount of slag phase for Furnace 2 this seems like a reasonable source. Furnace 1 has such a high amount that it becomes less likely to be the only cause unless the raw material contains a lot of ash content.

5.3 Composition of the silica phase

The silica phase is something all the furnaces have in common. The composition of the phase strongly suggest that it consists of silica fume. When the phase is compared to Microsilica in Figure 36 it shows that the silica phase has less trace elements than the Microsilica. For Furnace 2 the deviation is so low that the difference is almost accounted for by the standard deviation. This does mean that the phase is likely just silica fume for Furnace 2. The result from Furnace 1 does show a completely different story. There is practically no other elements than silica in it. Especially when this phase is compared to Microsilica from the same time period. It is substantially lower on all elements especially K_2O, Na_2O, Al_2O_3 and MgO. This is quite surprising since it indicates that a large portion of the fouling from Furnace 1 is purer than the resulting silica fume. The slag phase does encapsulate the silica phase for Furnace 1, where this could mean that the slag phase is liquid then binds the silica phase. There accuracy of the EPMA measurement might be off for the silica phase. Otherwise, there is a large deviation in

composition of Microsilica and all the areas just happened to have a higher purity. The silica phase for Furnace 3 does have the same tendencies where the phase is purer than the Microsilica. The images from Furnace 3 does however not show a very organised sample. The phases are very non-heterogeneous, and the phases are spread all over it does not really indicate liquid phases binding silica fume like for Furnace 1.

There are however other possibilities for the silica phase. The silica phase could have formed through condensation reactions: Equation 5 and Equation 6 or be the result of quartz fines from the raw material. The latter option is measured through XRD where Furnace 1 had 5.2%, Furnace 2 had 2.6% and Furnace 3 had 4.77%. This silica could potentially be anywhere inside the silica phase and could be hard to distinguish. The condensation option is also a factor since there is both silicon metal and ferrosilicon in the sample that has likely formed through condensation reactions. Both would produce a silica that has a very high purity.

5.4 Silicon and ferrosilicon

All the furnaces also have silicon metal and ferrosilicon. The silicon metal is expected to have formed due to unreacted SiO in the chimney that then react through a condensation reaction. There are structures that suggest condensation reactions because of typical brown condensate structures. The ferrosilicon is expected to have happen at the same time as the ferrosilicon. Often the ferrosilicon is at the outskirts of the silicon metal, but sometimes it is also separate. The iron source that reduces for Furnace 3 is from iron fines, but there should be no iron fines in Furnace 1 or Furnace 2. The iron could be iron oxide in the fouling or silica fume that is reduced by the CO gas. This would require a temperature at least above 1000°C. If there is unreacted SiO then there should also be unreacted CO. The SiO gas is indicative of unstable furnace operation that leads to an oxygen supply that is too low to react with all the CO and SiO.

Based on the Fedorov results the fouling from Furnace 3 is the one that is the most affected by silicon metal. Furnace 3 had measured 5.8% free Si. This result does indicate that roughly 5.8% of the fouling should also be SiO_2 formed through Equation 6. This would mean at at least 12% of the sample is the result of condensation reactions which is quite a lot. Since the only other alternative is Equation 4. This would require silicon carbide which is in the fouling as well. Some of the SiO could also have formed silicon carbide through Equation 5. Some of the measured free Si is also going to be ferrosilicon since the test cannot differentiate Fe^{2+} from pure Si. Based on the images from Furnace 3 it is safe to assume that majority of it is ferrosilicon. The amount of silicon metal in Furnace 1 is lower(1.9%) and Furnace 2 had even less(0.3%). Both have a lot less ferrosilicon which is not surprising since they are both silicon furnaces. Furnace 2 has such a small amount of silicon metal that it is unlikely that condensation reactions have a large effect on the formation of the fouling. Condensation does influence Furnace 1, but it would not be a large affect. Furnace 3 however seems to be affected by it based on the Fedorov results. But keep in mind that everything is relative. If the fouling forms at a higher rate the amount of silicon metal could be lower. Therefor it cannot be said for certain which furnace has the most stable operation, but it is likely Furnace 2.

5.5   Fusion temperature and prediction models

The results from the sessile drop furnace are quite conclusive in terms of how high the measured softening temperature is for the representative samples and a Microsilica sample. The softening temperature does not change a lot when the iron content is considerably increased. The result does not really differ that much between Furnace 1 and Furnace 2 even though the composition is quite different in terms of purity. That does suggest that the softening temperature does not differ a lot within the higher purity range of silica fume. The softening temperature seems to be consistently above or right below 1600°C. The high softening temperature does suggest that the off gas would very rarely be at a high enough temperature to form a liquid phase, but it is worth noting that the softening temperature is quite bad at measuring potential melt fractions. From the theory section it is also known that the presence of quartz fractions can skew the measured softening temperature even though most of the other ash particles are molten. The samples have shown to be quite non heterogeneous with silicon carbide, quartz, other crystalline forms and metals. The method of preparing the samples have shown to be quite good at making representative samples, but the distribution of elements that have a higher melting point like quartz and silicon carbide might raise the softening temperature. This is also why some models chose to use shrinkage starting temperature. How heterogeneous the sample is affects the measured softening temperature. Which is probably why the measured softening temperature of Microsilica is a lot higher than the rest. When as little as 10% of the particle melts that can heavily affect the chance for deposition of the particle.

The test was also ran in a reducing atmosphere which typically lowers the ash fusion temperature. Even in these conditions the softening temperatures are too high to say anything in terms of ideal temperatures for the off gas. The test was done according to an ISO standard. Deciding the softening temperature is quite the subjective task, but the difference between initial deformation temperature, softening temperature and hemispherical temperature was quite low for all the samples making the room for potential human error regarding observed temperature below 25°C. This combined with the low standard deviation below 12 for every sample over three parallels does suggest that the measured softening temperature according to the ISO standard have been done accurately.

All things considered it does not seem like testing the fouling for softening temperature gives a lot of information. Since the validity of ash fusion temperature tests for fouling samples have been questioned in the past, does raise concern regarding the validity. The process of fouling is considered a very complex process and at least for the silicon industry it does seem like the ash fusion test might simplify too much and not give any useful information. Especially when this is paired with the fact of how non heterogeneous the samples are and the potential effect that has on the softening temperature.

When the composition of the samples is tested with the five prediction models it becomes quite apparent that most of them predict temperatures way below the measured softening temperature. The model for Herbaceous material by Yu et al.[35] seem to break making one prediction above 5000C and another above 100000°C. The model by Suzhen et al.[37] seem to be the closest with the prediction for the samples from Furnace 1, Furnace 2 and for the Microsilica. The predicted softening temperature for the F1.1 is higher than F1.2 from the same furnace, but the resulting

softening temperature does not reflect that. This likely means that there are other factors like quartz, silicon carbide or metal content that effects the measured temperature. The metallic content was quite scattered in the EPMA and the quartz content measured by XRD was quite low for all the samples making it possible for large deviations on the amount in each sample. Considering the amount of sample sent to ICP-MS for analysis was 3 grams, then there is a potential for larger deviations on composition. The iron content in the samples from Furnace 3 seems to skew the predicted temperature from the same model quite low to roughly 1422°C, but the measured softening temperature is 1642°C. The iron should reduce the softening temperature because it requires a much lower temperature for reduction compared to silica and the experiments were done in reducing conditions(CO). This does not seem to be the case for Furnace 3, however. This might once again be because of content like quartz, silicon carbide and metal effecting the process of melting.

5.6   Short summary of mechanisms for formation

Furnace 1 potentially has lower melting phase creating a liquid which binds silica fume. Furnace 2 does not have enough slag phase to suggest a lower melting phase. The lack of a slag phase might mean that the fouling occurs through heat treatment so the reaction is essentially a crystallisation after deposit. The crystallisation also likely occurs during temperature spikes. Furnace 3 could have a lower melting point phase if the iron fines can be reduced and form a liquid in the chimney. The silica phase in all the furnaces is likely a result of silica fume, quartz and condensation reaction. All the furnaces have had a temperature above 820°C to crystallize and form cristobalite. The fusion temperature test is not useful for samples from the silicon industry and the softening temperature models can not be extrapolated to the composition of the silicon industry. Quartz is the result of fines for all the furnaces. The silicon carbide is most likely the result of condensation reactions or from the charge material, because there is no structure that suggest a reaction between carbon particles and SiO. The silicon metal is also likely the result of condensation reactions. A large portion of the fouling from Furnace 3 is the result of iron fines. The combination of EPMA and XRD gives a very good indication on underlying mechanisms for formation. Based on this short summary the potential steps to reduce fouling would be: reduce fines(quartz, iron, carbon), better process control to avoid temperature spikes and reduce the air inlet. These measures are more or less the same conclusions that Sintef[33] had back in 1993. There is potentially a possibility that Furnace 1 can also have a reduction in fouling tendency by investigating the source for the slag phase and see if it can be removed/reduced.

5.7   Validity of the XRD result

The XRD-result were quantified through a Rietveld refinement in Topas[9]. The result from Furnace 1 had a Rietveld weighted profile(RWP) value varying from 10.9-12.2, Furnace 2 had a RWP values between 10.6 and 15.3. Furnace 3 had a much higher RWP values with it varying from 15.8-18.1. While the Goodness of fit(GOF) for Furnace 1 was 3.3-3.8, 3.1-5.1 for Furnace 2 and 4.0-5.5 for Furnace 3.

This clearly indicates that the refinement was best for Furnace 1 and worst for Furnace 3. Since ideally the RWP should be below 10 and GOF between 1 and 2, but this is not the case for any

of the furnaces. What is the most important is to consider the system and if the resulting phases are possible and reasonable. All the phases for Furnace 1 agree with the results from both EPMA and ICP-MS. The system is also expected to have trace elements which of course could end up in the lattice which would lead to a worse fit. The fit was improved when the XRD was redone with alumina doping meaning the amorphous content is accounted for. All the samples were screened for two hours. The GOF will decrease the lower the step size is used since GOF is the ratio of RWP over R_{exp}(R_{exp} decreases with lower step size). This would mean that data has been over collected but the model obtained by fitting is better.

The simulated fit for one of the samples from Furnace 1 can be seen in Figure 41. The resulting graphs from all the furnaces look very similar to the figure where most of the peaks have been fitted. The degree that the tops have been fitted is by far the worst for Furnace 3 which is not surprising considering the Figure 19 where the peaks look very broadened and it looks very amorphous. The fit for all the refinements were made to exclude the data before 20° to optimize the fit, because there was just noise or no peaks before 20°. The result from this can then be used as a relatively good indicator for the phase distribution of the fouling of each furnace. The fit was also adjusted for alumina content measured by ICP-MS to have an accurate amount of alumina after doping with alumina. The result was also checked for contamination of Cu and W leading to distortion of peaks. The maximal amount of copper was quantified to be 340mg/kg through ICP-MS and 2.1mg/kg for tungsten. The small amount makes it likely that the potential wavelength contamination is negligible. The result from Furnace 3 has the highest uncertainty, while the difference between Furnace 2 and 1 could be caused by a better fitting because of one more phase(tridymite) to fit to for Furnace 1.
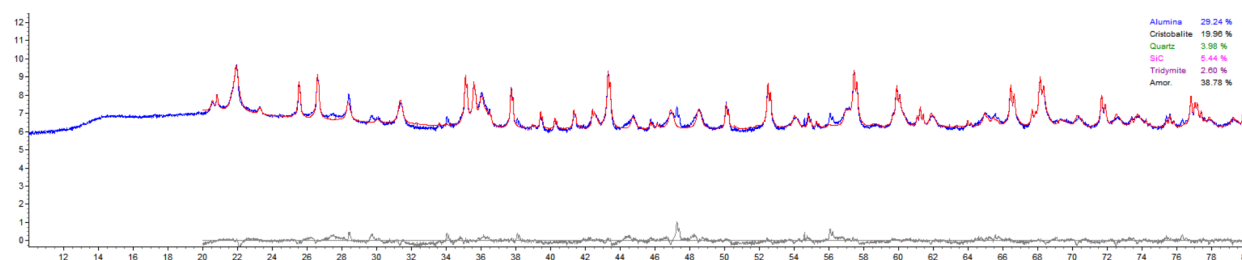
Figure 41: Graph from Topas 5[9] showing the simulated fir for the XRD curve for one sample from Furnace 1. The red line is the simulated fit.

6 Conclusion

The objective of this thesis has been to characterize fouling samples from three different furnaces to understand the underlying mechanism. The samples were characterized through XRD, EPMA, ICP-MS, SDF and Fedorov. The following conclusions from the characterization can be made:

- The samples have a good amount of crystalline phases as well as amorphous silica. The crystalline phases are expected to form above 800°C. Tridymite was quantified for two of the furnaces. The lack of a slag phase and less potassium seems to be the underlying cause. The fouling all contain quartz which indicates a high likeliness that this is the result of quartz fines from the raw material. The average temperature is very likely too low for crystallisation which means the crystallisation happens during temperature spikes.

- Silicon metal, silicon carbide and ferrosilicon is likely the cause of condensation reactions happening in the off gas. The silicon carbide could also be from the charge material. The presence of SiO and potential silicon carbide from the charge material does suggest unstable conditions of operation. It could be the result of large cavities in the furnace collapsing. The ferrosilicon is often found in the outskirts of the silicon metal phase for the silicon furnaces. Suggesting that the iron dissolves into the silicon metal.

- The presence of a slag phase in every furnace does suggest the potential of a lower melting phase working as a glue but based on Furnace 2 it does not seem to be a dominating or necessary factor in the formation of fouling.

- The softening temperature is quite high for the where the lowest was 1585°C. The high softening temperature would suggest very harsh conditions for the potential formation where the temperature of needs to spike quite high. With how non-heterogeneous the samples are it is possible that this increases the measured softening temperature. Silicon carbide, quartz and the metal phases could affect this. The much higher melting point tested on Microsilica likely means silicon metal reduces the measured softening temperature.

- The softening temperature models tested do not seem to be applicable to the fouling tested in this thesis. This might be the result of how non-heterogeneous the samples are again.

- The amount of silicon metal phase measured suggest that condensation reactions are not a dominating mechanism for the formation, but it does play a part.

- The fouling problem can potentially be reduced by removing fines from the raw material, reducing air flow and having a stable process operation to avoid temperature spikes. Furnace 1 could potentially benefit from further investigation to find the source/cause of the slag phase.

7 Further Work

- Investigation into melt fraction by simultaneous thermal analysis(STA). The softening temperature measurements might be affected by how non-heterogeneous the sample is. This type of test would potentially catch if the sample has a lower melting point.

- Microsilica could be heated and investigated to better understand the process of crystallisation. This should be done while quantifying the amount of amorphous material while increasing the temperature. How sudden spikes of temperatures effect the formation could also be done.

- Quantification of carbon in the fouling samples by Leco analysis. This would give a better understanding on how much carbon and silicon carbide make up of the fouling.

- A study of the rate the fouling forms while measuring temperature could give a better understanding of the effect of temperature and the importance of spikes in temperature.

- Testing fouling tendencies in a pilot scale setup for better controll over the parameters.

8 Bibliography

1. Anders Schei, Johan Tuset, and Halvard Tveit. Production of high silicon alloys. 01 1998.

2. Edin Henrik Myrhaug. Non-fossil reduction materials in the silicon process : properties and behaviour, 2003.

3. R. E. Pocovi, G. Villaflor, and J. E. Flores. Minimum transport velocities of mineral and metallic dusts in exhaust systems. 1997.

4. Cornelis Klein. Manual of mineralogy, 1993.

5. Shipeng Zhang, Shengnian Tie, and Fenjuan Zhang. Cristobalite formation from the thermal treatment of amorphous silica fume recovered from the metallurgical silicon industry. *Micro nano letters*, 13(10):1465–1468, 2018. ISSN 1750-0443.

6. G. Akdogan, H. Johto, and P. Taskinen. Phase equilibria study of k–o–si system in equilibrium with air. *Journal of the European Ceramic Society*, 34(15):4053–4058, 2014. ISSN 0955-2219. doi: https://doi.org/10.1016/j.jeurceramsoc.2014.05.007. URL `https://www.sciencedirect.com/science/article/pii/S0955221914002659`.

7. F. C Kracek. The ternary system: K2sio3—na2sio3—sio2. *The Journal of Physical Chemistry*, 36(10):2529–2542, 1932. ISSN 0092-7325.

8. Jørund Vangskåsen. Metal-producing mechanisms in the carbothermic silicon process, 2012. URL `http://hdl.handle.net/11250/249099`.

9. Bruker. Diffrac.topas. (v6.0.0.9), .

10. Kurt Aasly. Properties and behavior of quartz for the silicon process, 2008. URL `http://hdl.handle.net/11250/235844`.

11. Hans U Zettler. 12th conference of heat exchanger fouling and cleaning - 2017, aranjuez, spain. *Heat transfer engineering*, 41(2):113–114, 2020. ISSN 0145-7632.

12. Per K Kofstandm and Bjørn Pedersen. Silisium. `https://snl.no/silisium`. Fetched 1. oktober 2021.

13. U.s. geological survey, mineral commodity summaries, january 2022. `https://pubs.usgs.gov/periodicals/mcs2022/mcs2022.pdf`. Fetched 29. march 2022.

14. Viktor Myrvågnes. Analyses and characterization of fossil carbonaceous materials for silicon production, 2008.

15. M Barati, S Sarder, A McLean, and R Roy. Recovery of silicon from silica fume. *Journal of non-crystalline solids*, 357(1):18–23, 2011. ISSN 0022-3093.

16. Eli Ringdalen and Merete Tangstad. Reaction mechanisms in carbothermic production of silicon, study of selected reactions. In *International Smelting Technology Symposium*, pages 195–203. John Wiley Sons, Inc, Hoboken, NJ, USA, 2012. ISBN 1118291166.

17. Sarder S Barati M, McLean A, and R. Roy. Recovery of silicon from silica fume. 2011. Accessed 14. october 2021.

18. Jefri Shahriar, Bahram Rezai, F Motlagh, Younes Shekarian, and Mohammad Reza Aslani. the effect of density and particles size of -quartz and amorphous silica on flotation. *Amirkabir Journal of Science and Technology (ISSN: 1015-0951)*, 05 2014.

19. Monica Dapiaggi, Lucia Pagliari, Alessandro Pavese, Luciana Sciascia, Marcello Merli, and Fernando Francescon. The formation of silica high temperature polymorphs from quartz: Influence of grain size and mineralising agents. *Journal of the European Ceramic Society*, 35 (16):4547–4555, 2015. ISSN 0955-2219.

20. S. B HOLMQUIST. Conversion of quartz to tridymite. *Journal of the American Ceramic Society*, 44(2):82–86, 1961. ISSN 0002-7820.

21. F. C Kracek, N. L Brown, and G. W Morey. Equilibrium relations and factors influencing their determination in the system k2sio3–sio2. *Journal of physical chemistry (1896)*, 41(9): 1183–1193, 1937. ISSN 0092-7325.

22. Andrea Broggi. Condensation of sio and co in silicon and ferrosilicon production, 2021. ISSN 2703-8084. URL `https://hdl.handle.net/11250/2734899`.

23. Michal Ksiazek, Ida Kero, and Bernd Wittgens. Challenges in transporting the off-gasses from the silicon process. 12 2015.

24. Broggi Andrea and Merete Tangstad. *Condensation of SiO and CO in Silicon Production—A Literature Review: Proceedings of the First Global Conference on Extractive Metallurgy*, pages 697–716. 01 2018. ISBN 978-3-319-95021-1. doi: 10.1007/978-3-319-95022-8_55.

25. Daniel Perez Clos, Petter Nekså, Sverre Gullikstad Johnsen, and Ragnhild Elizabeth Aune. Investigation on scale formation in aluminium industry by means of a cold-finger. 2019. ISSN 2367-1181. URL `http://hdl.handle.net/11250/2634063`.

26. H Müller-Steinhagen, M. R Malayeri, and A. P Watkinson. Heat exchanger fouling and cleaning-2011. *Heat transfer engineering*, 34(8-9):653–654, 2013. ISSN 0145-7632.

27. Ulrich Kleinhans, Christoph Wieland, and Spliethoff Hartmut. Ash formation and deposition in coal and biomass fired combustion systems: Progress and challenges in the field of ash particle sticking and rebound behavior. *Progress in Energy and Combustion Science*, 68, 05 2018. doi: 10.1016/j.pecs.2018.02.001.

28. Daniel Perez Clos. Formation of hard grey scale(hgs) on the surface of a cold-finger in the aluminium production industry, 2021.

29. Introduction to coal utilization technologies. In *Clean Coal Engineering Technology*, pages 147–229. 2017. ISBN 9780128113660.

30. P Billen, J Van Caneghem, and C Vandecasteele. Predicting melt formation and agglomeration in fluidized bed combustors by equilibrium calculations. *Waste and biomass valorization*, 5 (5):879–892, 2013. ISSN 1877-2641.

31. Raj Gupta, T Wall, and L Baxter. *Impact of mineral impurities in solid fuel combustion.* Springer Science & Business Media, 2007.

32. Erich Raask. *Mineral impurities in coal combustion: behavior, problems, and remedial measures.* Hemisphere Pub, 1985.

33. Svend Graadahl and Stein Tore Johansen. Groing av gasskanaler sluttraport. *Sintef*, 68, 11 1993.

34. Mustafa Ozer, Omar M. Basha, Gary Stiegel, and Badie Morsi. 7 - effect of coal nature on the gasification process. In Ting Wang and Gary Stiegel, editors, *Integrated Gasification Combined Cycle (IGCC) Technologies*, pages 257–304. Woodhead Publishing, 2017. ISBN 978-0-08-100167-7. doi: https://doi.org/10.1016/B978-0-08-100167-7.00007-X. URL `https://www.sciencedirect.com/science/article/pii/B978008100167700007X`.

35. L.Y. Yu, L.W. Wang, and P.S. Li. Study on prediction models of biomass ash softening temperature based on ash composition. *Journal of the Energy Institute*, 87(3):215–219, 2014. ISSN 1743-9671. doi: https://doi.org/10.1016/j.joei.2014.03.011. URL `https://www.sciencedirect.com/science/article/pii/S174396711400021X`.

36. Michal Holubcik, Jozef Jandacka, and Milan Malcho. Ash melting temperature prediction from chemical composition of biomass ash. *The holistic approach to environment*, 5(3):119, 2015. ISSN 1848-0071.

37. Suzhen Miao, Qingyin Jiang, Hua Zhou, Jia Shi, and Zhikai Cao. Modeling and prediction of coal ash fusion temperature based on bp neural network. *MATEC Web of Conferences*, 40: 5010, 2016. ISSN 2261-236X.

38. Chungen Yin, Zhongyang Luo, Mingjiang Ni, and Kefa Cen. Predicting coal ash fusion temperature with a back-propagation neural network model. *Fuel (Guildford)*, 77(15):1777–1782, 1998. ISSN 0016-2361.

39. Ian Madsen, Nicola Scarlett, and Arndt Kern. Description and survey of methodologies for the determination of amorphous content via x-ray powder diffraction. *Zeitschrift fur Kristallographie*, 226:944–955, 12 2011. doi: 10.1524/zkri.2011.1437.

40. Bruker. Diffrac.eva. (v5.2.0.5), .

A   XRD graphs used for quantification
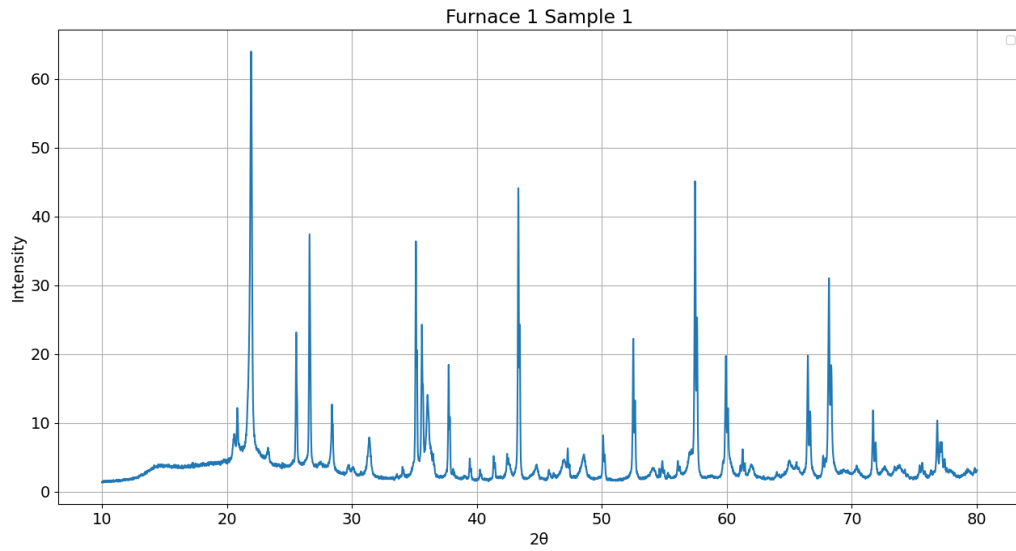
Figure 42: XRD for sample 1 from Furnace 1 doped with alumina for quantification.
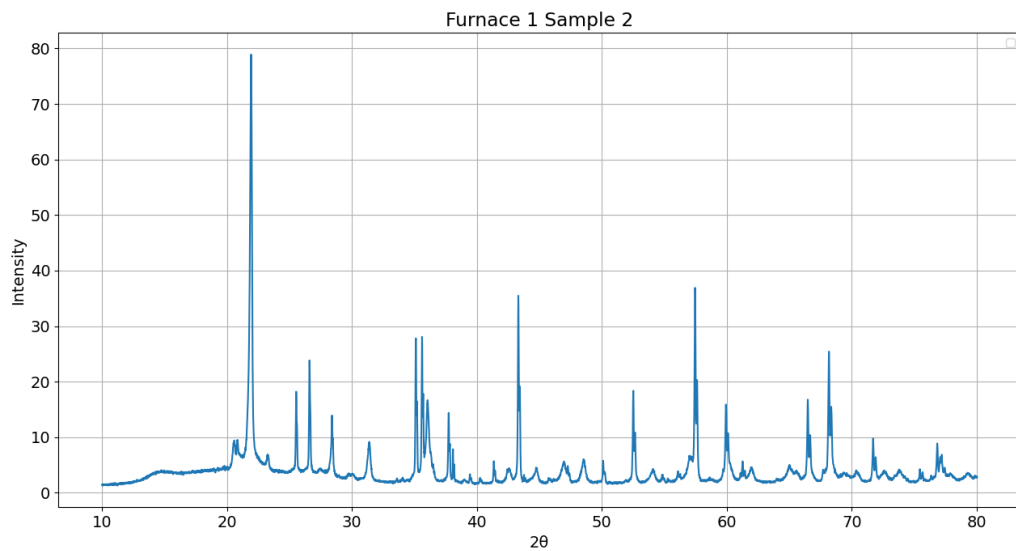
Figure 43: XRD for sample 2 from Furnace 1 doped with alumina for quantification.
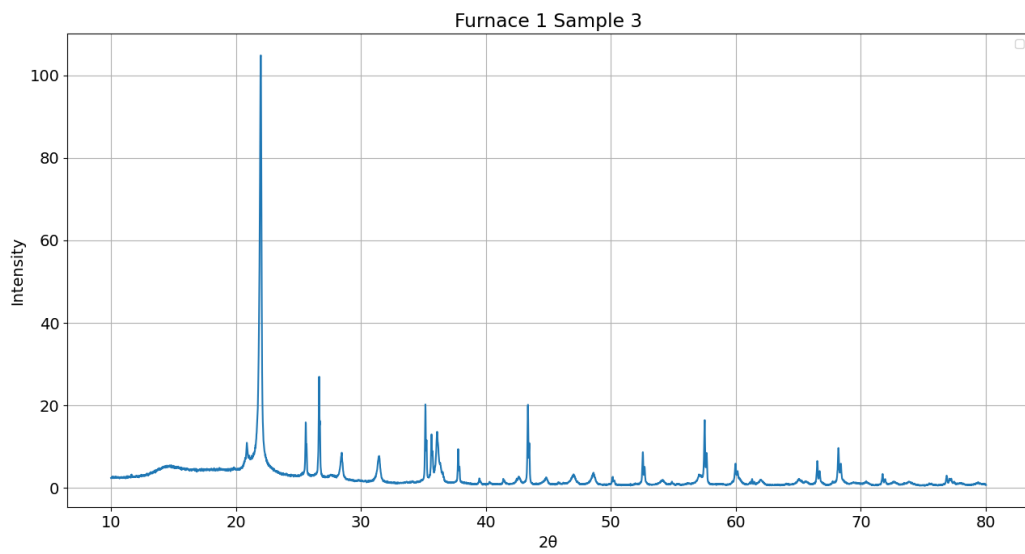
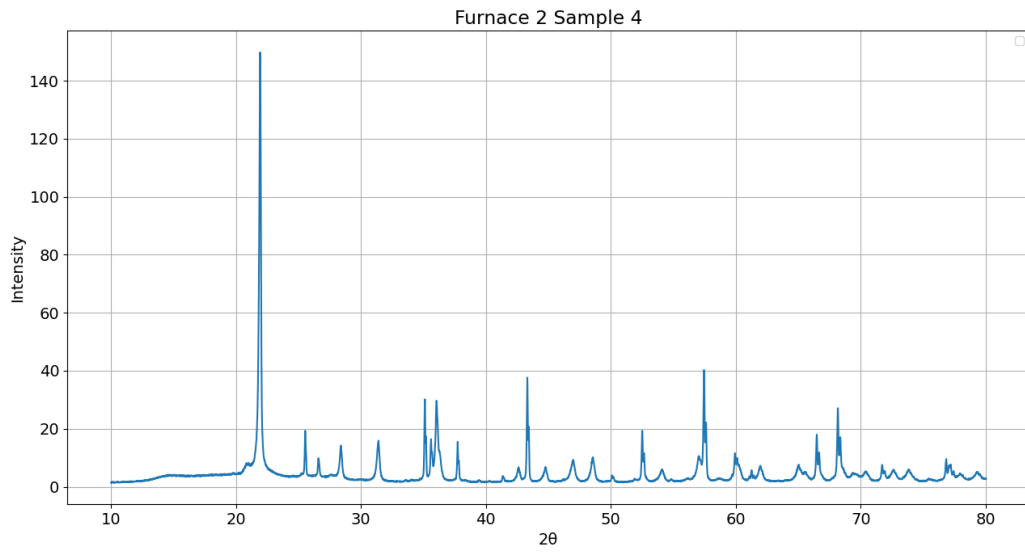Figure 44: XRD for sample 3 from Furnace 1 doped with alumina for quantification.
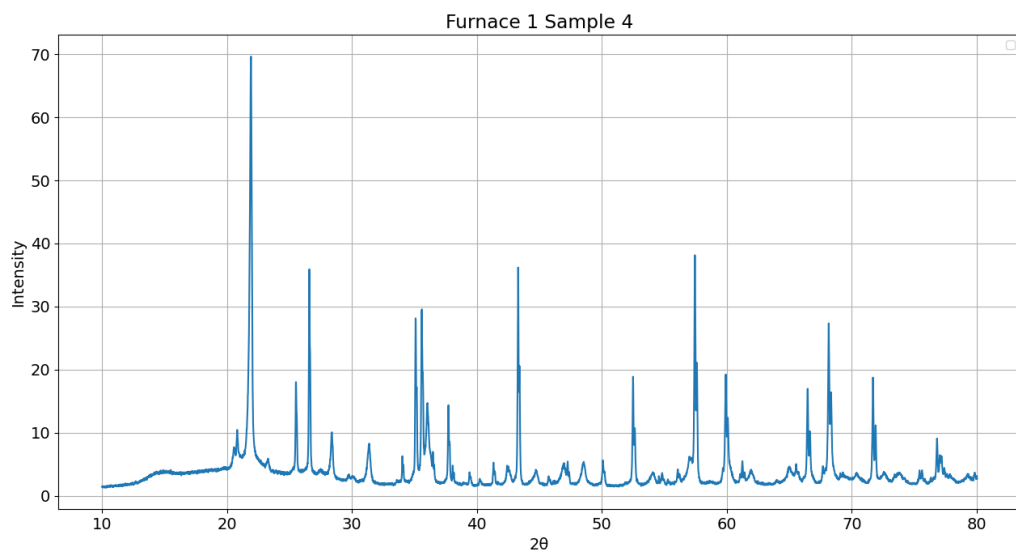
Figure 45: XRD for sample 4 from Furnace 1 doped with alumina for quantification.
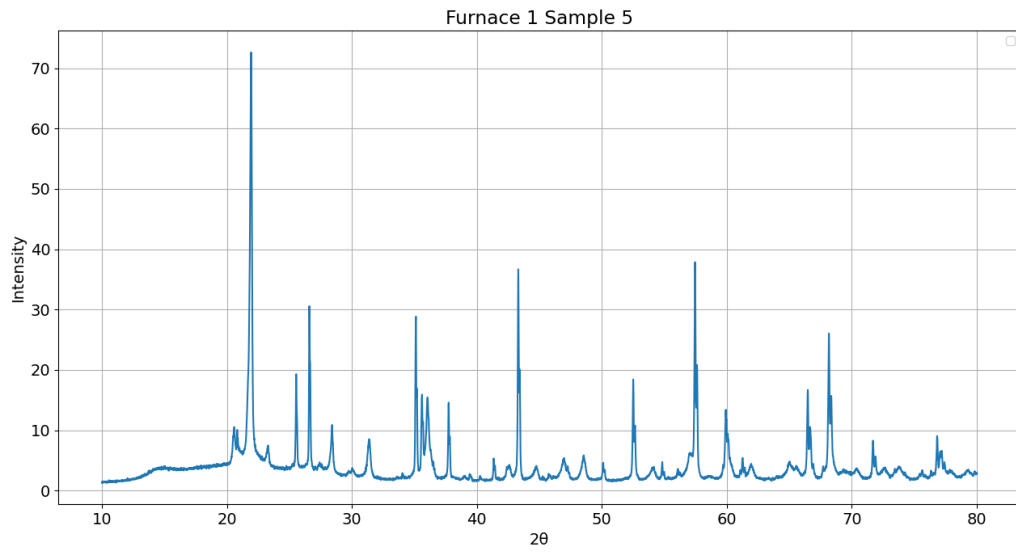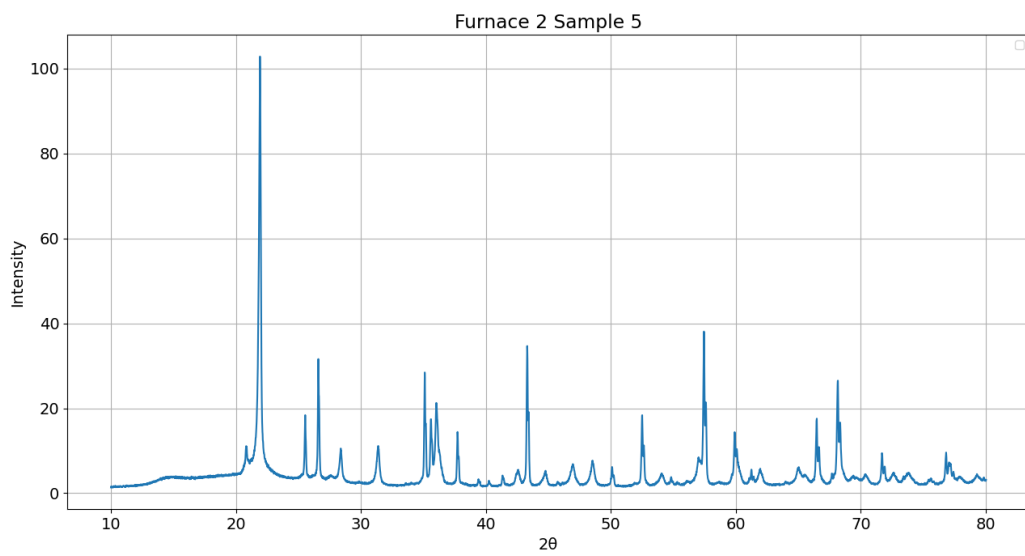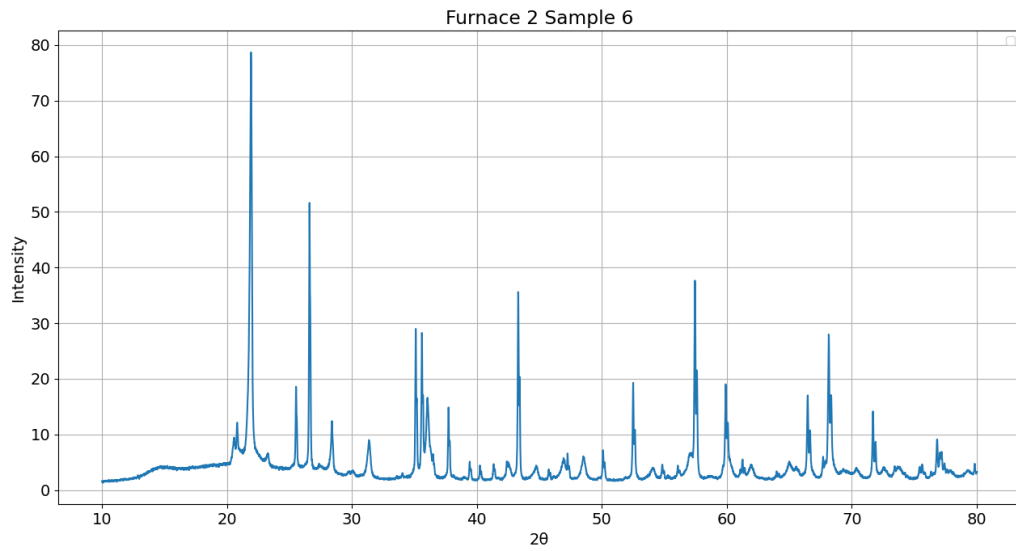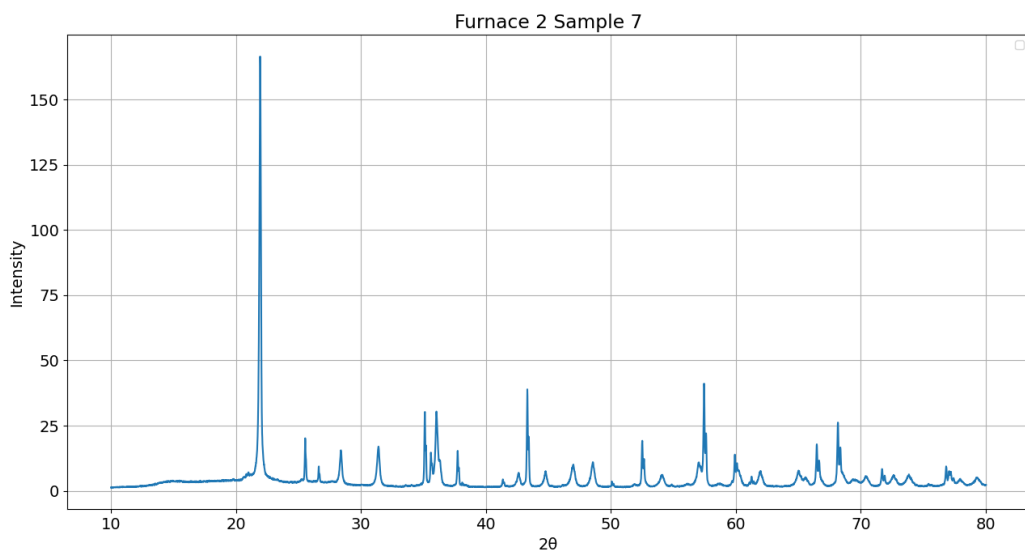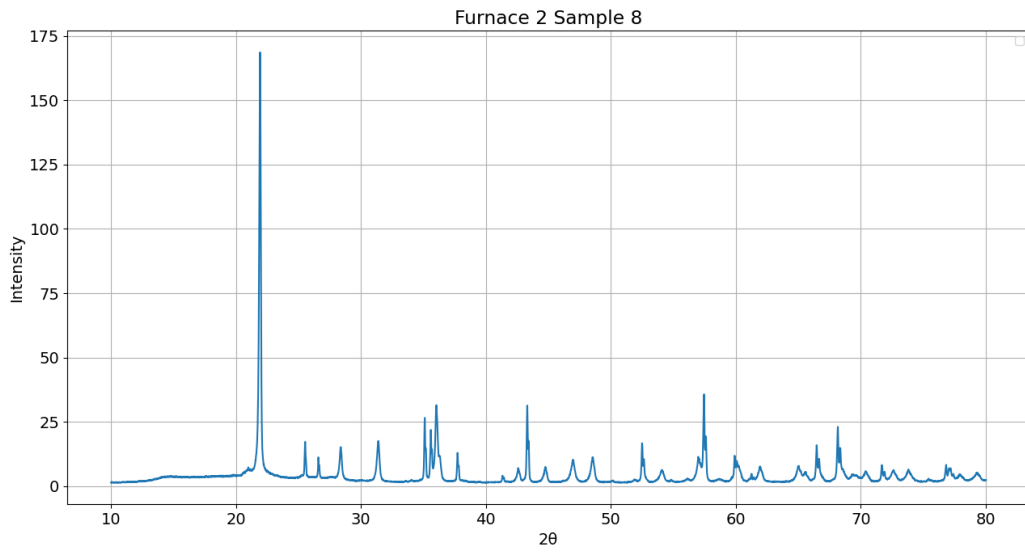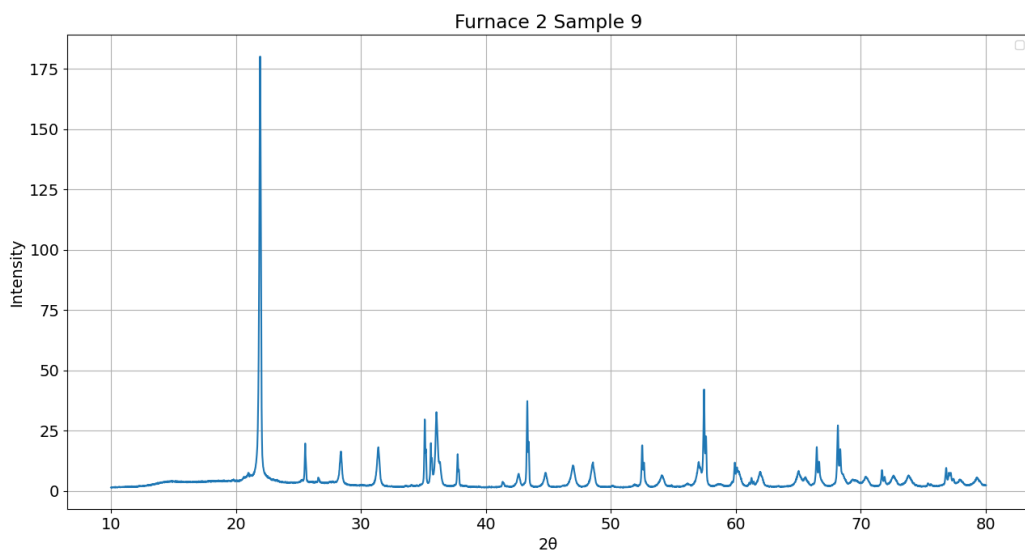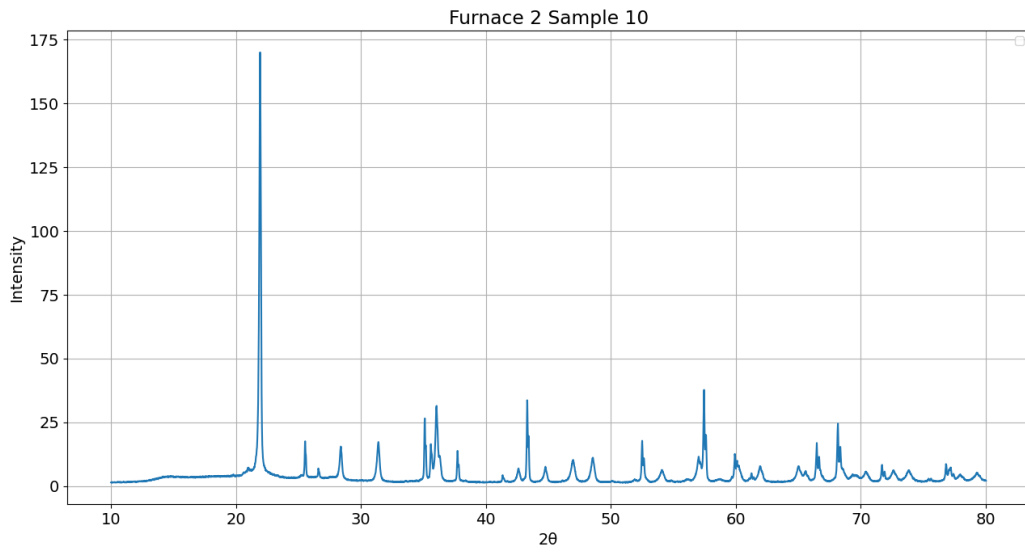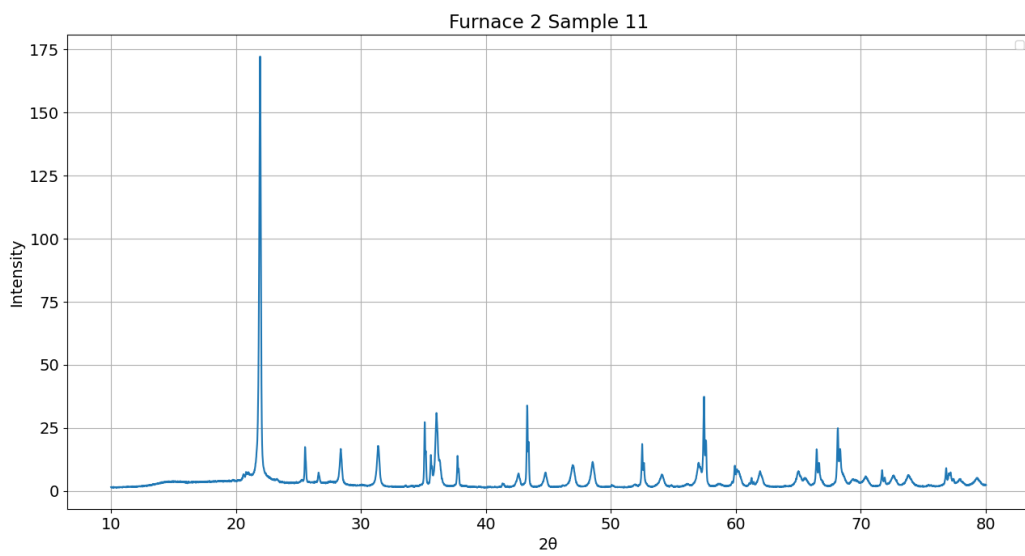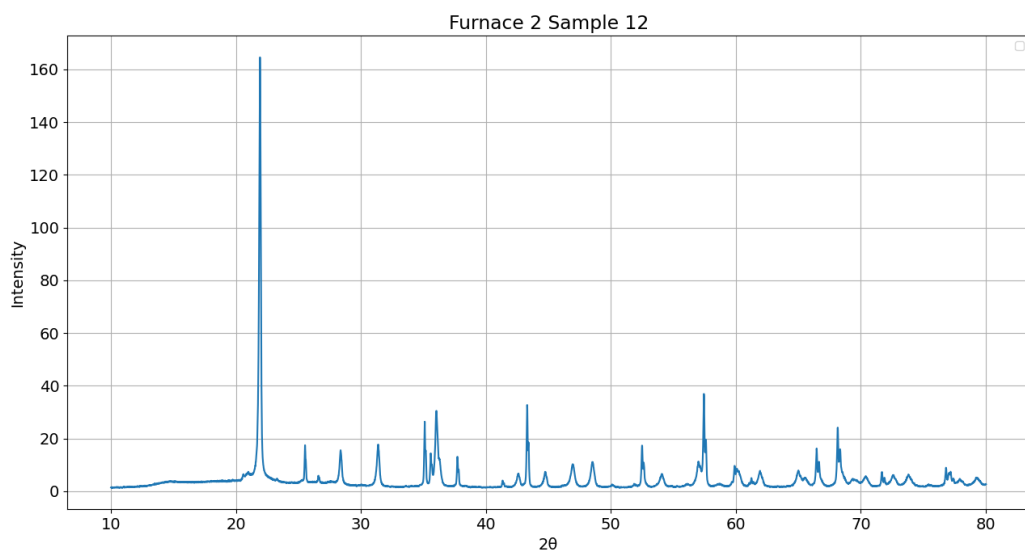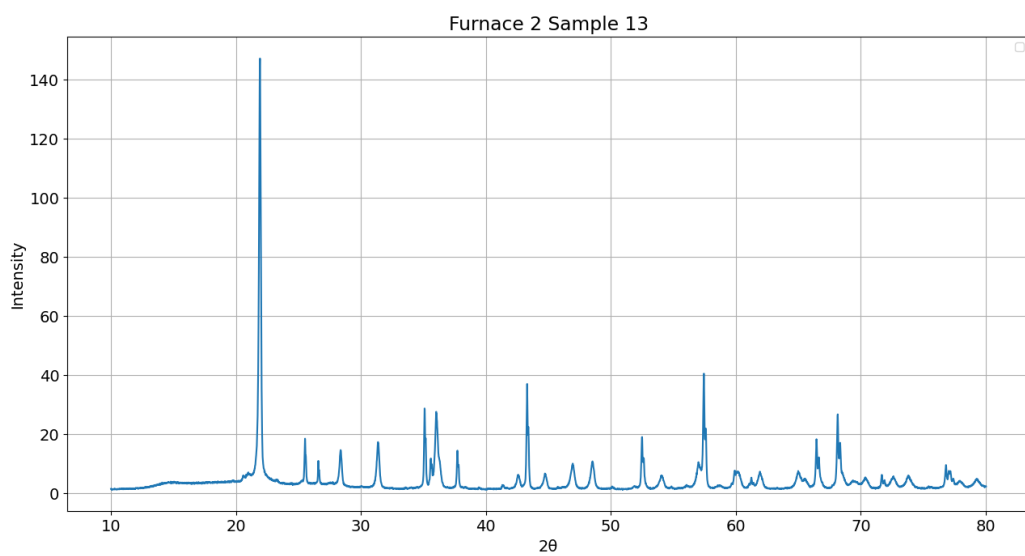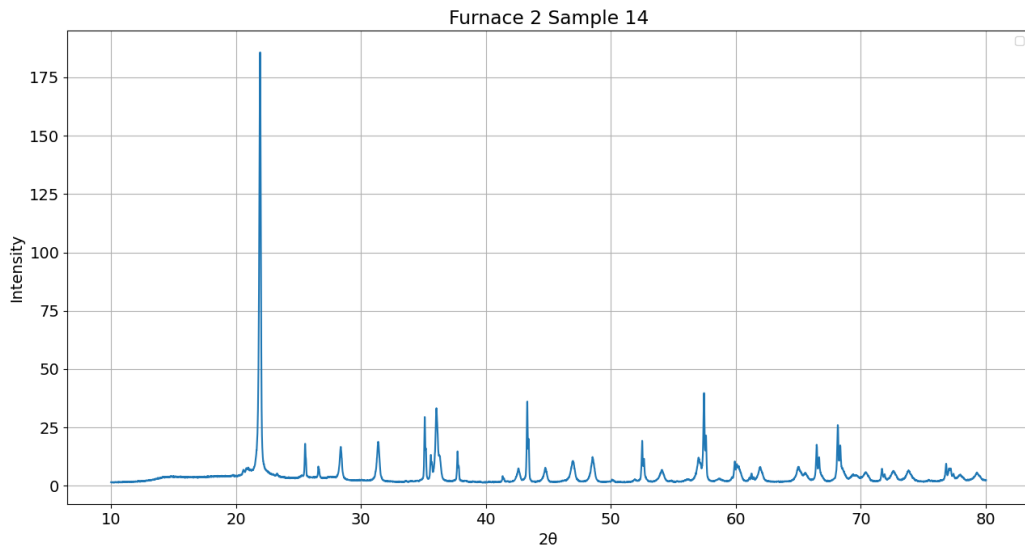
Figure 46: XRD for sample 5 from Furnace 1 doped with alumina for quantification.
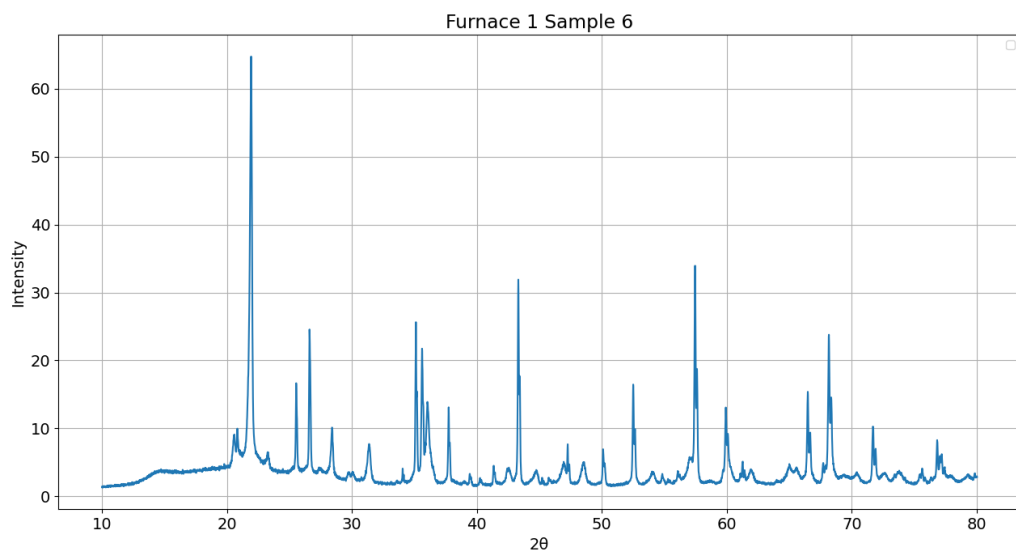
Figure 47: XRD for sample 6 from Furnace 1 doped with alumina for quantification.
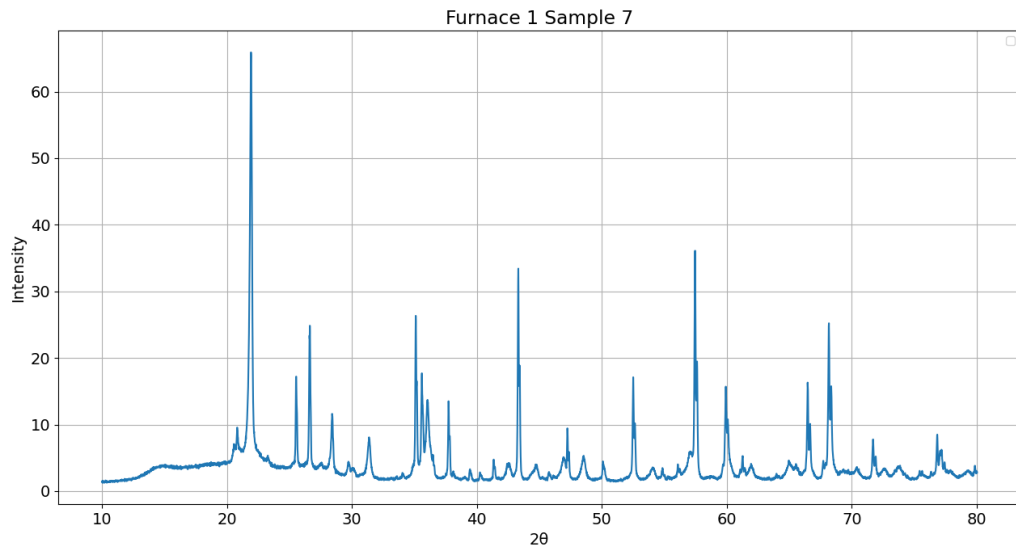
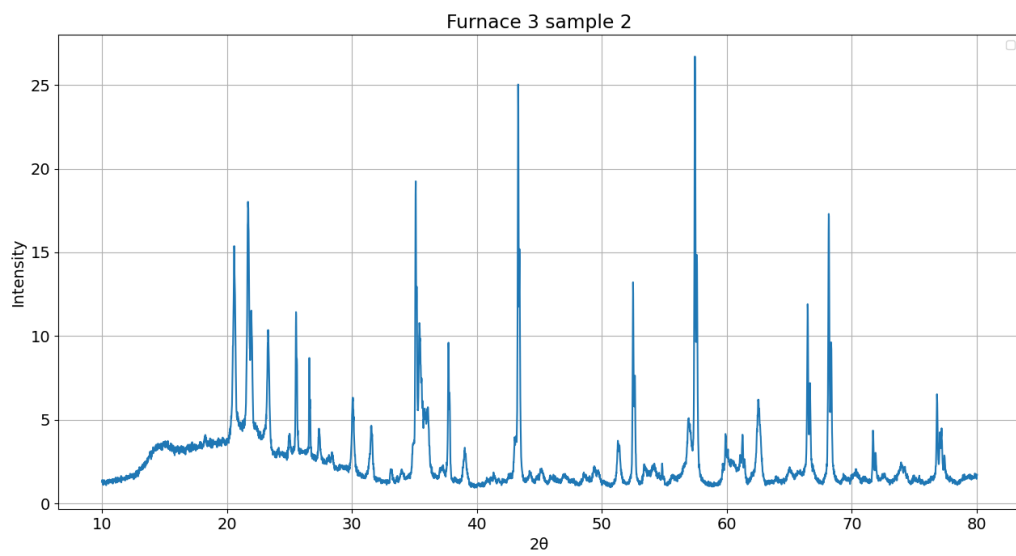Figure 48: XRD for sample 7 from Furnace 1 doped with alumina for quantification.
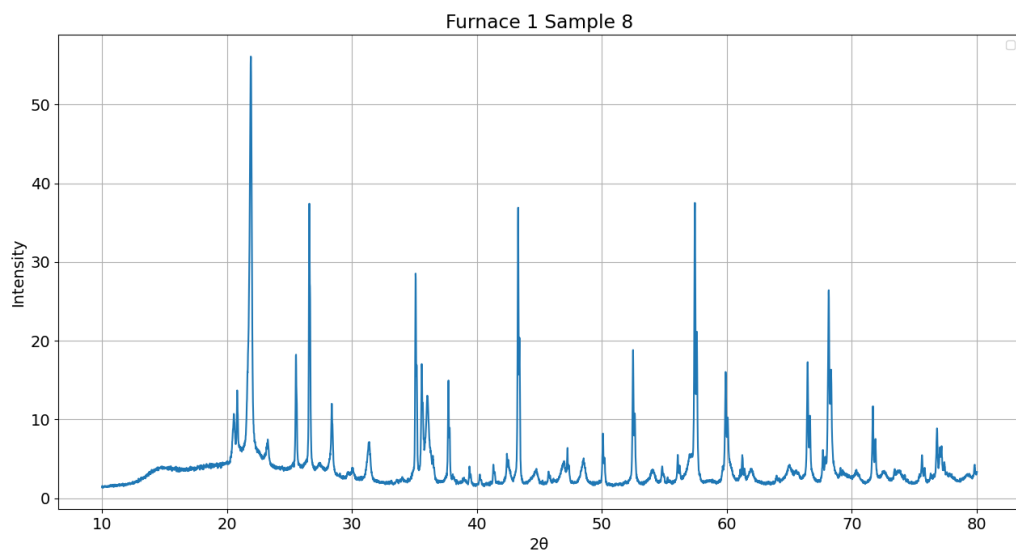
Figure 49: XRD for sample 8 from Furnace 1 doped with alumina for quantification.
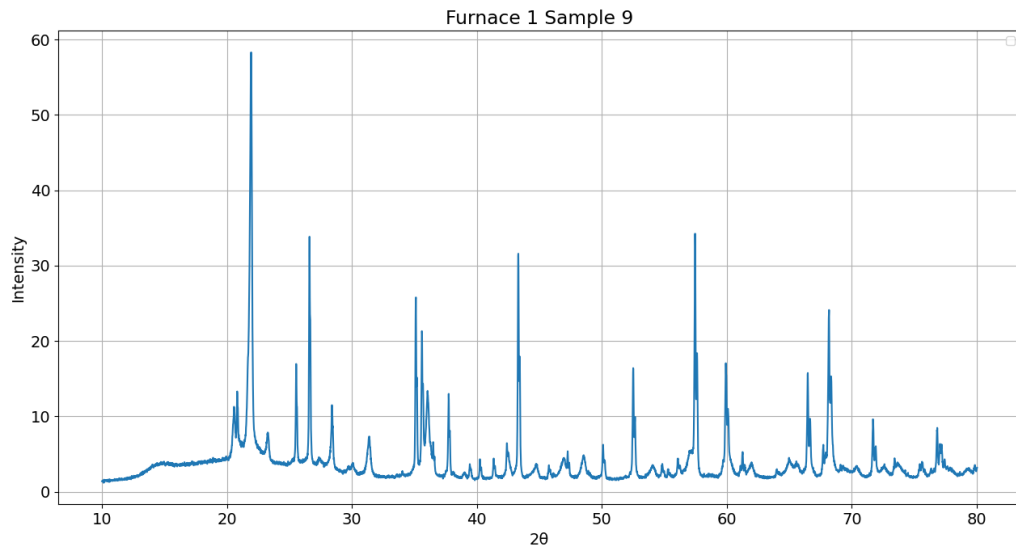
Figure 50: XRD for sample 9 from Furnace 1 doped with alumina for quantification.
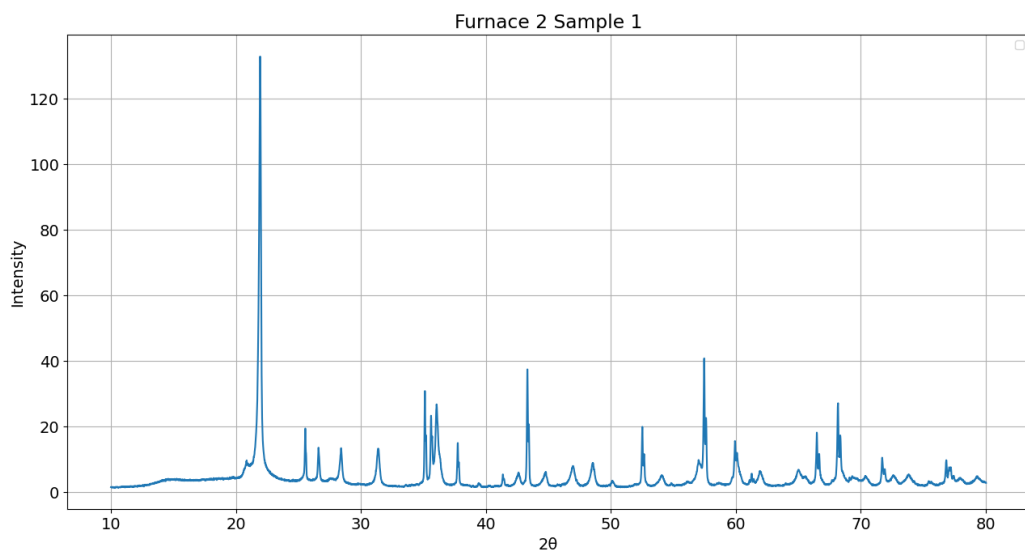
Figure 51: XRD for sample 1 from Furnace 2 doped with alumina for quantification.
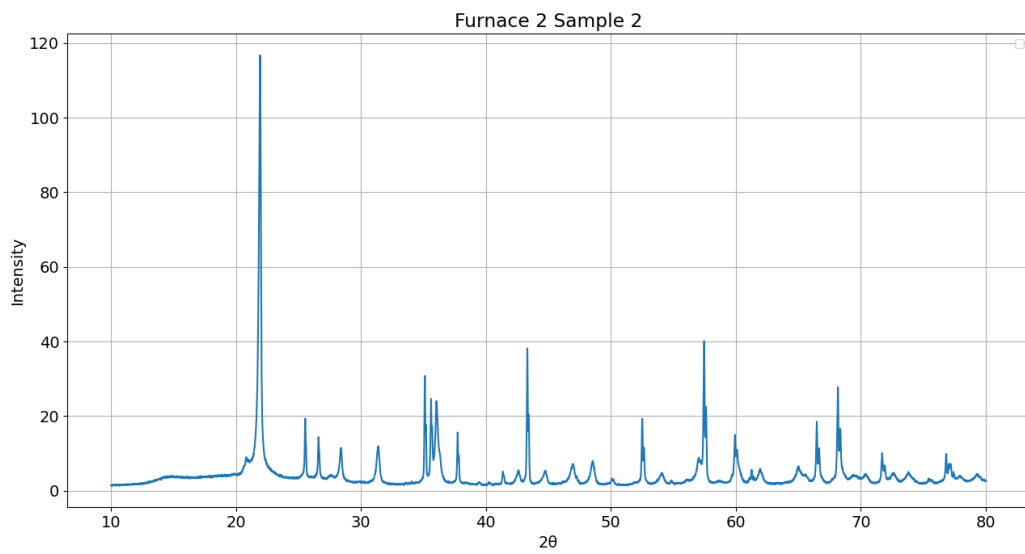
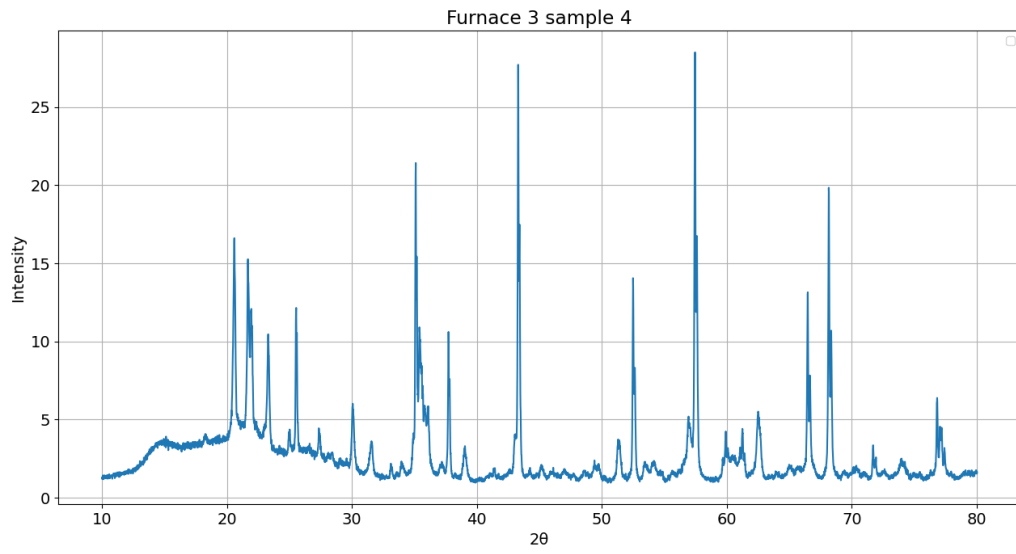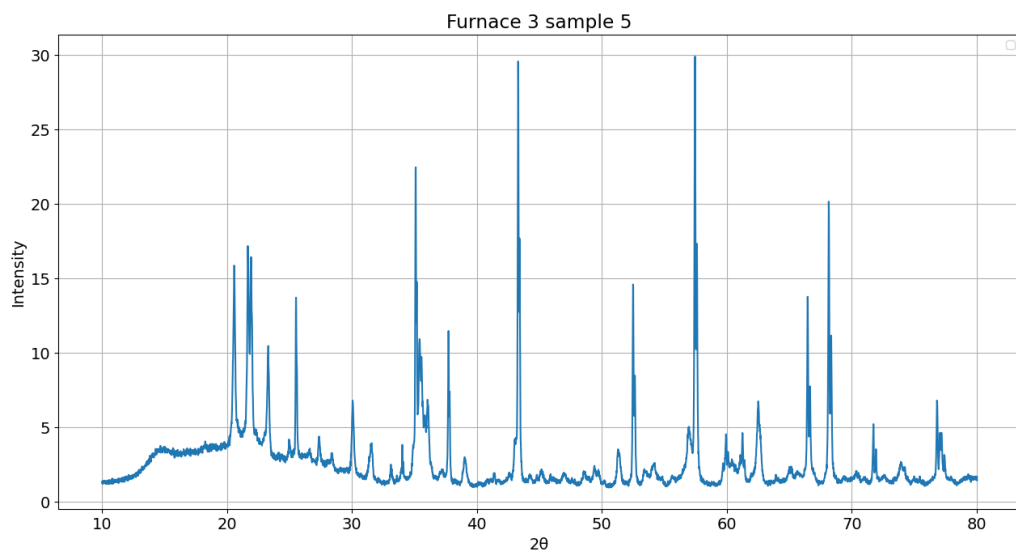Figure 52: XRD for sample 2 from Furnace 2 doped with alumina for quantification.
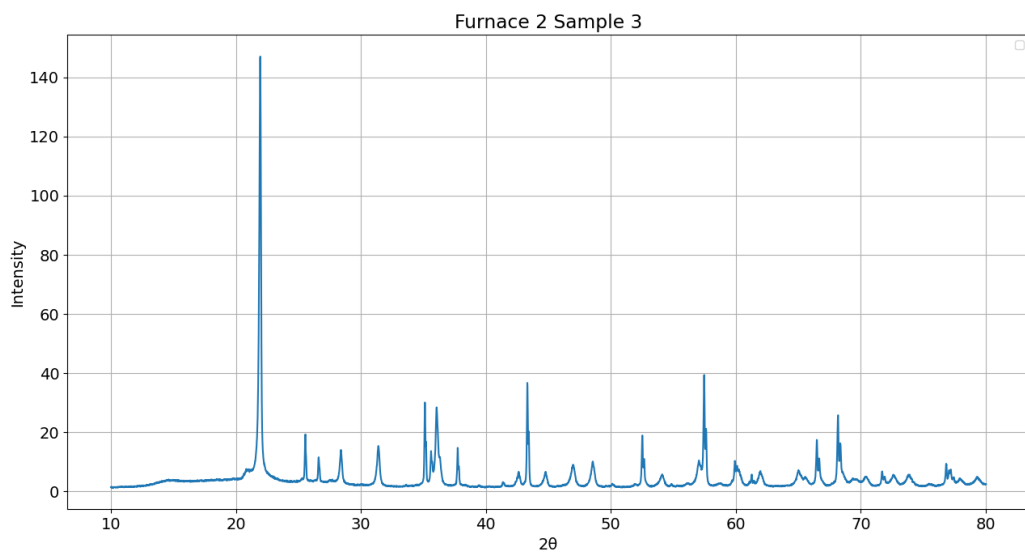
Figure 53: XRD for sample 3 from Furnace 2 doped with alumina for quantification.

Figure 54: XRD for sample 4 from Furnace 2 doped with alumina for quantification.

Figure 55: XRD for sample 5 from Furnace 2 doped with alumina for quantification.

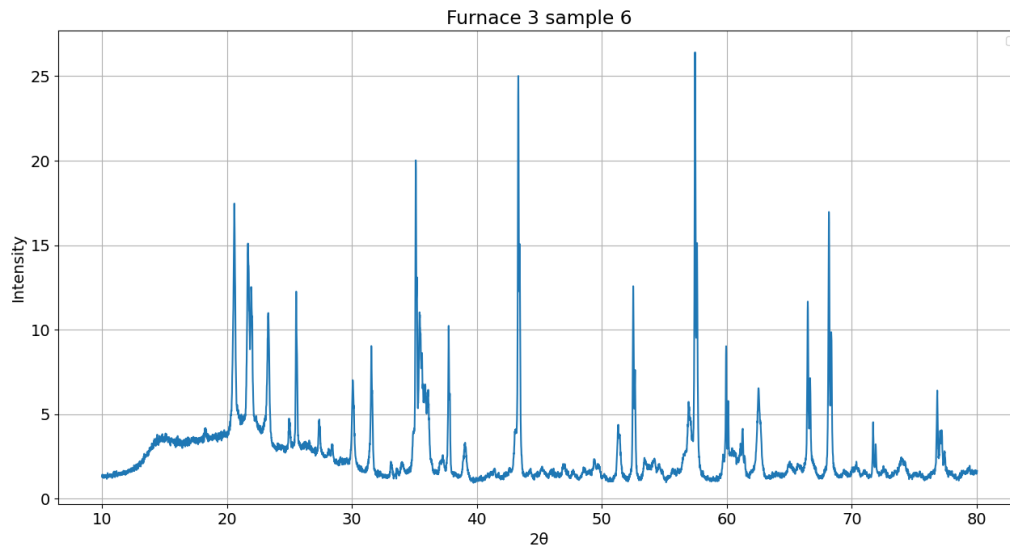Figure 56: XRD for sample 6 from Furnace 2 doped with alumina for quantification.

Figure 57: XRD for sample 7 from Furnace 2 doped with alumina for quantification.

Figure 58: XRD for sample 1 from Furnace 2 doped with alumina for quantification.

Figure 59: XRD for sample 9 from Furnace 2 doped with alumina for quantification.

Figure 60: XRD for sample 10 from Furnace 2 doped with alumina for quantification.

Figure 61: XRD for sample 11 from Furnace 2 doped with alumina for quantification.

Figure 62: XRD for sample 12 from Furnace 2 doped with alumina for quantification.

Figure 63: XRD for sample 13 from Furnace 2 doped with alumina for quantification.

Figure 64: XRD for sample 14 from Furnace 2 doped with alumina for quantification.

Figure 65: XRD for sample 1 from Furnace 3 doped with alumina for quantification.

Figure 66: XRD for sample 2 from Furnace 3 doped with alumina for quantification.

Figure 67: XRD for sample 3 from Furnace 3 doped with alumina for quantification.

Figure 68: XRD for sample 4 from Furnace 3 doped with alumina for quantification.

B   Raw ICP-MS results

Table 12: The ICP-MS results for Furnace 1 by ALS Scandinavia for the elements of most interest in terms of melting temperature and previous results given in g/kg.

Sample Number	Si g/kg	Na g/kg	K g/kg	Fe g/kg	Al g/kg	Mg g/kg	Ca g/kg	Ti g/kg	S g/kg	P g/kg	Mn g/kg
1	420	2.0	10	14	11	2.3	13	0.45	0.069	0.82	0.5
2	440	2.1	10	12	11	2.6	12	0.45	0.06	0.77	0.48
3	450	1.8	8.7	11	9.6	2.2	9.7	0.39	0.086	0.66	0.4
4	420	1.6	8.9	11	9.4	2.0	9.5	0.37	0.16	0.57	0.37
5	430	2.1	9.7	11	10	2.6	12	0.42	0.055	0.75	0.47
6	440	2.0	9.5	13	10	2.3	12	0.44	0.058	0.78	0.46
7	400	2.2	11	16	12	2.6	14	0.5	0.054	0.95	0.58
8	440	2.1	10	15	11	2.4	13	0.47	0.051	0.92	0.51
9	450	2.0	11	15	11	2.3	13	0.47	0.044	0.9	0.5

Table 13: The ICP-MS results for Furnace 2 by ALS scandinavia for the elements of most interest in terms of melting temperature and previous results given in g/kg

Sample Number	Si g/kg	Na g/kg	K g/kg	Fe g/kg	Al g/kg	Mg g/kg	Ca g/kg	Ti g/kg	S g/kg	P g/kg	Mn g/kg
1	470	1.8	1.5	2.4	2.8	1.1	4.0	0.072	1.7	0.13	0.11
2	490	1.6	1.7	2.7	3.5	1.5	6.5	0.097	0.18	0.14	0.15
3	460	1.9	1.8	1.8	3.1	1.3	4.3	0.079	0.68	0.15	0.12
4	460	2.1	1.9	3.5	4.6	1.7	8.4	0.160	0.018	0.15	0.17
5	460	2.1	1.7	3.4	4.0	1.5	6.5	0.130	0.010	0.18	0.17

Table 14: The ICP.MS results for Furnace 3 by ALS scandinavia for the elements of most interest in terms of melting temperature and previous results given in g/kg.

Sample Number	Si g/kg	Na g/kg	K g/kg	Fe g/kg	Al g/kg	Mg g/kg	Ca g/kg	Ti g/kg	S g/kg	P g/kg	Mn g/kg
1	380	1.7	3.9	300	4.2	3.5	3.0	0.17	0.036	0.23	5.1
2	320	1.5	4.3	240	3.6	3.2	2.8	0.16	0.052	0.23	4.3

C More x-ray mapping from EPMA images
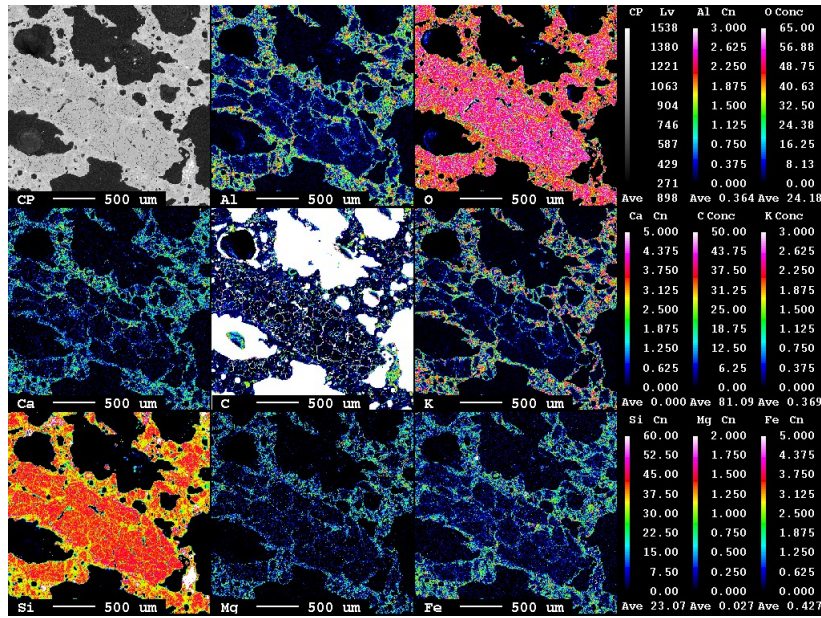
Figure 69: X-ray mapping of sample 1 from Furnace 1 the colour gradients on the right side are in wt%
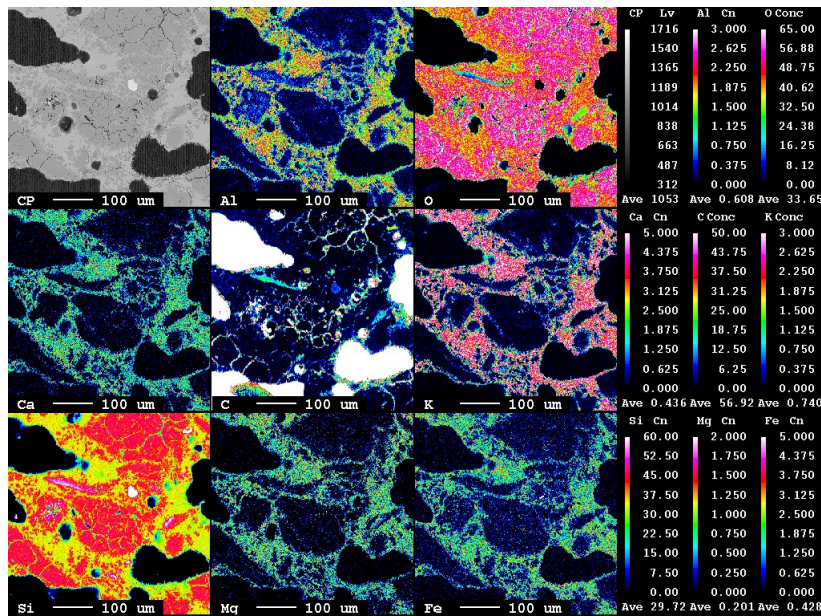
Figure 70: X-ray mapping of sample 1 from Furnace 1 the colour gradients on the right side are in wt%
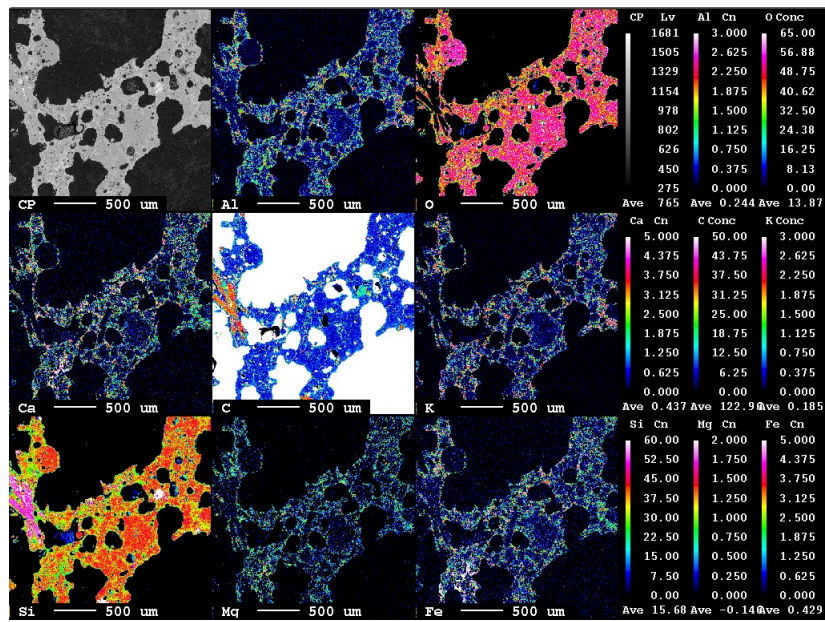
Figure 71: X-ray mapping of sample 2 from Furnace 1 the colour gradients on the right side are in wt%
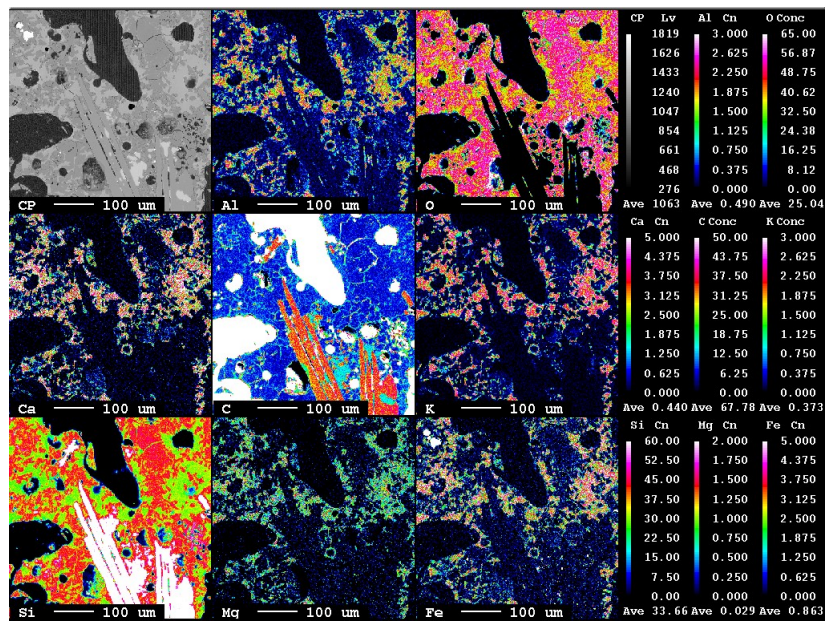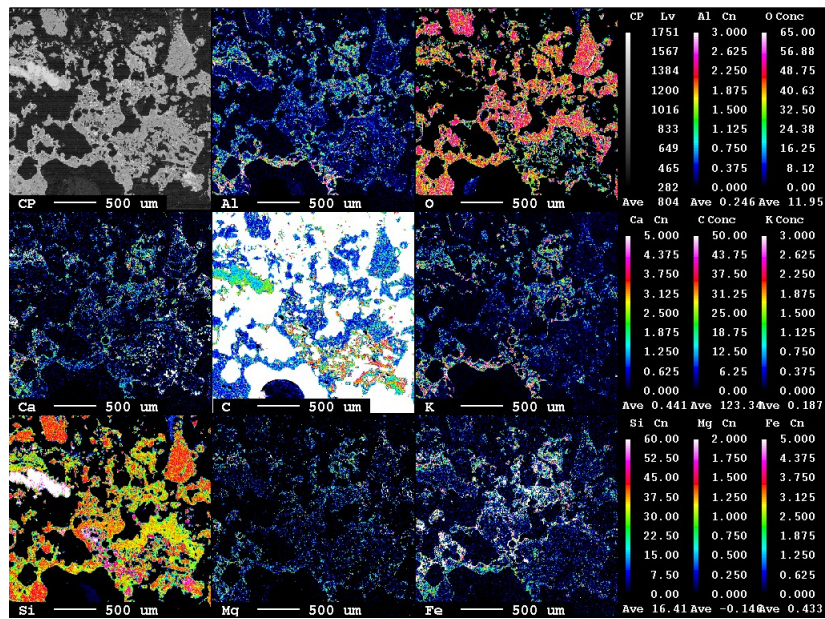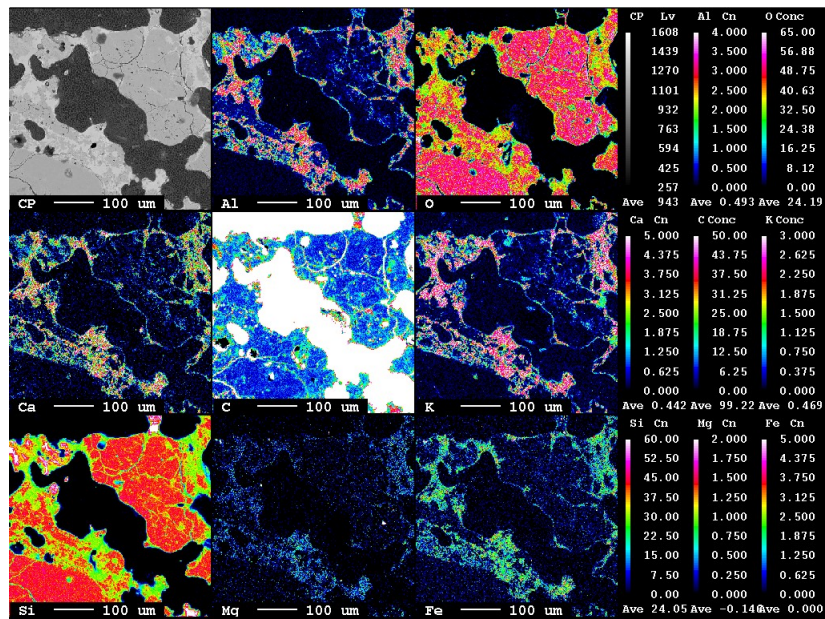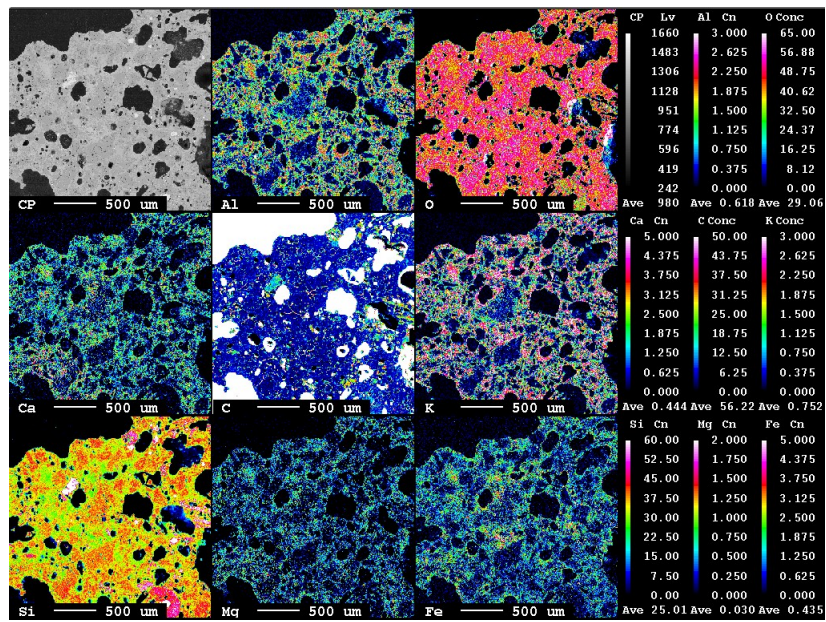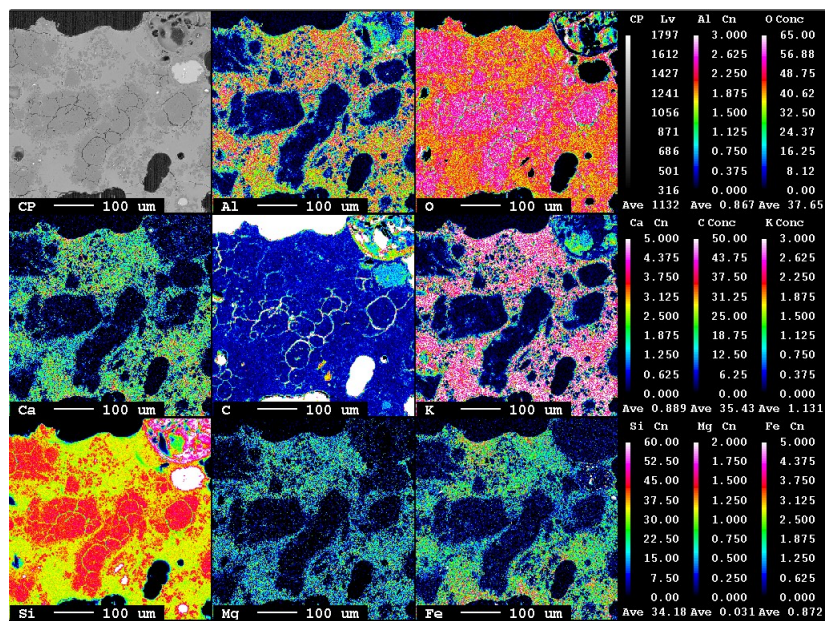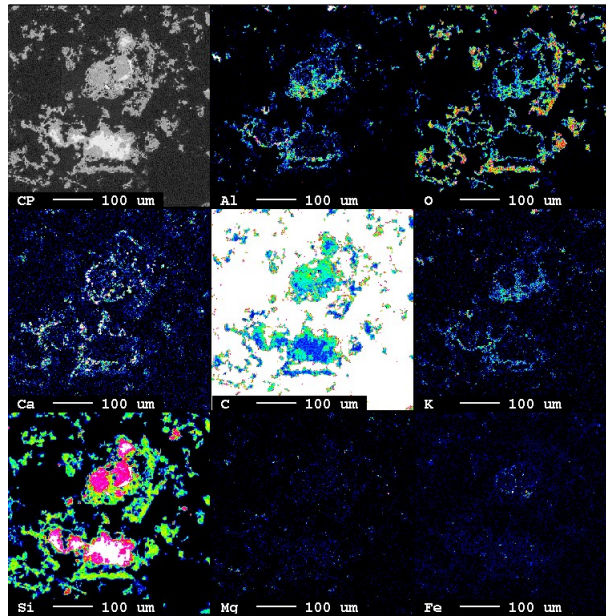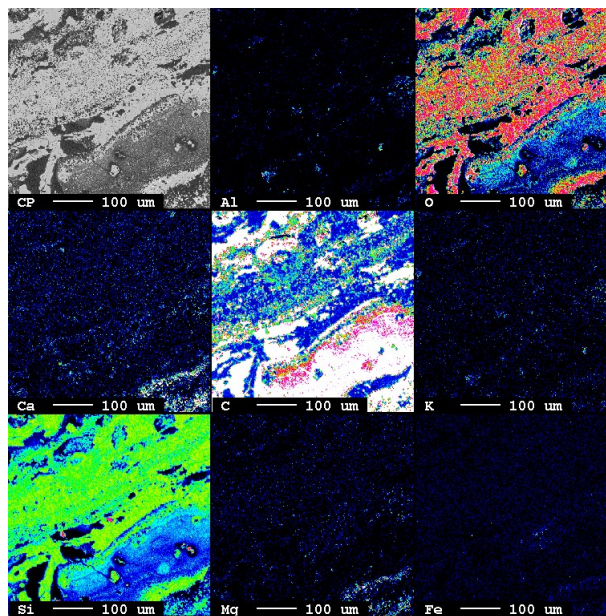

Figure 72: X-ray mapping of sample 2 from Furnace 1 the colour gradients on the right side are in wt%

Figure 73: X-ray mapping of sample 3 from Furnace 1 the colour gradients on the right side are in wt%
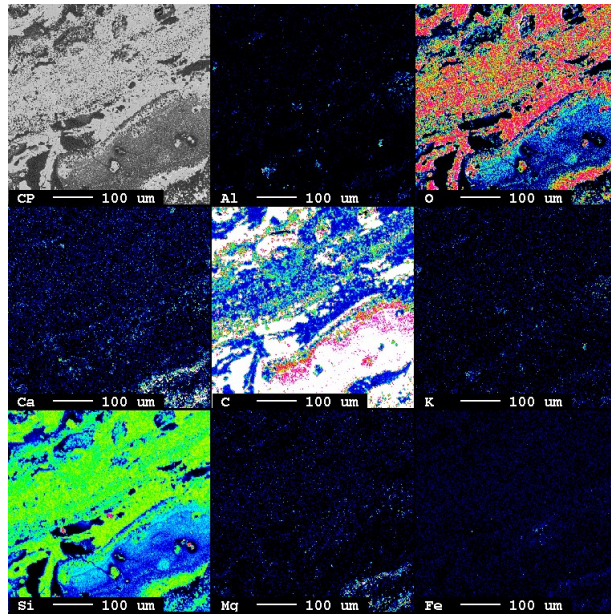

Figure 74: X-ray mapping of sample 3 from Furnace 1 the colour gradients on the right side are in wt%

Figure 75: X-ray mapping of sample 4 from Furnace 1 the colour gradients on the right side are in wt%

Figure 76: X-ray mapping of sample 4 from Furnace 1 the colour gradients on the right side are in wt%

Figure 77: X-ray mapping of sample 1 from Furnace 2 the colour gradients on the right side are in wt%
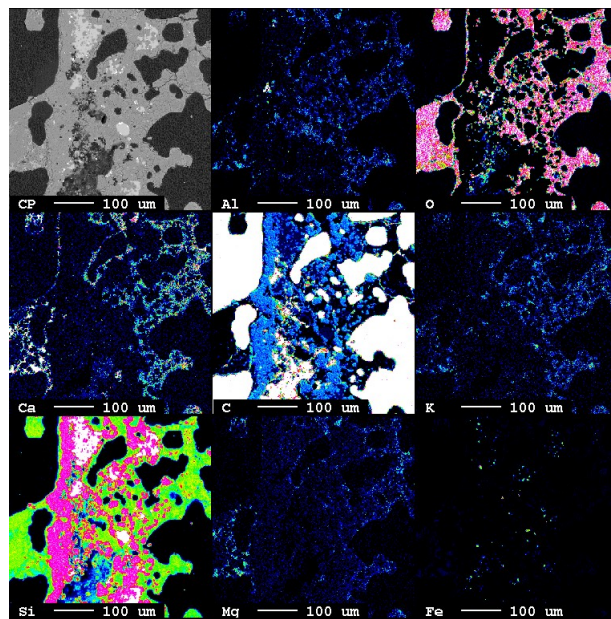

Figure 78: X-ray mapping of sample 2 from Furnace 2 the colour gradients on the right side are in wt%
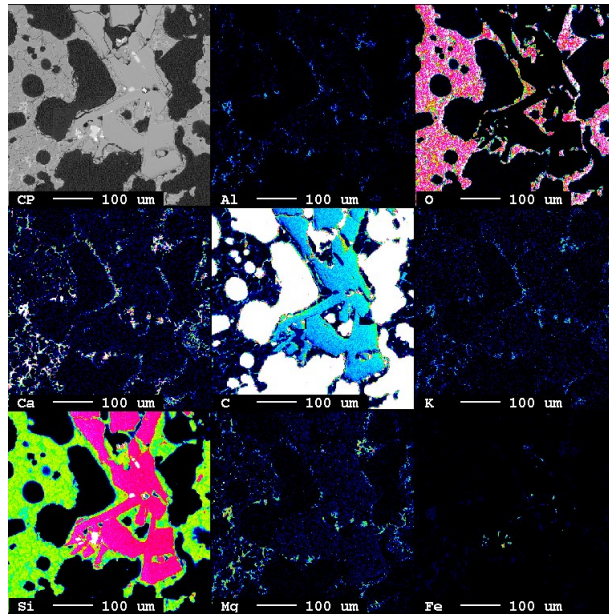
Figure 79: X-ray mapping of sample 3 from Furnace 2 the colour gradients on the right side are in wt%

Figure 80: X-ray mapping of sample 4 from Furnace 2 the colour gradients on the right side are in wt%

Figure 81: X-ray mapping of sample 5 from Furnace 2 the colour gradients on the right side are in wt%
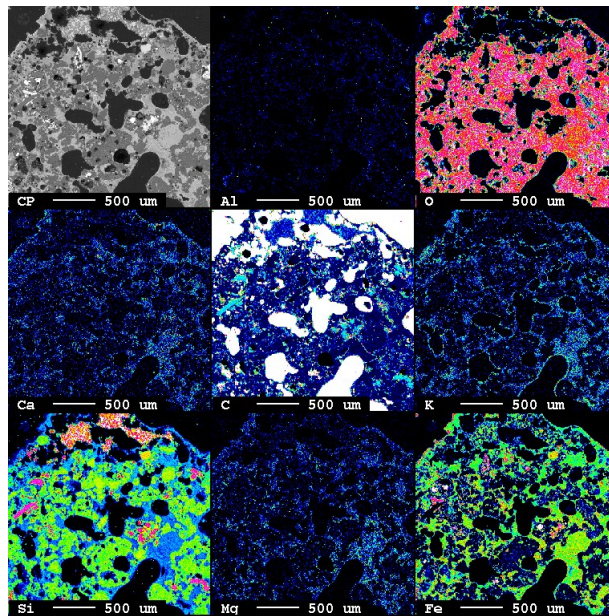

Figure 82: X-ray mapping of sample 1 from Furnace 3 the colour gradients on the right side are in wt%
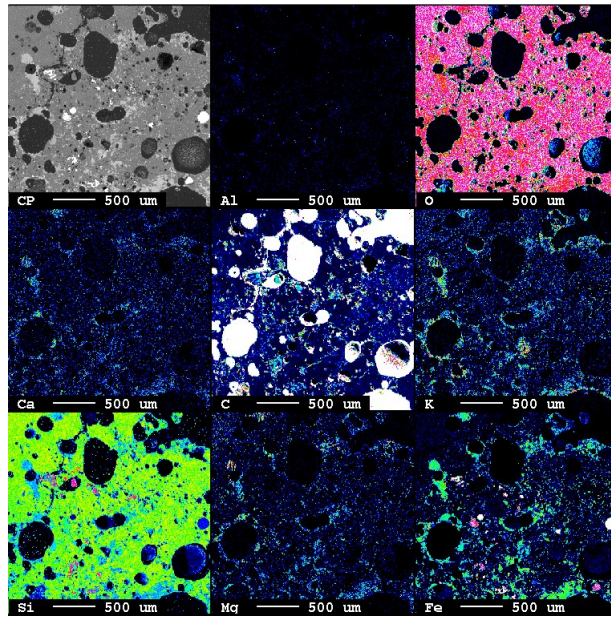
Figure 83: X-ray mapping of sample 2 from Furnace 3 the colour gradients on the right side are in wt%
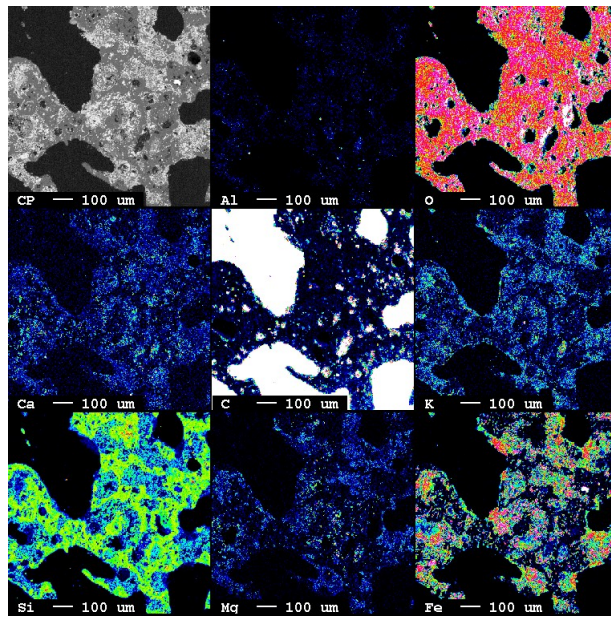

Figure 84: X-ray mapping of sample 3 from Furnace 3 the colour gradients on the right side are in wt%
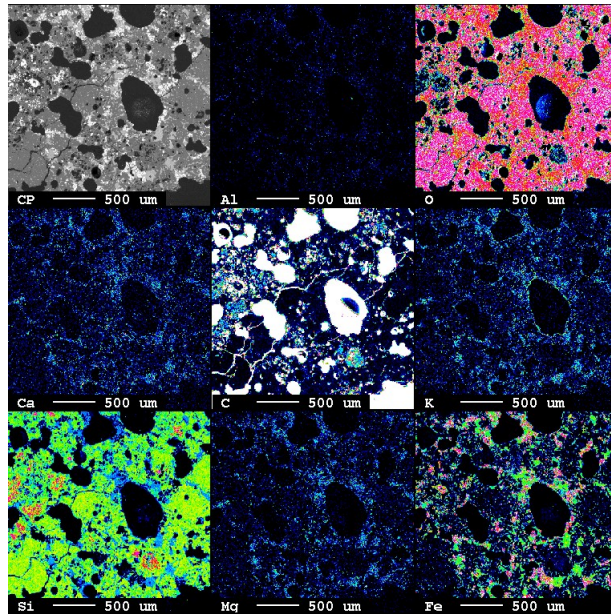
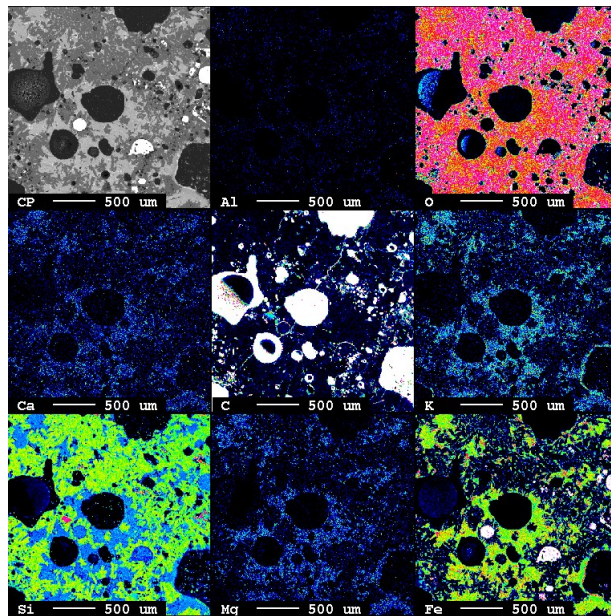Figure 85: X-ray mapping of sample 4 from Furnace 3 the colour gradients on the right side are in wt%

Figure 86: X-ray mapping of sample 5 from Furnace 3 the colour gradients on the right side are in wt%

D   Prediction models for ash fusion temperature

The two models from Yu et al.[35] used the following equations with the species in wt%.
Herbaceous based:

$$A' = \frac{SiO_2 + Na_2O + K_2O}{CaO + Al_2O_3 + Fe_2O_3}$$

$$ST = 1381 - 92.73A' + 4.874A'^2$$

Wood-based:

$$A = \frac{CaO + MgO}{SiO_2 + Al_2O_3 + K_2O + Fe_2O_3}$$

$$ST = 1098 + 181.5A - 19.15A^2$$

The model from Holubcik et al.[36] is using the following formulas. Species in wt%.
Dolomite index:

$$D_{IX} = \frac{CaO + MgO}{SiO_2 + CaO + K_2O + MgO + Al_2O_3}$$

$$f_{CMK} = \frac{CaO + MgO}{K2O}$$

$$f_{PH} = \frac{CaO + K_2O + MgO}{SiO_2 + Al_2O_3}$$

$$
\begin{aligned}
T = {} & 959.55 + 33.13SiO_2 + 285.91CaO - 400.69K2O + 134.70MgO \\
& + 977.82Al2O3 + 640.55D_{IX} - 3.28f_{CMK} - 32.84f_{PH}
\end{aligned}
\tag{9}
$$

The model by in the article of Suzhen et al.[37] the article does not say explicitly that the species are in weight percentage, but it is very likely due to it being how species are discussed earlier in the article. Also in the first equation $KNaO$ was assumed to mean the species K_2O and Na_2O.

$$b = Fe_2O_3 + CaO + MgO + K_2O + Na_2O$$

$$c = 1126.4 \cdot Al_2O_3 + 123.2055 \cdot b + 5217.4$$

$$587.6594 \cdot SiO_2 + 185.5634 \cdot b + 5374.5$$

Then different equations are picked based on size of previous numbers. If c is not larger than 23142, then

$$T2' = 923.2804 - 0.0183 \cdot c$$

if c is larger than 23142:

$$T2' = 0.0183 \cdot c + 136.7196$$

When e is smaller than 33273;

$$T2'' = 956.148 - 0.0161 \cdot e$$

when e is larger than 33273:

$$T2'' = 0.0151 \cdot e - 103.0041$$

Predicted softening temperature:

$$ST = ST2' + ST2''$$

Yin et al.[38] here it is assumed that the models use weight percentage since it was not given, and the text is quite indicative that it is wt%.

$$a = 100 - (SiO_2 + Al_2O_3 + Fe_2O_3 + CaO + MgO)$$

$$T_2 = 10.75SiO_2 + 13.03Al_2O_3 - 5.28Fe_2O_3 - 5.88CaO - 10.28MgO + 3.75a + 453$$

Erlend Hauge

NTNU
Norwegian University of
Science and Technology